PARSING THE DUAL ROLES OF CU/ZN SUPEROXIDE DISMUTASE (SOD1) IN OXIDATIVE STRESS PROTECTION AND REDOX SIGNALING

A Dissertation
Presented to
The Academic Faculty

by

Claudia Montllor Albalate

In Partial Fulfilment
Of the Requirements for the Degree
Doctor of Philosophy in the
School of Chemistry & Biochemistry

Georgia Institute of Technology

May 2021

PARSING THE DUAL ROLES OF CU/ZN SUPEROXIDE DISMUTASE (SOD1)

IN OXIDATIVE STRESS PROTECTION AND REDOX SIGNALING

Approved by:

Dr. Amit R. Reddi, Advisor
School of Chemistry and Biochemistry
Georgia Institute of Technology

Dr. Adegboyega K. Oyelere
School of Chemistry and Biochemistry
Georgia Institute of Technology

Dr. Loren D. Williams
School of Chemistry and Biochemistry
Georgia Institute of Technology

Dr. John F. McDonald
School of Biology
Georgia Institute of Technology

Dr. Matthew P. Torres
School of Biology
Georgia Institute of Technology

Date Approved: December 11th ,2020

This thesis is dedicated to my godfather Pere Ibars, who left us too soon, and my mother Lourdes Albalate Fernández, the strongest person I know.

“At the end of the day we can endure much more than we think we can”

- Frida Kahlo

ACKNOWLEDGEMENTS

The work presented in this dissertation would not have been possible without the contributions of many scientists. Although there is a single author name on this thesis, the help provided by numerous graduate students, postdoctoral fellows and professors that I have met at Georgia Tech and conferences has been essential for its completion. For this reason, I would like to first acknowledge my advisor Dr. Amit R. Reddi and thank him for the guidance, mentorship and knowledge provided during the past five years. I am very grateful to Dr. Reddi for his professional and personal advice, as well as for always being understanding and approachable. Graduate school can shape how you perceive yourself as a scientist and is a very vulnerable process, however, Dr. Reddi has always provided me with a comfortable environment where I always felt heard and have been able to grow as a scientist. His encouragement and enthusiasm have kept me motivated to answer new questions and find the best way to approach them. Dr. Reddi's enthusiasm for science is contagious and his way of thinking outside the box has deeply influenced me and shaped me as a scientist. I do not think I could have asked for a better advisor than Dr. Reddi.

I would like to extend my gratitude to my committee members, Drs. Loren D. Williams, Matthew P. Torres, Adegboyega K. Oyelere and John F. McDonald for their encouragement, time and academic advice.

I would especially like to thank Dr. Torres, who has immensely contributed in the third chapter of my thesis, by leading the mass spectrometry section of the paper and providing great expertise in yeast biology. I would also like to thank him for his encouragement.

Besides the scientists at Georgia Tech, I would also like to thank many scientists in the Redox Biology field. From the beginning, they have been extremely welcoming and kind to me and have provided me with lots of very valuable personal and professional advice, which has helped me enormously. I still remember my first conference, alone, surrounded by all these amazing scientists that I knew from all of the papers I had read, and feeling so small. Yet, they did not hesitate to approach and talk to me, making me feel like one of them. There are no words to describe how grateful I am to each of them and how much I appreciate their work and their enthusiasm.

The environment in which you develop yourself as a scientist has great impact on you, and I have been extremely lucky to have spent the time in graduate school surrounded by great scientists that have helped me and given me advice and personal support during these years. Therefore, I would like to thank all the members in the Reddi lab with which I have shared my time and lab space these past five years. Especially, I would like to thank Dr. Rebecca Donegan and Dr. Osiris Martinez-Guzmán. Rebecca is not only a great scientist that I admire and who has given me a lot of very valuable advice, she is also an amazing friend and mother. She is a person I really look up to and who I feel inspired by, and I cannot wait to see what she achieves in the near future. Osiris has provided me with all the knowledge in yeast biology I have, she is the person that spent time and effort showing me all the yeast techniques performed in the lab, and I could not ask for a better person to teach me; her patience and meticulousness in everything she does have deeply influenced me and, as a consequence, my work. She has not only been a great mentor, but also a great friend. We both share that Hispanic warm blood, and I do not know what I would have done without her hugs, her encouragement and her energy; only she knows how many tears and laughs we have shared, and they are all precious to me. I cannot thank both of them enough, I feel very lucky to have met them. Besides

Rebecca and Osiris, I would also like to thank Hyojung Kim and Alyson Colin, with whom I have worked together to develop the articles presented in my thesis work. And finally, Annalise, the graduate student who is taking on the Sod1 project. She is an amazing person with lots of enthusiasm, and I cannot wait to see what she discovers in the next couple years.

Why did I pursue a Ph.D. in Biochemistry? Probably because of many teachers and professors that have impressed me and helped me point towards this direction. For this reason, I would like to first acknowledge Max Marco, my biology teacher in High School. His enthusiasm, unconventional way of teaching Biology and exceptionally entertaining exams awoke my passion for Biology and Biochemistry. Thanks to him I decided to pursue a degree in Biochemistry, during which I had the immense honor to do an internship for Dr. Arturo Rojas and Dr. Loren D. Williams. Dr. Arturo Rojas, a professor in the Universidad Autónoma de Nueva León, in Monterrey, Mexico, gave me the first opportunity to work in a Cell Biology lab, where I realized my passion for Cell Biology research. A year later, I had the great opportunity to spend two months in the Williams lab at Georgia Tech, where I had one of the best experiences in my life. Dr. Williams is one of the people I am most grateful to; not only did he provide me with great mentorship and great expertise, but he also encouraged and believed in me. I would not be writing this thesis, here, today, without him helping me to get admitted at Georgia Tech as a graduate student. Thank you, Dr. Williams. I would also like to acknowledge Jessica Bowman and Marcus Bray, my internship mentor, who helped me immensely during my time in the Williams lab and from whom I learned a lot.

Although Graduate school has been a very valuable experience in my life, it has come with great challenges and up and downs. Having a great group of friends has been

monumental for me these years, it has kept me sane and constantly encouraged. So, I would like to thank my great friends from Graduate School, including Dr. Abraham Jordan, Dr. Osiris Martínez-Guzmán, Dr. Eric Drew, Dr. Zachary Hood, Dr. Samuel Evans, Dr. Rio Febrian, Dr. Marc Fernández and soon-to-be Drs. Stephen Zambrzycki and Samantha LaVoi. I will never forget our bonfires, hiking trips, shot walks and many other moments. I love and will miss them greatly. I would also like to thank the Evans family: Reilly, Sam, Mrs. Anne and Mr. Jeff Evans. They invited me to spend my very first Thanksgiving in the USA with them, and since then, we have shared fantastic experiences. I love and appreciate the Evans family so much.

Besides the friends I have in the USA, my friends back home have been a great support. The trips to Barcelona where I got to see them and share beers and lots of laughs recharged my batteries to go back to research with eagerness. I would like to thank the "Jefes": Tito, Uri, Carles, Álex, Rebe, Marta, Gemma, Porto, Adri, Albert, Inés and Eric, most of which I have known since I was two years old, in fact, I could say they are my extended family. I have been also immensely lucky to share my time in the United States with Marta and Rebe, which has allowed us to make great trips together. I love them so much. Although Rebe was only in the US for a year, Marta, or may I say Dr. Marta Sans-Escofet, continues to live here and we continue to spend every Thanksgiving together, one of the dates I always look forward to the most. I would also like to thank my great friends Monica and Ari, who have been always there for me and are one of the best people in my life. I would also like to acknowledge Manu, my great friend from college, my study mate, my favorite gossiper, the person with who I shared the experience of doing an internship at Georgia Tech. He has been a great friend and supporter these past years and I will always be grateful to him. Finally, I would like to acknowledge my best friend, Juancho. He has been an integral piece of my life for these past years and has been my most important support, who has always believed in me and in what I would be able to

achieve. He inspires me, and that has helped me become a better person and a better scientist. Am I not the luckiest person to have all these people in my life?

During Graduate School I have also met my partner, Santi. In him I have found my best friend and a person I really admire. I do not think I would have been able to go through these years without him; his enthusiasm, passion and curiosity has kept me motivated to never give up. Also, all the trips and amazing experiences we have shared have been essential for me to get a dose of fresh air and keep going through the numerous frustrations these past years. With Santi, I met Santi's family, a family that has welcomed me from the very beginning and that has been an immense support throughout the years they were living in the US. Ana, Manuel and Carlos, thank you so much for welcoming me, you are a very important part of my life now and I really appreciate and love you all.

Lastly, but not least, I would like to thank my family. The Albalate family, or the Woody Allen family, as we call it, has had a huge impact in who I am today, and I miss them every day of my life we are apart. I would like to especially thank my mother Lourdes and my sisters Júlia and Carla, they are very special to me and have been instrumental in my life. My mother, who is the strongest person I know, has always been my inspiration and is the reason I try to be a better person every day; from her I got my work ethic, my drive and strength to never give up. Without her I would not be where I am today, and I cannot thank her enough for her unconditional love and for everything she has done for me. My sister Júlia has been a great support throughout these years. I do not think I could count how many hours we spent on the phone, crying, laughing and trying to get the best out of every situation. She is my charm, my better half, and I admire and love her unconditionally. Carla has also been very important to me during this process. She is a person with who I can laugh and who has always believed in me. I am sure she will achieve great things with her talent and her personality. I love her very much. Finally, I would also

like to thank my father, Ramon, who more than a father has been a coach; his sport advice applied to real life has been very valuable for me throughout these years. He always used to tell me that I have to be a good loser to be a good winner, and that to smile in the race I have to cry training, and now I understand how right he was.

This section is rather lengthy, which is proportional to my gratefulness to all these people that have supported and helped me become who I am today.

TABLE OF CONTENTS

LIST OF TABLES

LIST OF FIGURES

LIST OF SYMBOLS AND ABBREVIATIONS

[4Fe-4S]	4 Iron- 4Sulfur cluster
Aco1	Aconitase
ACN	Acetonitrile
ATP	Adenosine triphosphate
BCA	Bicinchoninic acid
BCS	Bathocuproinedisulfonic acid disodium salt
ºC	Degrees Celsius
CAT	Catalase
Cu	Copper
Cys	Cysteine
DHE	Dihydroethidium
DMEM	Dulbecco's Modified Eagle Medium
DMSO	Dimethyl sulfoxide
DNA	Deoxyribonucleic acid
DTT	Dithiothreitol
Dvl	Disheveled

EDTA	Ethylenediaminetetraacetic acid
EGFR	Epidermal Growth Factor Receptor
EPR	Electron Paramagnetic Resonance
ER	Endoplasmic Reticulum
EV	Empty Vector
FALS	Familial amyotrophic lateral sclerosis
Fe	Iron
FE	Median Fold Enrichment
G	Gravity
G6PD	Glucose 6-phosphate dehydrogenase
GAL	Galactose
GAPDH	Glyceraldehyde 3-phosphate dehydrogenase
GFP	Green Fluorescent Protein
GLU	Glucose
GO	Gene Ontology
GPx	Glutathione Peroxidase
GSH	Glutathione
H_2O_2	Hydrogen peroxide

HEK293	Human Embryonic Kidney 293 cells
HIF	Hypoxia Inducible Factor
HIS	Histidine
hSod1	Human Sod1
IMS	Mitochondrial intermembrane space
Iodo-TMT	Iodoacetyl Tandem Mass Tag
kDa	Kilodalton
L	Liter
LC/MS	Liquid chromatography Mass Spectrometry
LEU	Leucine
Leu1p	Isopropylmalate isomerase
Lys	Lysine
µg	Microgram
µL	Microliter
µM	Micromolar
mM	Millimolar
Mn	Manganese
ms	Millisecond

MS	Mass spectrometry
mPEG-mal	Methoxy polyethylene glycol maleimide
NADH	Dihydronicotinamide adenine dinucleotide
$NADP^+$	Nicotinamide-adenine dinucleotide phosphate
NADPH	Dihydronicotinamide-adenine dinucleotide phosphate
Ni	Nickel
NOX	NADPH Oxidase
O_2	Oxygen
$O_2^{\bullet -}$	Superoxide radical
OD_{600}	Optical density read at 600nm
$^{\bullet}OH$	Hydroxyl radical
Opti-MEM	Opti- Modified Eagle Medium
Ox	Oxidized
oxPPP	Oxidative phase of the Pentose Phosphate Pathway
PAGE	Polyacrylamide Gel Electrophoresis
PBS	Phosphate-buffered Saline
PCR	Polymerase Chain Reaction
PMSF	Phenylmethylsulfonyl fluoride

pO_2	Oxygen pressure
PPP	Pentose Phosphate Pathway
PQ	Paraquat
Prdx	Peroxiredoxin
Prx-SO_3	Sulfinic acid oxidized Peroxiredoxin
PSMs	Protein Spectral Matches
PTMs	Post-translational modifications
ROS	Reactive oxygen species
RPLC	Reverse phase liquid chromatography
RPM	Revolutions per minute
SC	Synthetic complete medium
SCE	Synthetic complete medium enriched with Ergosterol and Tween
S. cerevisiae	*Saccharomyces cerevisiae*
SILAC	Single Isotope Labeling by/with Amino acid in Cell culture
SIRT	Sirtuin
Sod1	Cu/Zn Superoxide dismutase
*sod1*Δ	Sod1 knock out strain
Sod2	Mn Superoxide dismutase

SDS-PAGE	Sodium Dodecyl Sulfate- Polyacrylamide Gel Electrophoresis
TAP	Tandem Affinity Purification
TCA	Trichloroacetic acid
TdT	Terminal deoxynucleotidyl transferase
TEMED	N,N,N′,N′-Tetramethylethylenediamine
ß-TrcP	ß-Transducin Repeat-Containing Protein
Tris	Tris(hydroxymethyl)aminomethane
Trx	Thioredoxin
TUNEL	Terminal deoxynucleotidyl transferase dUTP nick End labeling
UbL	Ubiquitin Ligase
URA	Uracil
UV/Vis	Ultraviolet- visible spectroscopy
Wnt	Wingless
WT	Wild type
Yck	Yeast casein kinase
YPD	Yeast Peptone Dextrose
ySod1	Yeast Sod1
Zn	Zinc

ZrO	Zirconium oxide

SUMMARY

Superoxide dismutases (SODs) are a highly conserved class of antioxidant enzymes that serve on the frontline of defense against reactive oxygen species (ROS). SODs, which detoxify superoxide radicals ($O_2^{\bullet-}$) by catalyzing their disproportionation into molecular oxygen (O_2) and hydrogen peroxide (H_2O_2), are rather unusual "antioxidant" enzymes in that they catalyze the production of one ROS – H_2O_2 – while scavenging another – $O_2^{\bullet-}$. While much is known about the necessity for $O_2^{\bullet-}$ detoxification, it is less clear what the physiological consequences of SOD-derived H_2O_2 are. Given that hormetic levels of H_2O_2 are important for physiological redox signaling and also act as a pro-growth signal, SODs, especially Cu/Zn SOD (Sod1), which accounts for the majority of intracellular SOD activity in eukaryotes and is localized virtually everywhere in the cell except the mitochondrial matrix, may be key to promote various redox signaling pathways.

My thesis work has been focused on parsing the dual roles of Sod1 in oxidative stress protection and redox signaling. I have found that the vast majority of Sod1 is dispensable for protection against $O_2^{\bullet-}$ toxicity using *Saccharomyces cerevisiae* and human cell lines as model organisms (Chapter 2 and 3, respectively). However, the bulk of Sod1 is required for proteome-wide H_2O_2-based redox signaling, including regulation of the of yeast casein kinase (Yck1, Chapter 2), the canonical Wnt signaling pathway (Chapter 3) and a molecular circuit that links O_2 availability to the production of NADPH, a key cellular reductant that regenerates thiol-based antioxidant enzymes (Chapter 4). Altogether, my work finally explains the physiological necessity for an "antioxidant" enzyme like Sod1 to produce an oxidant – namely that the H_2O_2 that Sod1 produces is used to stimulate NADPH-dependent ROS scavenging and redox regulate a large network of metabolic enzymes.

In the first part of my thesis work, described in Chapter 2, I discovered that < 1% of the total cellular Sod1 pool is required for protection against superoxide damage in yeast. Superoxide toxicity stems from the oxidative inactivation of 4Fe-4S clusters, resulting in defects in a number of pathways containing Fe/S dependent metabolic enzymes, and toxicity from the iron released from damaged clusters. The iron leads to deleterious redox reactions that oxidatively damage DNA, lipids, and proteins. By profiling cell wide markers of superoxide toxicity, including Fe/S cluster enzyme activity, DNA damage, and membrane fragmentation, in cell lines expressing a regulatable *SOD1* promoter, I found that an undetectable (< 1%) amount of Sod1 is sufficient for superoxide resistance in air. Instead, the bulk of Sod1 is required to promote the stabilization of Yck1, a glucose sensing plasma membrane casein kinase previously found to be stabilized in a Sod1-dependent manner. This led me to conclude that the majority of Sod1 plays a more important role as a source for hormetic H_2O_2 than for scavenging $O_2^{\bullet-}$.

In Chapter 3, I extend my findings from yeast to mammalian cells, and found that ~50-80% depletion of Sod1 in human embryonic kidney cells using RNA interference does not result in oxidative stress but does impact casein kinase signaling in the Wnt pathway. The Yck1 homology in humans, CK1γ, is an integral component of the Wnt signaling pathway, which is necessary for embryonic development and is prooncogenic when hyperactivated. I found that silencing Sod1 does not affect cell proliferation or the expression of a panel of antioxidant enzymes, consistent with bulk Sod1 being dispensable for oxidative stress protection. However, Sod1 silencing resulted in reduced CK1γ expression and attenuated Wnt signaling and Wnt-dependent cell proliferation. Thus, as in yeast, bulk Sod1 is dispersible for oxidative stress protection but seemingly required for redox signaling in human cell lines.

Having established that bulk Sod1 is dispensible for protection from superoxide toxicity, in the third section of my thesis, described in Chapter 4, I probed the physiological roles of Sod1-derived spatio-temporal bursts of H_2O_2. As part of this effort, I discovered that an important but previously unknown antioxidant function of Sod1 is to integrate O_2 availability to stimulate production of NADPH, a key cellular reductant that regenerates peroxide-scavenging thiol peroxidases and catalases. The mechanism involves Sod1-derived H_2O_2 oxidatively inactivating the catalytic Cys residue in the glycolytic enzyme, glyceraldehyde phosphate dehydrogenase (GAPDH), which in turn re-routes carbohydrate flux through the oxidative phase of the pentose phosphate pathway (oxPPP) to increase NADPH. Sod1 senses O_2 via $O_2^{\cdot -}$ generated from mitochondrial respiration and a NADPH oxidase, Yno1. The oxidation of GAPDH is exclusively dependent on and rate limited by Sod1, suggesting that Sod1 provides a highly localized pool of H_2O_2 in close proximity to GAPDH, likely via transient interactions between Sod1 and GAPDH. These findings broaden the antioxidant role of Sod1 to include stimulation of NADPH production, which offers more expansive protection against redox stress than just defending against $O_2^{\cdot -}$, which most Sod1 is dispensable for as determined in Chapter 2. Moreover, in collaboration with the laboratory of Matthew Torres, we employed mass spectrometry based redox proteomics approaches to identify cell-wide targets of Sod1-dependent protein oxidation. This analysis revealed that Sod1 is a master regulator of metabolism and the thiol redoxome.

Overall, my findings shed light on a broader role for Sod1 that extends beyond just superoxide scavenging as was previously thought. Given that changes in Sod1 expression and activity are a central aspect of the pathogenesis of a number of diseases, including many cancers and neurodegenerative disorders, my thesis work highlights how metabolic rewiring due to Sod1-based redox control may underlie the progression of human disease

and may inspire new Sod1-based therapeutics and aid to understand the effectiveness of anti-Sod1 therapeutic interventions in cancer.

CHAPTER 1. INTRODUCTION

1.1. General Thesis Introduction

Over the years, there has been an increasing interest in understanding the role of reactive oxygen species (ROS) in physiology and disease. At first, ROS were perceived as toxic molecules, and it was not until the early 90s that some ROS, and, in particular H_2O_2, were starting to be recognized as potential signaling molecules. One of the main cellular sources of peroxide are superoxide dismutases (SODs) that protect against superoxide toxicity by disproportionating superoxide radicals into hydrogen peroxide and molecular oxygen. From the different types of SODs, Cu/Zn SOD, or Sod1, constitutes the most abundant and widespread SOD and accounts for most SOD activity in the cell. As such, Sod1 may have a broader physiological impact, both as an antioxidant and in promoting redox signaling. In fact, Sod1 has been implicated in several cancers and neurodegenerative diseases, such as familial amyotrophic lateral sclerosis (FALS). However, whether the contribution of Sod1 towards pathology is related to its antioxidant capacity or perturbed redox signaling is still enigmatic.

The work described below arose from one simple question: Given that superoxide radicals, $O_2^{\bullet-}$, are spontaneously disproportionated at a relatively fast rate, 10^5 $M^{-1}s^{-1}$, and that Sod1 disproportionates $O_2^{\bullet-}$ at a diffusion-limited rate, 10^9 $M^{-1}s^{-1}$, why are such large quantities of Sod1 generated? This motivated me to establish the relative contributions of Sod1 towards superoxide protection versus redox signaling and to identify cell-wide Sod1-catalyzed H_2O_2 redox relays. This will shed light on a better perception of the role of Sod1 in cell biology and disease. My thesis motivation was to challenge how we perceive Sod1 in physiology.

1.2. Reactive Oxygen Species (ROS): A Byproduct of Life in Air

Reactive oxygen species (ROS) are the byproduct of aerobic metabolism. ROS result from the incomplete 4 electron reduction of oxygen (O_2) to water (H_2O), producing superoxide ($O_2^{\bullet-}$), hydrogen peroxide (H_2O_2), or hydroxyl radicals ($^{\bullet}OH$). These ROS can oxidize and damage various biomolecules, including [4Fe-4S] cluster-containing enzymes, nucleic acids [1], lipids and proteins [2]. One of the main sources of ROS in the cell is the mitochondrial electron transport chain (ETC) [3], where electrons are transferred across the different respiratory complexes to a final acceptor molecule, oxygen, to generate an electrochemical gradient that powers ATP synthesis. Leakage of electrons from complex I or complex III in the ETC to the mitochondria intermembrane space (IMS) can partially reduce oxygen to generate superoxide radicals. Besides the ETC, there are additional sources of $O_2^{\bullet-}$ within the cell, such as NADPH oxidase enzymes (NOX). NOX generate $O_2^{\bullet-}$ from NADPH and O_2 and are mainly found tethered to the membranes of different compartments in the cell and the plasma membrane, contributing to $O_2^{\bullet-}$ build-up in the cytosol or outside the cell [4], respectively.

Since cells are constantly exposed to ROS, they require a complex network of antioxidant systems, including superoxide and hydrogen peroxide scavengers. Superoxide dismutases (SODs), which require metals for catalysis, are the main antioxidant defense against superoxide in the cell [5] and act to disproportionate two molecules of superoxide into hydrogen peroxide and molecular oxygen. Most cells express two intracellular SOD isoforms: Cu/Zn superoxide dismutase (SOD1), localized virtually everywhere in the cell including the mitochondrial IMS [6, 7], except the mitochondrial matrix; and Mn superoxide dismutase (SOD2), exclusively localized in the mitochondrial matrix (**Figure 1.1**). Mammalian cells express a third SOD isoform, SOD3,

an extracellular Cu/Zn SOD. Additional antioxidant systems in the cell scavenge H_2O_2, including thiol peroxidases (i.e. peroxiredoxins, Prxs) [8], glutathione peroxidases (GPx) [9] and catalases (CAT) (**Figure 1.1**). All these antioxidant systems rely on NADPH, a vital cellular reductant, for their regeneration [10, 11]. This intricate antioxidant network protects the cell from oxygen and oxidative insults [12]. However, when these antioxidant systems are overwhelmed by the ROS burdens, there is an imbalance between ROS levels and the antioxidant capacity that prevent ROS damaging effects, resulting in *oxidative stress*.

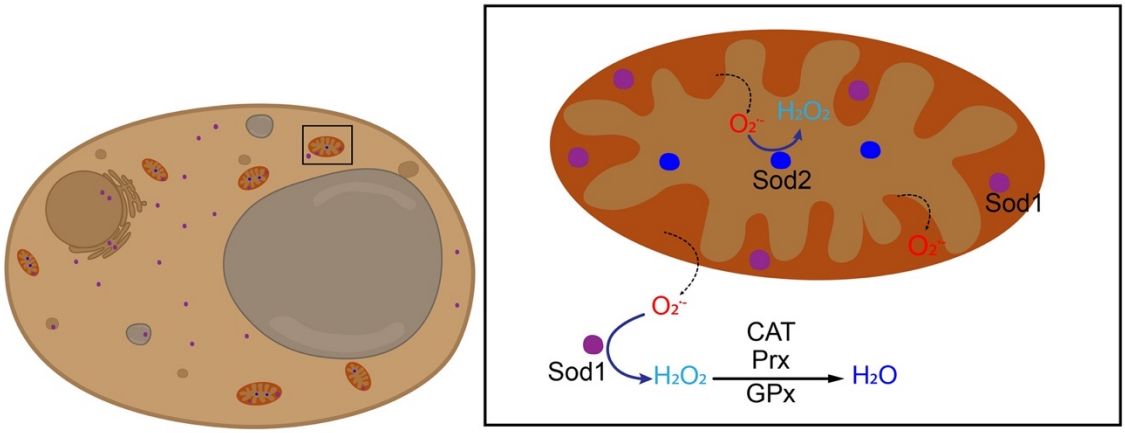

Figure 1.1. Antioxidant systems in the cell. Sod2, Mn superoxide dismutase; Sod1, Cu/Zn superoxide dismutase; CAT, catalase; Prx, thiol peroxidase; GPx, Glutathione peroxidase.

1.2.1. Brief History of Reactive Oxygen Species

Over the last hundred years, there has been an increasing interest in understanding the role of free radicals in biology, given their ample involvement in both physiology and disease. It is been long known that living organisms have a paradoxical relationship with molecular oxygen, in that it is necessary for life but toxic. However, the molecular mechanisms underlying oxygen toxicity were not understood until 1954, when Gershman proposed the *free radical theory of oxygen toxicity,* proposing that oxygen is toxic due to its ability to form free radicals [13], confirmed later the same year by Commoner and co-workers *via* electron paramagnetic resonance (EPR) [14]. Interestingly, they found that the level of free radicals detected *via* EPR spectroscopy correlated with metabolic activity, in alignment with previous hypothesis that suggested that free radicals may be involved in biological oxidation-reduction reactions. These findings inspired Harman to propose the *free radical theory of aging*, after observing that irradiation of living organisms induced mutations, cancer and aging, speculating that the irradiation drove the liberation of free radicals, specifically hydroxyl radicals, that caused aging [15]. Given that the concentration of free radicals increased with increasing metabolic activity, Harman suggested that hydroxyl radicals may arise from the utilization of oxygen by respiratory complexes that contain iron centers in the electron transport chain. Not long after, xanthine oxidase, an enzyme capable of generating superoxide radicals and reducing cytochrome c, was identified and characterized [16].

A decade later, in 1969, Mc Cord and Fridovich contributed to the understanding of free radical metabolism with the seminal discovery of a novel enzymatic activity for erythrocuprein, a Cu-containing enzyme found in erythrocytes. They found that erythrocuprein catalytically disproportionates superoxide into hydrogen peroxide to protect against superoxide toxicity [17], corresponding to the first description of a superoxide

dismutase. Erythrocuprein is now commonly known as Cu/Zn superoxide dismutase or Sod1. The high abundance of superoxide dismutase detected across different animal tissues, led them to propose that superoxide dismutase may have a vital role in protecting the organism against superoxide toxicity. Later findings, including that reactive oxygen species (ROS) arise from cellular respiration [18, 19] and that ROS include radical and non-radical oxygen species [20] set the stage for the multitude of findings that contribute towards understanding the role of ROS in physiology and disease.

1.2.2. Superoxide Radicals

Superoxide is a negatively charged free radical formed *via* single electron reduction of oxygen. It is not very reactive by itself [21], however, its harmful effects arise from the secondary ROS species generated as a consequence of superoxide-dependent reactions. For instance, superoxide radicals ($O_2^{\bullet-}$) oxidatively inactivate [4Fe-4S] clusters in enzymes, by univalently oxidizing the cluster, which perturbs its stability and results in degradation and release of a ferrous iron atom (Fe^{2+}). The released ferrous iron, which overwhelm the Fe detoxification systems in the cell, generates hydroxyl radicals ($^{\bullet}OH$) *via* the Fe-catalyzed reduction of H_2O_2, i.e., Haber-Weiss and Fenton reactions. $^{\bullet}OH$, is a very strong univalent oxidant that non-selectively reacts at diffusion-limited rates with most biomolecules that are in close proximity, including DNA, lipids and proteins. As a consequence, superoxide build-up induces DNA double strand (ds) breaks and mutations, lipid peroxidation causing membrane fragmentation and protein carboxylation that results in protein degradation and inactivation [1]. Moreover, the inactivation of [4Fe-4S] cluster- containing enzymes in the cytosol, i.e., isopropyl malate isomerase, and the mitochondria, i.e. aconitase, ultimately impacts cell metabolism. For instance, in baker's

yeast, oxidative inactivation of Fe-S clusters in homoaconitase and isopropylmalate isomerase leads to lysine and leucine auxotrophy, respectively. Notably, endogenous superoxide is unlikely to be toxic to cells, since these phenotypes are only observed when cells are devoid of superoxide dismutases (SOD). Although cells generate $O_2^{\bullet-}$ at a high rate, i.e. 5μM/s in *E. coli*, SODs, which disproportionate superoxide to H_2O_2 very efficiently, maintain very low steady-state levels of $O_2^{\bullet-}$, at only 0.1nM [22].

Superoxide is largely generated in the mitochondrial electron transport chain (ETC) as a result of aerobic metabolism [3], and its production is practically proportional to physiological [O_2] within the cell [23, 24]. Leakage of electrons from Complex I, predominantly, and Complex III in the ETC, generates superoxide radicals upon reduction of molecular O_2, especially when the mitochondria is not actively producing ATP via respiration [3, 25]. Accidental electron leakage supports the notion that superoxide is toxic; however, enzymes capable of producing superoxide support its potential role as a signaling molecule. NADPH oxidases (NOX) are transmembrane enzymes that generate superoxide by transferring electrons from NADPH to oxygen and account for a major source of cellular superoxide, especially after some stimuli. Although superoxide is unlikely to be a signaling molecule, due to its intrinsic low stability and solubility, it can be disproportionated spontaneously or by Sod1, at a very fast rate, to H_2O_2 in the vicinity of its generation site. H_2O_2, which is fairly stable, lasting up to 1ms, is a signaling molecule that exhibits high reactivity towards thiols in cysteine residues of target proteins and regulates their activity *via* cysteine oxidation.

1.2.3. Hydrogen Peroxide: Friend or Foe?

Hydrogen peroxide is a cytotoxic molecule due to its reactivity towards ferrous iron, that results in the generation of the highly cytotoxic ROS, hydroxyl radical, which readily reacts with DNA, proteins and lipids and oxidizes them. This yields DNA double strand breaks, protein carbonylation and membrane fragmentation, respectively [26].

Although initially perceived as a toxic molecule, over the last two decades enough evidence has been compiled to prove that H_2O_2 can also function as a signaling molecule. What makes H_2O_2 recognized as a signaling messenger? Mainly, it is intrinsically stable (up to 1ms) and reactive towards cysteine thiols on redox-regulated proteins [27]. Moreover, given that H_2O_2 is a non-charged species, it can diffuse freely through membranes, or *via* aquaporins [28, 29]. This allows H_2O_2 to easily diffuse throughout the cell, where, as a result of the disparate compartmentalization of antioxidant enzymes across different organelles, will elicit distinct responses in each cellular compartment.

How does H_2O_2 act as a signaling molecule? H_2O_2 reversibly oxidizes cysteine thiols yielding sulfenic acid (R-SOH), which is unstable and susceptible to nucleophilic attack by a neighboring cysteine thiol, potentially leading to disulfide bond generation. Alternatively, sulfenic acids can be further reversibly or irreversibly oxidized by additional H_2O_2 molecules to sulfinic ($R\text{-}SO_2H$) and sulfonic acid ($R\text{-}SO_3H$), respectively. Redox switches, which encompass reversible oxidation of thiols, especially active site thiols, regulate protein activity, stability and localization, consequently turning on/off signaling pathways. Some of the elucidated H_2O_2-dependent cellular processes include growth factor signaling pathways [30-32], proliferation [33, 34], metabolic switches [35], gene expression [36-38], apoptosis [39], cell migration [40] and cell morphology regulation [41].

The cytosolic H_2O_2 concentrations are estimated to be between 1-10nM [42] and can transiently rise up to 0.5-0.7μM during redox signaling events [43]; this physiological

oxidative stress is referred to as *oxidative eustress* [42, 44, 45]. Yet, concentrations above 1μM promote *oxidative distress*, favoring cellular oxidative damage, cell growth arrest and potential cell death [46, 47]. Interestingly enough, concentrations of H_2O_2 are rather constant across life domains, hinting conserved redox switches, as well as similar susceptibility to oxidative stress when exposed to higher concentrations of H_2O_2.

Even though H_2O_2 exhibits high reactivity towards many substrates, especially the higher the concentration is inside the cell, its concentration is tightly regulated by multiple enzymes that reduce and disproportionate H_2O_2 to H_2O, including peroxiredoxins and catalases, respectively. Peroxiredoxins are very abundant thiol peroxidases, accounting for 1% of total soluble protein, that exhibit high reactivity towards peroxide (with second rate constants spanning between 10^5-10^8 $M^{-1}s^{-1}$ [48]). Nonetheless, cysteine thiols in redox regulated proteins are much less numerous in the cell and exhibit second rate constants towards peroxide of 10-100 $M^{-1}s^{-1}$. How can redox regulated protein thiols get oxidized in a sea of peroxide scavenging enzymes? [49]. This may be explained by cellular spatio-temporal concentrations of H_2O_2 in close vicinity of the target redox-regulated protein. On one hand, H_2O_2 can be generated at close vicinity of the redox regulated protein bypassing any H_2O_2 competitors; or peroxiredoxins, although competing with the target protein for peroxide, may deliver redox equivalents, once oxidized, via transient intermolecular disulfide exchange [36, 50, 51]. This is known as a *redox relay* (**Figure 1.2**, left). Alternatively, local bursts of H_2O_2 may lead to transient overoxidation and inactivation of peroxiredoxins, facilitating a transient spatio-temporal rise in H_2O_2 concentration, that allows H_2O_2 to reversibly oxidize the cysteinyl of the target protein. This process is known as the *floodgate effect* [52] (**Figure 1.2**, right). These two plausible mechanisms are not necessarily mutually exclusive and likely explain redox signaling *in vivo*.

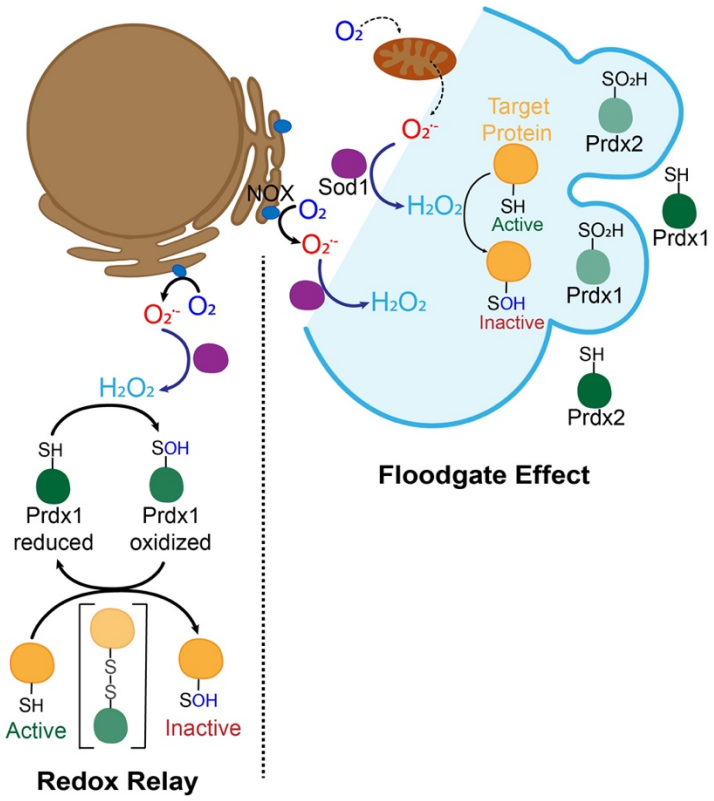

Figure 1.2. Redox signaling mechanisms. Floodgate effect (right) vs redox relay (left). Sod1, Cu/Zn superoxide dismutase; Prdx1, peroxiredoxin 1; Prdx2, peroxiredoxin 2; NOX, NADPH oxidase.

The necessity for spatio-temporal bursts of peroxide for physiological redox signaling, requires superoxide generation at close vicinity. The main sources of cellular superoxide are mitochondrial respiration and NADPH oxidases (NOX), membrane tethered enzymatic sources of superoxide [53]. NOX are widely distributed throughout the cell, distinctly turning on individual redox relays adjacent to specific compartments [54, 55]. There are several elucidated mechanisms that illustrate how superoxide and hydrogen peroxide work in synchrony to elicit a redox signaling relay. For instance, upon cellular exposure to growth factors or other signals, plasma membrane NOX are turned on and subsequently yield superoxide generation extracellularly, that can be disproportionated to H_2O_2 outside the cell by Sod3 or inside the cell after influx, through the chloride channel-3 [56], by Sod1.

The intracellular H_2O_2 can oxidize target cysteine thiols to initiate redox signaling cascades [57], such as induction of EGFR dimerization and activation [30].

Why are only unique cysteine thiols oxidized by hormetic concentrations of H_2O_2? The microenvironment of the cysteine thiolate may dictate its reactivity towards peroxide. This includes local polarity and neighboring amino acids that influence the redox potential and lower the thiol pK_a, whereby the thiolate form is favored at neutral pH, enhancing its susceptibility to be oxidized by H_2O_2.

However, due to the lack of tools to efficiently measure intracellular concentrations of H_2O_2, there is still little understanding on how spatio-temporal bursts are triggered and what are the sources of peroxide that promote each redox signaling pathway. Most of the studies to this day rely on the addition of exogenous and possibly physiologically irrelevant concentrations of peroxide that elicit responses that may not occur under hormetic H_2O_2 concentrations. Therefore, it is necessary to identify where peroxide arises from to understand how each redox relay is regulated. Given that Sod1 is a major enzymatic source of peroxide in most organisms and human cell types, my thesis work has provided new insight into Sod1-dependent physiological redox relays, which will influence how we perceive physiological redox signaling.

1.3. Superoxide Dismutases

Superoxide dismutases catalyze the disproportionation of two superoxide anions into hydrogen and molecular oxygen and comprise the cellular frontline defense against superoxide toxicity. SODs are unique, compared to the rest of antioxidant enzymes, in that they protect against one type of ROS, superoxide, and generate another ROS species, hydrogen peroxide, as a byproduct. Although peroxide generation was perceived as an incidental reaction and neglected by most, recent work is starting to shed light on the physiological significance of SOD catalyzed H_2O_2. In particular, my thesis work has vastly contributed on how we perceive SODs, concretely Cu/Zn superoxide dismutase.

SODs disproportionate superoxide at diffusion-limited rates, achieved *via* electrostatic guidance towards a transition metal that facilitates superoxide disproportionation. There are three different classes of SODs that exhibit different protein folding patterns and catalytic metal ions, including the Cu/Zn SOD, also known as Sod1 or Sod3, MnSOD/FeSOD and NiSODs. Most eukaryotes express two intracellular superoxide dismutases, a Manganese-containing SOD (MnSOD, Sod2) that is exclusively localized in the mitochondrial matrix, and a Copper/Zinc SOD (Cu/ZnSOD, Sod1) that is localized virtually everywhere in the cell, including the cytosol, mitochondrial intermembrane space (IMS), endoplasmic reticulum (ER), nucleus and peroxisomes. Additionally, humans express a third extracellular Cu/Zn SOD, Sod3 [58-60]. Regarding MnSOD or Sod2, it has recently been found that in eukaryotes a fraction of Sod2 can acquire Fe instead of Mn [61] when Sod2 is exposed to high iron concentrations [62, 63] or when Sod2 is acetylated at lysine residues 68 and 122 [64, 65]. This Fe-bound Sod2 fraction is either inactive [62] or exhibits peroxidase activity, instead of dismutase activity, associated with several physiological consequences that are starting to be discerned, such as stem cell reprograming and tumorigenesis [64, 65].

Iron SOD (FeSOD) and MnSOD appear to have a common ancestor, however, they have diverged so much that in most species the metals cannot functionally substitute each other. While FeSOD is found in plant plastids, bacteria and in primitive eukaryotes, MnSOD is found in most eukaryotes, exclusively in the mitochondria, and some bacteria [66, 67]. However, there are some bacterial species that express a cambialistic SOD, which can interchangeably use Fe or Mn for catalysis [68, 69].

Nickel SOD (NiSOD) is the most recently characterized SOD, and was identified in *Streptomyces* [70, 71] and cyanobacteria [72]. Bioinformatic analysis suggest that NiSOD is not only found in actinobacteria from marine and soil environments, but also in proteobacterial species, that include pathogenic species, such as chlamydia [67, 73].

Given that my thesis work is fixated on eukaryotic Sod1 or Cu/Zn superoxide dismutase, I will focus the next sections on Sod1 biology and its roles in physiology.

1.3.1. Cu/Zn Superoxide Dismutase (SOD1): More than a Superoxide Scavenger

Sod1 is a highly conserved, from bacteria to humans, and abundant protein that accounts for ~80-90% total SOD cellular activity, in yeast and a wide arrange of human cell types, and approximately 1% total soluble protein, corresponding to a concentration of ~10-40μM in most mammalian cell lines [57, 74, 75]. Sod1, unlike the rest of SODs, is localized virtually everywhere in the cell, including the intermembrane space of the mitochondria (IMS), nucleus, cytosol and peroxisomes, except the mitochondrial matrix where Sod2 resides. Sod1 is a homodimeric protein, with each monomer bound to a copper and zinc ions, [76, 77] essential for catalysis, that encompasses disproportionation of two superoxide molecules into hydrogen peroxide and molecular oxygen.

The importance of this enzyme for aerobic life has been demonstrated in several model organisms; ablation of *SOD1* in *E. coli*, yeast, drosophila [78] and mice [79, 80] results in several hallmarks of oxidative stress. For instance, *SOD1*$^{-/-}$ mice show higher incidences of hepatocellular carcinoma and signs of considerable oxidative damage at early stages of life (3 months of age) [80], which is also translated into a shorter life span. Similarly, *SOD1*-deficient *Drosophila* mutants exhibit increased spontaneous DNA damage and are unable to tolerate DNA-repair defective mutations, in addition to reduced lifespan and infertility [78]. Also, baker's yeast strains that lack *SOD1* (*sod1*Δ) are defective in lysine and methionine biosynthetic pathways and show several markers of oxidative stress, including protein carbonylation, degradation of Fe/S clusters in enzymes and DNA damage (**Figure 1.3**) [81, 82]. The phenotypes observed in cells devoid of *SOD1* are due to superoxide toxicity, which can oxidize iron-sulfur cluster ($[4Fe\text{-}4S]^{2+}$) cofactors in proteins and release of ferrous iron (Fe^{2+}) in the process. Therefore, the hallmarks of superoxide toxicity in yeast include amino acid auxotrophy due to inactivation of 4Fe/4S cluster enzymes, including aconitase or homoaconitase and isopropyl malate isomerase, the inactivation of which causes Lysine and Leucine auxotrophy, respectively. Also, yeast *sod1*Δ exhibit methionine auxotrophy due to NADPH depletion. The Ferrous iron released from the oxidation of 4Fe/4S cluster can reduce H_2O_2 to generate hydroxyl radicals *via* Fenton chemistry, a highly reactive species that oxidizes and damages DNA and membrane lipids. The requirement for Sod1 in aerobic cultures is also supported by the high rate at which *sod1*Δ yeast exhibit suppressor mutations, including suppressor mutations at the *PMR1* locus that rescue most oxygen toxicity phenotypes, which confer an enhanced aerobic growth advantage [83].

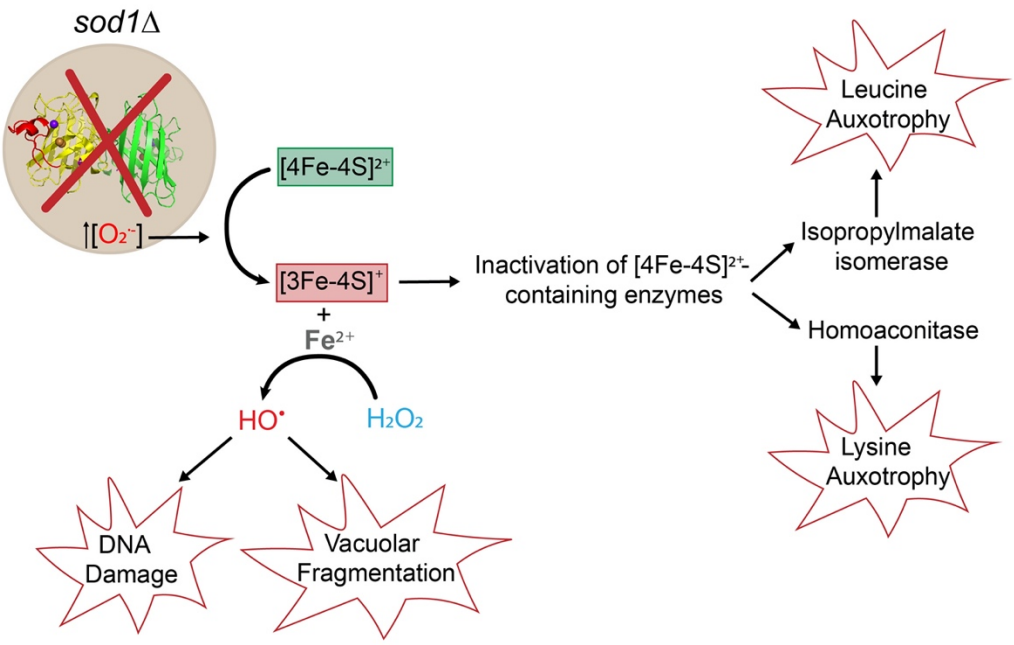

Figure 1.3. Schematic representation of *SOD1* null yeast (*sod1*Δ) characteristic phenotypes due to superoxide build-up.

SODs are unique antioxidant enzymes in that they protect against one ROS, $O_2^{\bullet-}$, to generate another one, H_2O_2. Given that Sod1 is so abundant and ubiquitous, that it disproportionates superoxide at a diffusion-limited rate (10^9 $M^{-1}s^{-1}$), and that superoxide itself can be spontaneously disproportionated at a relatively fast rate (10^5 $M^{-1}s^{-1}$), there may be an additional requirement for Sod1. Besides superoxide protection, Sod1 may promote hormetic H_2O_2 levels to support certain redox relays in signaling pathways. During my thesis, I have put my efforts in understanding the relative contribution of Sod1 between superoxide protection and spatio-temporal H_2O_2 generation to promote redox signaling.

1.3.1.1. SOD1 Structure and Maturation

Sod1 is a homodimeric and relatively small protein, with each monomer bound to a copper and zinc ions (**Figure 1.4**). The copper ion, required for catalysis, is coordinated by four or three histidine residues, depending on the Cu oxidation state, and lies at the base of the electrostatic loop, where catalysis takes place [84-86]. Zinc, which is coordinated by three histidine residues and one aspartate, not only provides structural stability [87], but also increases the redox potential of the catalytic Cu (II) ion [77, 88].

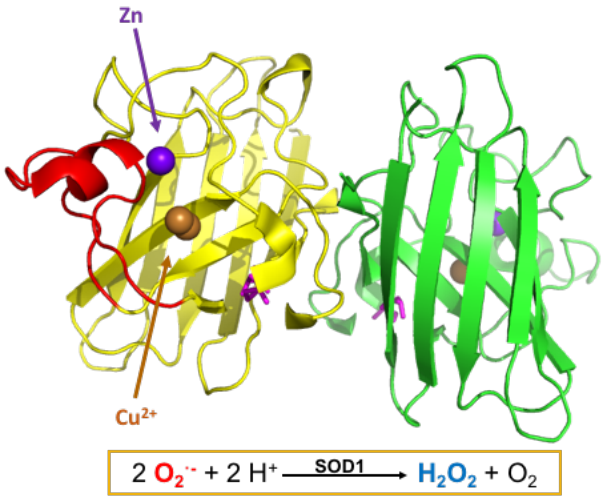

Figure 1.4. Cu/Zn Superoxide dismutase (Sod1) structure and reaction equation. Crystal structure of Sod1 homodimer (PDB ID 2C9V). The two monomers are represented in green and yellow and the zinc (Zn) and copper (Cu) ions are represented in purple and gold, respectively.

Nascent Sod1 is monomeric and inactive and requires the copper chaperone Ccs1 to be converted to its active homodimeric form, where each monomer is forming a disulfide bond between cysteine residues 57 and 146. Yeast Sod1 (ySod1) is entirely dependent on Ccs1 for maturation and activity [89], except when the culture medium is supplemented with exogenous copper [90]. Likewise, *Drosophila melanogaster* devoid of Ccs1 do not exhibit Sod1 activity and are sensitive to oxidative stress [91]. However, expressing

human Sod1 (hSod1) in *ccs1*Δ yeast results in ~ 25% Sod1 activity, due to the ability of a subset of hSod1 to acquire copper independently of Ccs1 and oxygen [92, 93]. This is also true for Sod1 from various metazoans, all lacking a proline residue at the position 144. The two major differences between Ccs1 dependent and independent pathways are the requirement for copper availability and molecular oxygen [93, 94]. According to this, Ccs1 requires copper for Sod1 disulfide bond formation, whereas Ccs1-independent Sod1 disulfide formation can take place even under copper depleted conditions. Moreover, the non-requirement for molecular oxygen allows metazoans to retain Sod1 activity over a wide range of pO_2, to fit their molecular complexity [93, 95]. How does hSod1 acquire copper independently of Ccs1 and O_2? The mechanism is still unclear, although it is known that this auxiliary pathway requires glutathione (GSH) for copper delivery to Sod1 and is dependent on the presence of non-proline residues at positions 142 and 144. Conversely, yeast Sod1 contains proline residues at positions 142 and 144 (P142, P144), located at the C-terminus of Sod1, which may facilitate Ccs1-dependent copper acquisition by limiting the flexibility of the protein. And, given they are juxtaposed to Cys-146 of Sod1 critical disulfide, they might also affect the pKa of the cysteine residues whereby the disulfide is less prone to oxidation [92, 93]. Interestingly, mutating P144 of ySod1, can switch ySod1 to a Ccs1-independent molecule [93].

Ccs1 is composed of three domains: D1, which contains a *MXCXXC* copper-binding domain that acquires Cu(I) from the copper transporter Ctr1; D2, a domain with high sequence and structural analogy to Sod1 that facilitates the interaction with immature Sod1 at the homodimeric interface [96, 97]; and D3, the C-terminus domain that contains a *CXC* motif, essential for Sod1 activation [98]. The mechanism by which Ccs1 forms active metallated Sod1 involves all Ccs1 domains. First, Ccs1 D3 domain interacts between the disulfide beta barrel and the electrostatic loop of Sod1 to expose the electropositive cavity, followed by the delivery of Cu(I) from D1 to the entry site, where

superoxide radicals are concomitantly attracted to, promoting Cu (I) oxidation to Cu (II) and H_2O_2 formation. H_2O_2 oxidizes Sod1 Cys-146, yielding sulfenic acid, that subsequently forms an intermolecular disulfide bond with Ccs1 Cys229, followed by a disulfide exchange reaction between Sod1 Cys146 and Cys57, yielding mature Sod1, terminating Ccs1-Sod1 interaction [99].

1.3.1.2. Sod1 Localization

While Sod2 is exclusively confined to the mitochondrial matrix, Sod1 is widely spread throughout the cell, including the cytosol, mitochondrial intermembrane space (IMS) [7, 100], peroxisomes [101], lysosomes [102], ER [103, 104] and nucleus [74, 105].

Although previously thought to be primarily cytosolic, a fraction of Sod1 is localized in the IMS, as observed in yeast [7] and mammalian cell lines [6]. The accumulation of Sod1 in the IMS is highly dependent on its copper chaperone, Ccs1, also partitioned between the cytosolic and mitochondrial pools [7]. Although the regulatory mechanisms behind Sod1 partitioning between the two compartments have only begun to unravel, it is conceivable that the fraction of Sod1 metallated by cytosolic or mitochondrial Ccs1, which prevents mitochondrial import or export, respectively, is an evident contributor. Ccs1 and Sod1 are imported through the translocator of the outer membrane (TOM) in its apo form and once in the IMS, upon intermolecular disulfide bond with Mia40, Ccs1 forms its intramolecular disulfide bond that traps it in the IMS. Mia40 is subsequently reoxidized by the sulfhydryl oxidase, Erv1, which relies on active mitochondrial respiratory chain to function [106-108]. Imported apoSod1 interacts with oxidized Ccs1, promoting the formation of Sod1 intramolecular disulfide bond and its retention in the IMS.

What is the physiological function of Sod1 in the mitochondrial IMS? Complex I, not present in yeast, and complex III of the respiratory electron transport chain can leak

electrons to the IMS yielding superoxide formation upon oxygen reduction [109, 110]. Mitochondrial Sod1 may prevent mitochondrial $O_2^{\bullet-}$ from exiting the mitochondria and damaging extramitochondrial cell components [7, 111]. Indeed, my thesis work has shown that expressing IMS-targeted Sod1 is sufficient to protect against cell-wide markers of superoxide toxicity in yeast [112].

1.3.1.3. Sod1 Post-Translational Modifications

The intricate regulation of Sod1 *via* post-translational modifications (PTMs) that dynamically regulate both its location and activity, suggests that the role of Sod1 may be more significant than just protecting against superoxide toxicity.

In yeast and human cells, it was found that in response to high concentrations of H_2O_2, the cell cycle checkpoint regulating Mec1/ATM effector Dun1/Cds1 kinase phosphorylates Sod1 at residues Serine 60 and 99 to induce Sod1 nuclear import to regulate oxidative stress resistance and repair gene expression. This hints a potential novel non-canonical function of Sod1 as a transcription factor [105]. Sod1 has been additionally found to be phosphorylated at Serine 39 in yeast or Threonine 40 in human cell lines by the nutrient sensing mTORC1 in response to nutrient availability to inactivate Sod1 [113]. These findings show that mTORC1 intricately regulate redox homeostasis *via* Sod1 in response to nutrient availability. Besides phosphorylation, Sod1 is also found to be acetylated at lysine 122 (K122), partially regulated by SIRT5, which regulates its partitioning between the mitochondrial IMS and the cytosol, affecting respiratory *vs.* fermentative energy metabolism, as a consequence [114, 115].

Besides the aforementioned described PTMs, there are many other identified PTMs in human Sod1 [114], however, the consequences of such PTMs are still enigmatic

or only starting to unfold. These PTMs add a layer of complexity to Sod1 biology and are imperative to perceive spatio-temporal Sod1 catalyzed H_2O_2 signaling.

1.3.1.4. Sod1: A Pivotal Mediator of Cell-wide Redox Signaling

As described above, loss of *SOD1* in model organisms evokes oxidative damage resulting in reduced lifespan and carcinogenesis. Besides oxidative damage, perturbation of Sod1-dependent redox relays, required for cell physiology, may also contribute towards the observed phenotypes.

Sod1 comprises a major source of peroxide that is spread throughout the cell. As such, it is conceivable that it may promote cell-wide redox signaling relays. However, until recently, very little was known about the relative contributions of Sod1 between superoxide protection and redox signaling. My thesis work has significantly contributed on how we perceive Sod1 in biology, since we have found that less than 1% of total Sod1 is required for superoxide protection in yeast, and that this miniscule fraction is localized in the mitochondrial IMS. Instead, large amounts of extracellular Sod1 are required for Sod1-dependent redox relays [112]. This was further demonstrated in mammalian cell lines, showing that while loss of a large fraction of Sod1 does not induce oxidative stress or affect cell proliferation; the bulk of Sod1 is required to promote the canonical Wnt signaling pathway, and Wnt-induced cell proliferation. Moreover, my later work has identified a novel Sod1-dependent redox relay by which Sod1 integrates oxygen availability to inactivate GAPDH and promote the pentose phosphate pathway to generate NADPH, a vital cell reductant that promotes reduction and regeneration of antioxidant systems, such as peroxiredoxins. Altogether, my findings recognize Sod1 as a master regulator of the cellular redox landscape by being a direct source of H_2O_2 to oxidize thiols and by promoting NADPH/$NADP^+$ redox balance to facilitate reversible redox signaling.

To this day there has been several studies that prove Sod1 to be a key contributor of a great variety of redox signaling pathways. According to this, Sod1 catalyzed H_2O_2 has been shown to integrate glucose and oxygen availability to repress respiration [35], promote growth factor activation [116], tyrosine phosphatase inactivation [31], transcription of antioxidant genes [105], cell proliferation [117] and differentiation. For instance, Sod1-catalyzed H_2O_2 promotes proliferation by favoring Epidermal Growth Factor Receptor (EGFR) dimerization and activation *via* reversible oxidation of an active cysteine thiol. This response is further amplified, due to the ability of a privileged pool of Sod1-derived H_2O_2 to oxidize the active site cysteine thiol in the protein tyrosine phosphatase (PTP1B) and inactivate it, preventing it from inactivating EGFR [31, 116]. This makes Sod1 a potential oncogene, however, its antioxidant capacity would posit it as a tumor suppressor. What role does Sod1 play in cancer, then? We are still far away from a definite answer, but something is clear, multiple cancer types rely on Sod1 [118], therefore, Sod1 is a potential therapeutic target to suppress carcinogenesis. In fact, multiple Sod1 inhibitors have been proven effective in promoting cancer cell apoptosis and growth arrest [117, 119-121]. It is conceivable, however, that untargeted Sod1 inhibition may result in disruption of redox signaling pathways and redox homeostasis in healthy tissues. Our work has also shown that Sod1 regulates the prooncogenic Wnt signaling pathway, which further poses Sod1 as a key protein in promoting carcinogenesis. For this reason, it is imperative that we understand the absolute contributions of Sod1 in redox signaling to perceive the advantages of inhibiting Sod1 in cancer treatment, as well as the contribution of Sod1 in the progression of other diseases, such as, familial amyotrophic lateral sclerosis (FALS) and metabolic diseases.

1.4. Scope of Thesis

In this dissertation I will describe our results on i) the discovery that extra-mitochondrial Cu/Zn superoxide dismutase is dispensable for superoxide protection but required to mediate peroxide signaling in *Saccharomyces cerevisiae*, ii) the finding that a small fraction of Sod1 is required for oxidative stress protection, but the bulk of Sod1 regulates the canonical Wnt signaling pathway in human cell lines and iii) the role of Sod1 in integrating oxygen availability to redox regulate NADPH production and the thiol redoxome.

In Chapter 2, I will describe our published work in which we find that most of the superoxide scavenging enzyme Cu/Zn superoxide dismutase (Sod1) is dispensable for superoxide protection using *Saccharomyces cerevisiae* as a model organism. According to this, less than 1% of total Sod1 is sufficient to rescue cell-wide markers of superoxide toxicity. Moreover, we found that this minuscule necessary fraction is localized in the mitochondrial intermembrane space. Instead, large quantities of extramitochondrial Sod1 are required for redox control of Yck1 signaling. The findings exposed in this chapter force us to re-evaluate the physiological role of bulk Sod1, proposing that eukaryotes express high levels of Sod1 to promote redox signaling.

In Chapter 3, I will lay out the recently accepted work led by Dr. Bindu Chandrasekharan in which we found that Sod1 regulates casein kinase gamma (CK1γ) expression in human embryonic kidney 293 (HEK293) cells and that it is required for canonical Wnt signaling and Wnt-dependent cell proliferation. Moreover, we find that the requirement of a minuscule fraction of Sod1 for superoxide protection versus the bulk of Sod1 for redox signaling is conserved from yeast to mammalian cell lines.

In Chapter 4, I will present our latest, soon to be published, findings in which, using *Saccharomyces cerevisiae* and mammalian cell lines, we discovered that a major new aspect of Sod1 antioxidant function is to integrate oxygen (O_2) availability to promote NADPH production to sustain life in air. In detail, Sod1 senses O_2 *via* $O_2^{\bullet-}$ from mitochondrial respiration and a yeast NADPH oxidase, Yno1, to oxidatively inactivate the glycolytic enzyme glyceraldehyde phosphate dehydrogenase (GAPDH), *via* Sod1-catalyzed H_2O_2. This in turn re-routes the carbohydrate flux towards the oxidative phase of the pentose phosphate pathway (oxPPP), where most cellular NADPH is generated, necessary to support cellular antioxidant systems. We found that the aerobic oxidation of GAPDH is exclusively dependent and rate-limited by Sod1. Moreover, using mass spectrometry we identified proteome-wide targets of Sod1-dependent redox signaling. Our findings in this chapter confers a new perception on the antioxidant role of Sod1 and posits Sod1 as a master regulator of metabolism and the thiol redoxome.

Lastly, in Chapter 5 I will present the conclusions of my work and some future directions. I will discuss the implications of my new findings on how we perceive Sod1 and redox signaling in biology and will lay out future experiments that will contribute towards elucidating additional Sod1-catalyzed H_2O_2 redox relays and better understanding its implication in physiology and pathology.

In short, the findings presented in this thesis indicate that the role of Sod1 in cell biology is much broader than just superoxide protection and provide a bright new perception of Sod1 in physiology and redox signaling.

CHAPTER 2

Extra-mitochondrial Cu/Zn-Superoxide Dismutase (Sod1) is Dispensable for Protection Against Oxidative Stress but Mediates Peroxide Signaling in *Saccharomyces cerevisiae*

This chapter is adapted from the previously published work: Montllor-Albalate, C., Colin, A. E., Chandrasekharan, B., Bolaji, N., Andersen, J. L., Outten, F. W., Reddi, A. R. “Extra-mitochondrial Cu/Zn-Superoxide Dismutase (Sod1) is Dispensable for Protection Against Oxidative Stress but Mediates Peroxide Signaling in *Saccharomyces cerevisiae*” *Redox Biology*. 21 (2019) 101064. The author of this document contributed to this work by conceiving, designing and performing most experiments of the paper, except detection of labile iron using EPR spectroscopy, enzyme assays (aconitase and isopropyl malate isomerase), TUNEL assay and vacuolar fragmentation analysis, making figures with help of the corresponding author and co-writing the manuscript with input from all authors.

2.1. Abstract

Cu/Zn Superoxide Dismutase (Sod1) is a highly conserved and abundant metalloenzyme that catalyzes the disproportionation of superoxide radicals into hydrogen peroxide and molecular oxygen. As a consequence, Sod1 serves dual roles in oxidative stress protection and redox signaling by both scavenging cytotoxic superoxide radicals and producing hydrogen peroxide that can be used to oxidize and regulate the activity of downstream targets. However, the relative contributions of Sod1 to protection against oxidative stress and redox signaling are poorly understood. Using the model unicellular eukaryote, Baker's yeast, we found that only a small fraction of the total Sod1 pool is

required for protection against superoxide toxicity and that this pool is localized to the mitochondrial intermembrane space. On the contrary, we find that much larger amounts of extra-mitochondrial Sod1 are critical for peroxide-mediated redox signaling. Altogether, our results force the re-evaluation of the physiological role of bulk Sod1 in redox biology; namely, we propose that the vast majority of Sod1 in yeast is utilized for peroxide-mediated signaling rather than superoxide scavenging.

2.2. Introduction

Superoxide ($O_2^{\bullet-}$) and hydrogen peroxide (H_2O_2) are cytotoxic reactive oxygen species (ROS) that are also essential for the redox control of a multitude of physiological processes. $O_2^{\bullet-}$ toxicity is largely due to its ability to oxidize and inactivate [4Fe-4S] cluster-containing enzymes, which releases iron (Fe) in the process [26, 57, 122, 123]. The liberated Fe, upon complexation by appropriate ligands, promotes deleterious redox reactions, and in particular produces hydroxyl radicals ($^{\bullet}OH$) via the Fe-catalyzed reduction of H_2O_2 *i.e.* Haber-Weiss and Fenton reactions [123, 124]. Once formed, $^{\bullet}OH$ indiscriminately oxidizes lipids, proteins, and nucleic acids, leading to membrane disruption, protein misfolding and aggregation, and DNA fragmentation, respectively. While $O_2^{\bullet-}$ itself is not likely to be a signaling molecule [125], it rapidly disproportionates into H_2O_2 ($k \sim 10^5\ M^{-1}\ s^{-1}$ at pH = 7.0), a well-established signaling molecule [125, 126], that can lead to the reversible oxidation of cysteine residues in a number of downstream targets[127], including phosphatases [31, 128, 129], kinases [30, 130], metabolic enzymes [131], and transcription factors [132, 133], to regulate protein activity.

The dual roles of $O_2^{\bullet-}/H_2O_2$ in oxidative stress and redox signaling necessitates that the concentration and localization of these ROS are regulated in a manner that

enables signaling but mitigates oxidative damage. In terms of localization, a number of metabolic sources of H_2O_2 and $O_2^{\bullet-}$ are present throughout the cell, including $O_2^{\bullet-}$-generating NADPH oxidases (NOX) that have been found in the nucleus, endoplasmic reticulum (ER), cell membrane, and mitochondria [54, 134], mitochondrial respiratory Complexes I and III [135-137], and enzymes that release $O_2^{\bullet-}$ and/or H_2O_2, *e.g.* xanthine oxidase (cytosol) [138, 139], monoamine oxidase (mitochondria) [140], cytochrome P450's (ER) [141], and globins (cytosol) [142, 143]. In terms of concentration, detoxification systems have evolved to limit the levels of $O_2^{\bullet-}$, *e.g.* superoxide dismutases (SODs), and H_2O_2, *e.g.* catalase (CAT), glutathione (GSH) peroxidases (GPx), and peroxiredoxins (Prx) [144]. Of these ROS scavenging systems, SODs, which catalyze the disproportionation of $2O_2^{\bullet-}$ into H_2O_2 and O_2, are unique in that they simultaneously affect both [$O_2^{\bullet-}$] and [H_2O_2]. As a consequence, SODs play dual roles in both defending against $O_2^{\bullet-}$ toxicity and regulating H_2O_2-mediated redox signaling [57, 144].

Most eukaryotes express two intracellular SODs, a Mn-containing SOD2 that is exclusively localized to the mitochondrial matrix [145], and a highly abundant Cu/Zn SOD1 that is present virtually everywhere else [17], including the mitochondrial intermembrane space (IMS) [100, 146], nucleus [147], endoplasmic reticulum (ER) [148], and peroxisomes [149]. SOD1-deficient organisms, from yeast to mice, are oxidatively stressed and have reduced life spans. For example, SOD1-/- mice have a higher incidence of liver cancer, neuronal damage, and loss of muscle mass [80, 150-154]. Drosophila mutants of SOD1 are infertile and have dramatically reduced life spans [155]. In *Saccharomyces cerevisiae* (Baker's yeast), *sod1*Δ cells have defects in a number of metabolic pathways due to oxidative damage of critical [4Fe-4S] cluster containing enzymes [124, 156-158], as well as membrane and DNA fragmentation [147, 158, 159] due to increases in "free" or labile iron [160, 161], which promote hydroxyl radical formation

[124]. In total, cell biological and biochemical studies across multiple organisms indicate Sod1 protects Fe-S cluster enzymes from $O_2^{\bullet-}$ damage and further oxidative stress due to Fe and $^{\bullet}OH$ toxicity.

From the perspective of redox signaling, Sod1-derived H_2O_2 was found to regulate the oxidation of protein tyrosine phosphatases [31] and the tyrosine kinase growth factor receptor [116]. In addition, Sod1 was also found to provide a source of H_2O_2 that stabilizes a pair of plasma membrane casein kinases, Yck1 and Yck2, that control nutrient sensing and energy metabolism [35].

Sod1 is a highly abundant protein in various organisms [20, 162], and in yeast is present at concentrations of ~10-20 μM [163, 164], accounting for ~80-90% of total cellular Sod activity[165]. Given that Sod1 disproportionates $O_2^{\bullet-}$ at diffusion-limited rates ($k \sim 10^9$ $M^{-1}s^{-1}$)[166], the rationale for producing such large quantities of Sod1 has been enigmatic. Moreover, the relative contributions of Sod1 towards protection against $O_2^{\bullet-}$ toxicity and H_2O_2-mediated redox signaling are not well understood [57]. Herein, using Baker's yeast as a eukaryotic model, we find that only a small fraction of total Sod1 is required for protection against $O_2^{\bullet-}$ toxicity and that this pool is localized to the mitochondrial intermembrane space (IMS). Instead, we find that much larger amounts of extra-mitochondrial Sod1 are critical for peroxide-mediated redox control of Yck1 signaling. Given that an exceedingly small fraction of Sod1 is required for protection against $O_2^{\bullet-}$ and much larger quantities are seemingly required for peroxide-mediated redox signaling, our results challenge us to re-evaluate the physiological role of bulk Sod1. We propose that eukaryotes express high levels of Sod1 to maintain appropriate peroxide fluxes to facilitate redox signaling, whereas superoxide detoxification can be handled by a relatively miniscule amount of Sod1.

2.3 Results

2.3.1. The vast majority of Sod1 is dispensable for protection against superoxide toxicity.

In atmospheric oxygen (21% O_2), *sod1*Δ cells exhibit a number of markers of $O_2^{\bullet-}$ toxicity. This includes elevated [$O_2^{\bullet-}$] [167], $O_2^{\bullet-}$-mediated inactivation of a number of [4Fe-4S] enzymes [124, 158, 168], including aconitase (Aco1), isopropylmalate isomerase (Leu1), and homoaconitase (Lys4), increased labile Fe due to its release from oxidized Fe-S clusters [158, 160, 161], and vacuolar [159] and DNA [147] fragmentation due to deleterious Fe-mediated redox reactions. Collectively, these defects lead to reduced aerobic growth [165], decreased lifespan [169], and a number of metabolic defects, including perturbations to redox homeostasis [157], energy metabolism [35, 170] and a number of amino acid auxotrophies [124, 156-158], *e.g.* defects in the biosynthesis of leucine (due to inhibition of Leu1), lysine (due to inhibition of Lys4), and methionine (due to reduced pentose phosphate pathway activity and NADPH). Using the galactose-inducible *GAL1* promoter to drive *SOD1* expression in the background of *sod1*Δ cells, we sought to determine the amount of Sod1 required to rescue various cell-wide markers of oxidative stress. As shown in **Fig. 2.1a**, titration of galactose (GAL) resulted in undetectable (0.000 - 0.005% w/v GAL), intermediate (0.006% - 0.008% w/v GAL), and high (> .01% w/v GAL) levels of Sod1 expression and activity. Concentrations > 0.01% GAL consistently resulted in near WT-levels of Sod1 expression and activity. Most interestingly, only 0.005% GAL, a concentration that results in the induction of an undetectable amount of Sod1 activity and polypeptide (**Fig. 2.1a**), rescues major hallmarks of $O_2^{\bullet-}$ toxicity, including sensitivity to paraquat, a $O_2^{\bullet-}$-generating agent (**Fig. 2.1b**), lysine auxotrophy (**Fig. 2.1c**), the activity of mitochondrial and cytosolic [4Fe-4S]

cluster containing enzymes, Aco1 (**Fig. 2.1d**) and Leu1 (**Fig. 2.1e**), respectively, cellular [$O_2^{\bullet -}$] as measured by dihydroethidium (DHE) fluorescence (**Fig. 2.1f**), electron paramagnetic resonance (EPR)-detectable labile Fe pools (**Fig. 2.1g**), vacuolar fragmentation as imaged by FM4-64 (**Fig. 2.1h** and **i**), and DNA damage as assessed by terminal deoxynucleotidyl transferase (TdT)-mediated dUTP nick end labeling (TUNEL) (**Fig. 2.1j**). Parenthetically, it is important to note that at the excitation and emission wavelengths chosen to measure DHE fluorescence, there are contributions from both superoxide specific, *e.g.* 2-hydroxyethidium, and non-specific, *e.g.* ethidium or ethidium/ethidine dimers, DHE oxidation products [171]. Thus, while our DHE fluorescence measurements are not specific for superoxide per se, the differences in DHE fluorescence we observe reflect Sod1-dependent DHE oxidation products. Altogether, these results indicate that the vast majority of Sod1 is dispensable for protection against superoxide toxicity.

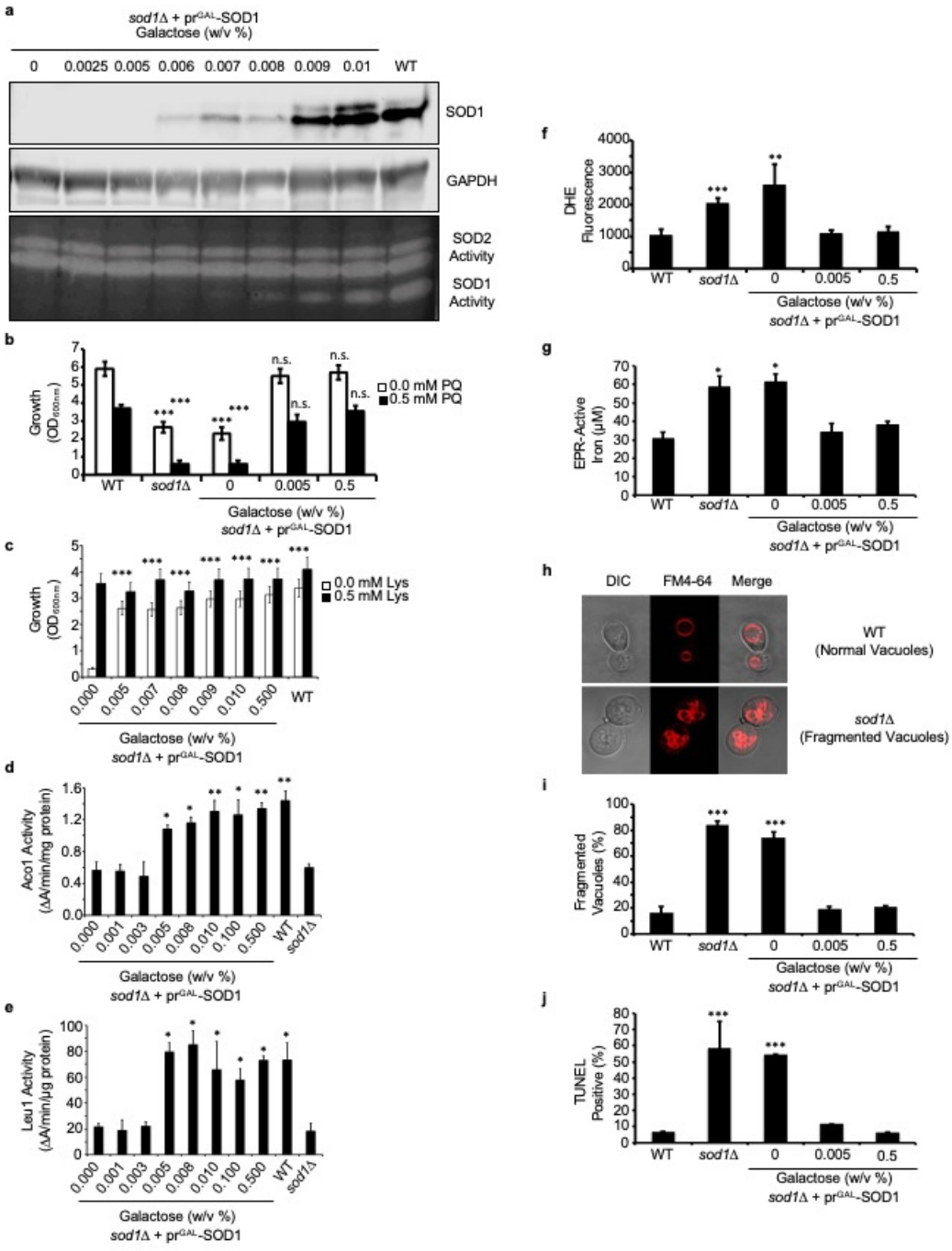

Figure 2.1. The vast majority of Sod1 is dispensable for protection against superoxide toxicity. (**a** and **b**) Titration of galactose (GAL) into cultures of sod1::*LEU2* (*sod1*Δ) cells expressing the *GAL1* driven Sod1 expression vector (pr^{GAL}-SOD1; pAR1026) results in the expression of low (≤ .005% GAL), intermediate (0.006% - 0.008% GAL), and high (≥ 0.009% GAL) expression and activity of Sod1. The immunoblots and activity gels depicted are representative of multiple trials across different batches of media. (**c**) Paraquat (PQ) sensitivity of WT and *sod1*Δ cells compared to *sod1*Δ + pr^{GAL}-SOD1 cells expressing none (0% GAL), low (0.005% GAL) or high (0.5% GAL) levels of Sod1 as

measured by solution turbidity. (**d**) Lysine (Lys) auxotrophy, (**e**) aconitase (Aco1) activity, and (**f**) isopropylmalate isomerase (Leu1) activity of *sod1*Δ + pr^{GAL}-SOD1 cells is measured as a function of Sod1 expression and compared to WT and/or *sod1*Δ cells. (**g**) Representative immunoblot and activity gel from a different batch of media showing the reproducibility of the low undetectable induction of Sod1 by 0.005% GAL in *sod1*Δ + pr^{GAL}-SOD1 cells. (**h**) DHE detectable superoxide was monitored in WT, *sod1*Δ, and *sod1*Δ + pr^{GAL}-SOD1 cells expressing none (0% GAL), low (0.005% GAL), or high (0.5% GAL) Sod1. (**i**) EPR detectable labile Fe, (**j** and **k**) FM4-64 visualized vacuolar fragmentation, and (**l**) DNA damage using the TUNEL assay was monitored in *sod1*Δ + pr^{GAL}-SOD1 cells expressing none (0% GAL), low (0.005% GAL), or high (0.5% GAL) Sod1. In panels **k** and **l**, approximately ~100 cells were counted from each culture condition in triplicate and scored for (**k**) having single or multiple fragmented vacuoles, as depicted in panel **j**, or (**l**) being non-fluorescent or fluorescent in the FITC channel. Error bars indicate the average ± s.d. of triplicate (**c**, **d**, **h**, **k**, **l**) or duplicate (**e**, **f**, **i**) cultures. The statistical significance relative to WT (**c**, **h**) or *sod1*Δ cells cultured with 0% GAL (**d**, **e**, **f**, **i**, **k**, **l**) is indicated by asterisks using a two-sample t-test. * $P < 0.05$, ** $P < 0.01$, *** $P < 0.001$, n.s. not significant.

2.3.2. IMS-targeted Sod1 is sufficient to protect against cell-wide markers of $O_2^{\bullet-}$ toxicity.

We next sought to determine if the localization of Sod1 is important for protection against cell-wide markers of superoxide toxicity. Mitochondria are a major source of ROS and $O_2^{\bullet-}$ due to electron leakage during cellular respiration, and in particular from Complex III, which can release $O_2^{\bullet-}$ into the mitochondrial matrix and IMS [135]. Deletion of Sod1, which is in-part localized to the mitochondrial IMS [100, 146], but not Sod2, which exclusively resides in the mitochondrial matrix, results in lysine auxotrophy due to the $O_2^{\bullet-}$-dependent inhibition of matrix-localized homoaconitase (Lys4). This suggests that $O_2^{\bullet-}$ leakage into the IMS occurs to a greater extent than into the matrix and the ultimate source of matrix $O_2^{\bullet-}$ is from the IMS. In order to determine the extent to which IMS-localized Sod1 protects against oxidative stress, including in the mitochondrial matrix, an allele of Sod1 that is exclusively targeted to the IMS, SOD1-IMS, due to fusion of the Sco2 IMS localization sequence [35, 172] was expressed in *sod1*Δ cells (**Fig. 2.2a**). Interestingly, we found that SOD1-IMS rescues cell-wide markers of $O_2^{\bullet-}$-toxicity, including paraquat

sensitivity (**Fig. 2.2b**), lysine auxotrophy (**Fig. 2.2c**), the activity of mitochondrial and cytosolic [4Fe-4S] cluster containing enzymes, Aco1 (**Fig. 2.2d**) and Leu1 (**Fig. 2.2e**), respectively, cellular [$O_2^{\bullet-}$] as measured by dihydroethidium (DHE) fluorescence (**Fig. 2.2f**), Phen Green-detectable labile Fe (**Fig. 2.2g**), vacuolar fragmentation as imaged by FM4-64 (**Fig. 2.2h**), and DNA damage as assessed by terminal deoxynucleotidyl transferase (TdT)-mediated dUTP nick end labeling (TUNEL) (**Fig. 2.2i**). The effects of SOD1-IMS on defending against $O_2^{\bullet-}$ toxicity are distinct from mitochondrial matrix localized Sod2. Unlike *sod1*Δ cells, *sod2*Δ mutants do not exhibit lysine, leucine, or methionine auxotrophies, stunted aerobic growth, or growth defects on respiratory carbon sources, *e.g.* 3% glycerol (**Fig. 2.2j**). Notably, SOD1-IMS expression is sufficient to rescue growth of *sod1*Δ cells on glycerol (**Fig. 2.2j**). Altogether, these results indicate that IMS-localized Sod1 alone can protect against cell-wide superoxide toxicity and that the source of matrix and extra-mitochondrial $O_2^{\bullet-}$ is from the IMS.

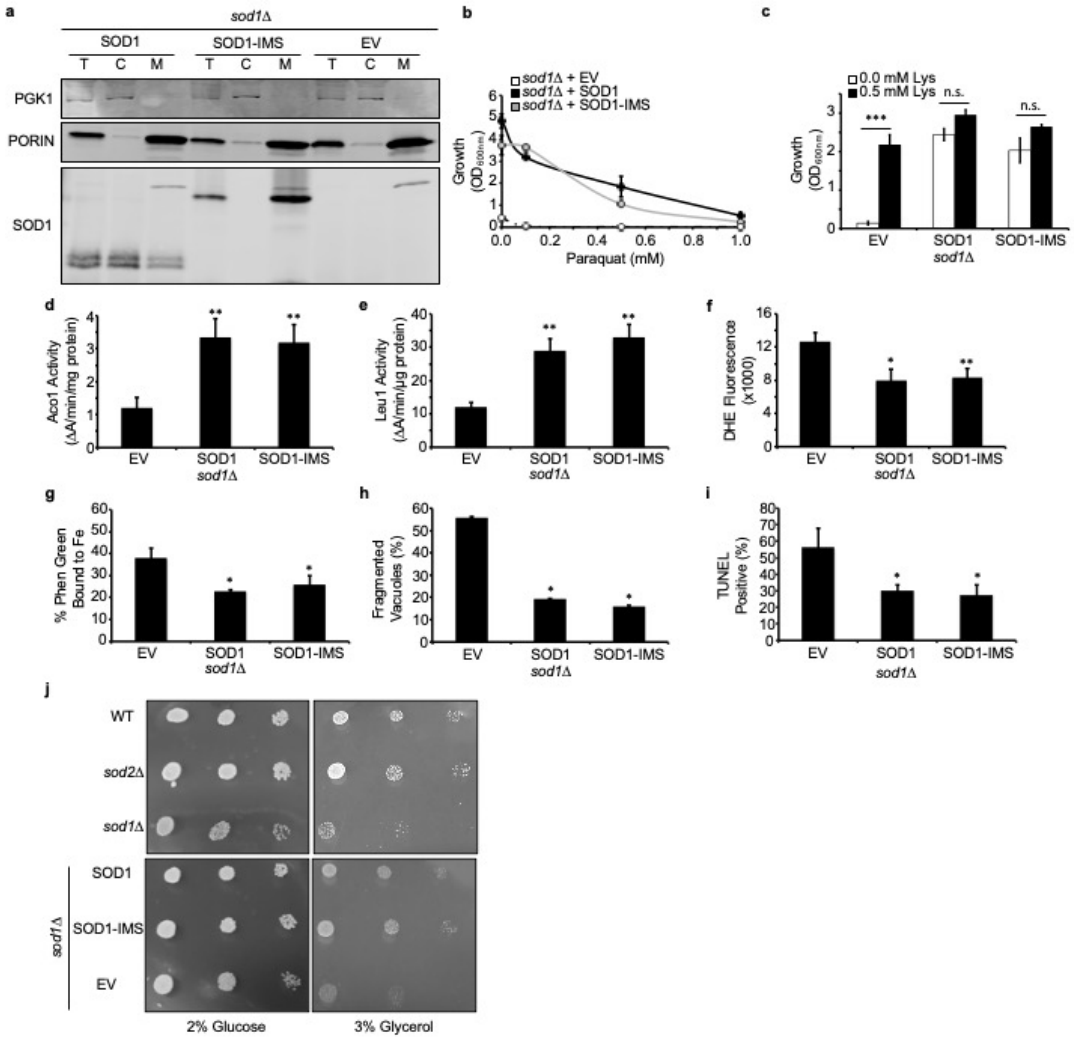

Figure 2.2. IMS-targeted Sod1 is sufficient to protect against cell-wide markers of superoxide toxicity. (**a**) Immunoblot and Sod activity gel of *sod1*::*kan*MX4 (*sod1*Δ) cells expressing empty vector (EV; pRS415), WT *SOD1* (SOD1; pRS415-SOD1), or mitochondrial IMS targeted SCO2-SOD1 (SOD1-IMS; pRS415-SCO2-SOD1. (**b**) Paraquat (PQ) sensitivity, (**c**) lysine (Lys) auxotrophy, (**d**) aconitase (Aco1) activity, (**e**) isopropylmalate isomerase (Leu1) activity, (**f**) DHE-detectable superoxide, (**g**) Phen-Green detectable labile Fe, (**h**) vacuolar fragmentation, and (**i**) TUNEL-detected DNA fragmentation in *sod1*Δ cells expressing EV, SOD1, or SOD1-IMS. (**j**) Respiratory (3% glycerol) versus fermentative (2% glucose) growth of WT, *sod1*::*kan*MX4, *sod2*::*kan*MX4, *sod1*::*kan*MX4 + pRS415, *sod1*::*kan*MX4 + pRS415-SOD1, *sod1*::*kan*MX4 + pRS415-SCO2-SOD1 was tested by spotting 10^4, 10^3, and 10^2 cells on YP media plates containing 2% glucose or 3% glycerol for 3 days. In panels **h** and **i**, approximately ~100 cells were counted from each culture condition in triplicate and scored for (**h**) having single or multiple fragmented vacuoles, as depicted in **Figure 1j**, or (**i**) being non-fluorescent or fluorescent in the FITC channel. Error bars indicate the average ± s.d. of triplicate cultures. The statistical significance relative to EV cells and/or between pairwise comparisons denoted by the black lines is indicated by asterisks using a two-sample t-test. * $P < 0.05$, ** $P < 0.01$, *** $P < 0.001$, n.s. not significant.

2.3.3. High concentrations of Sod1 are required for Yck1 signaling.

Given that the vast majority of extra-mitochondrial Sod1 is apparently dispensable for protection against superoxide toxicity, we next sought to determine the relative contribution of Sod1 towards H_2O_2-mediated redox signaling. In *Saccharomyces cerevisiae*, the only known case of Sod1-mediated redox signaling to date involves a pathway in which Sod1 derived H_2O_2 regulates the stability of a pair of plasma membrane tethered casein kinases, Yck1 and Yck2, that integrate nutrient sensing with energy metabolism [35]. Sod1, which physically associates with the C-terminus of Yck1, produces a local flux of H_2O_2 that prevents the degradation of Yck1. In the absence of Sod1, its substrate, $O_2^{\bullet-}$, or a $O_2^{\bullet-}$-generating NADPH oxidase, Yno1[173], Yck1 is degraded through a mechanism that is currently unknown [35]. The loss of Yck1 shifts energy metabolism from fermentation to respiration. Notably, IMS-localized Sod1 does not contribute towards the regulation of Yck1 stability [35]. Most interestingly, unlike numerous hallmarks of superoxide-toxicity, Yck1 stability is very sensitive to Sod1 expression. Titration of Sod1 using the GAL-inducible SOD1 expression system results in a positive correlation between Sod1 activity and Yck1 expression at Sod1 levels that exceed the minimal threshold required to protect against superoxide toxicity (**Fig. 2.3a**). Similarly, inhibiting Sod1 activity using the copper chelator BCS results in a dose-dependent decrease in Yck1 expression (**Fig. 2.3b**). Altogether, we find that redox signaling via the Sod1/H_2O_2/Yck1 signaling axis is far more sensitive to fluctuations in bulk Sod1 activity than protection against cell-wide markers of superoxide toxicity, which only requires a vanishingly low amount of Sod1 activity.

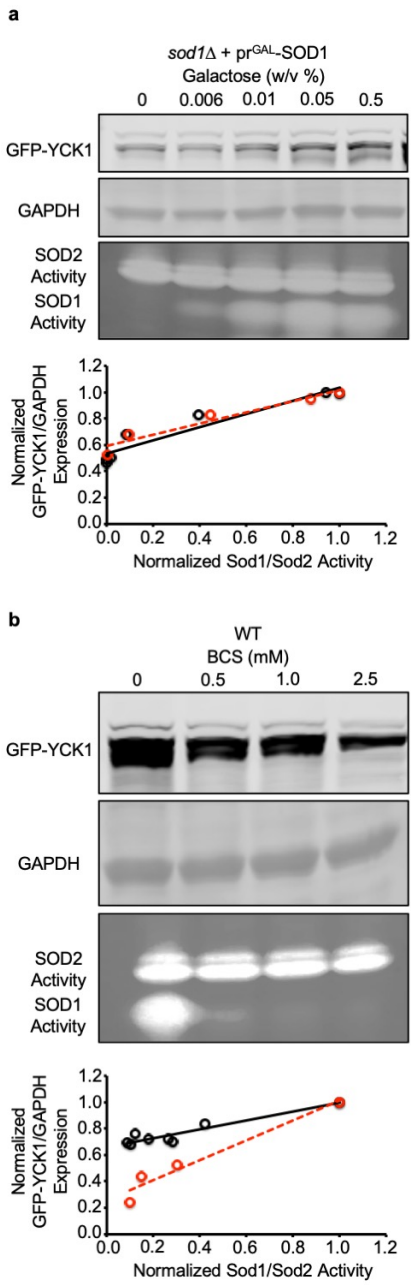

Figure 2.3. Yck1 expression is more sensitive to fluctuations in Sod1 expression and activity than various markers of superoxide toxicity. (**a**) Titration of galactose (GAL) into cultures of sod1::*LEU2* (*sod1*Δ) cells co-expressing the *GAL1* driven Sod1 expression vector (pr^{GAL}-SOD1; pAR1026) and the *TEF1* driven GFP-Yck1 expression vector (pAR113) results in a positive correlation between Sod1 activity and Yck1 expression. (**b**) Titration of the copper chelator, BCS, into cultures of sod1::*LEU2* cells expressing the *TEF1* driven GFP-Yck1 expression vector (pAR113) results in a positive correlation between Sod1 activity and Yck1 expression. In the correlation plots, relative GFP-Yck1 expression is measured as the ratio of GFP-Yck1 to GAPDH signal intensities as determined from densitometry of the immunoblots. Sod1 activity is expressed as a normalized activity relative to the maximal activity observed in each experimental set, *i.e.* 0.5% GAL in GAL titrations or 0 mM BCS in BCS titrations.

2.4. Discussion

Since the seminal discovery of Sod1 in 1969 [17], there was great controversy surrounding its proposed physiological function in $O_2^{\bullet-}$ scavenging due to the low reactivity of $O_2^{\bullet-}$ with various biomolecules, *e.g.* nucleic acids, proteins, and lipids, and the short lifetime of $O_2^{\bullet-}$ due to its rapid un-catalyzed disproportionation, $k \sim 10^5\ M^{-1}\ s^{-1}$ at pH 7.0[174, 175]. In fact, it was proposed that Sod1 had other unknown functions in biology and that it coincidentally catalyzed $O_2^{\bullet-}$ disproportionation [175]. This controversy was largely put to rest with the realization that [4Fe-4S] cluster containing enzymes are primary targets of $O_2^{\bullet-}$, which can oxidize and destroy Fe-S clusters with rate constants up to $10^7\ M^{-1}\ s^{-1}$ [26, 57, 122, 123]. In fact, most of the pathological hallmarks of Sod1 deletion and $O_2^{\bullet-}$ toxicity are due to the diminished activity of certain Fe-S cluster enzymes and inhibition of the corresponding metabolic pathways they operate in, increased labile Fe due to the destruction of Fe-S clusters, and Fe-mediated oxidative stress that results in the damage of lipids, proteins, and nucleic acids. However, given that Sod1 is amongst the most abundant proteins, constituting as much as 0.5% of total yeast protein [176], and disproportionates $O_2^{\bullet-}$ at diffusion-limited rates ($k \sim 10^9\ M^{-1}s^{-1}$), the rationale for producing large quantities of Sod1 has been a mystery. Indeed, herein, using the model unicellular eukaryote, *Saccharomyces cerevisiae* (Baker's yeast), we find that the vast majority of Sod1 is dispensable for protection against numerous cell-wide markers of $O_2^{\bullet-}$ toxicity, including cellular [$O_2^{\bullet-}$], loss of Fe-S cluster enzyme activity, increased labile Fe, and vacuolar and DNA damage (**Fig. 2.1**).

As SODs are the only enzymes that simultaneously affect both [$O_2^{\bullet-}$] and [H_2O_2], they play dual roles in defending against $O_2^{\bullet-}$ toxicity and regulating H_2O_2-mediated redox signaling. While the bulk of Sod1 is dispensable for protection against $O_2^{\bullet-}$ toxicity, we find

that Sod1-mediated peroxide regulation of Yck1 and Yck2 is far more sensitive to fluctuations in Sod1 expression and activity (**Fig. 2.3**). However, if anything, logic dictates that Sod1 would have more influence on superoxide scavenging than peroxide-mediated signaling given that it facilitates the production of 1 H_2O_2 molecule per 2 $O_2^{\bullet-}$ molecules. This paradox can be resolved by considering that the biological targets of $O_2^{\bullet-}$ toxicity are limited in scope, primarily Fe-S proteins, necessitating that very little Sod1 is required to protect against $O_2^{\bullet-}$ damage. In contrast, peroxide-mediated signaling may require large amounts of Sod1 in order to ensure that a sufficient concentration is present in locations proximal to sites of $O_2^{\bullet-}$ generation, *e.g.* NADPH oxidases, so as to provide an adequate flux of H_2O_2 for the redox control of downstream targets. Directly testing this hypothesis is not trivial due to the technical challenges associated with measuring localized pools of H_2O_2. Moreover, given that *sod1*Δ cells exhibit profound metabolic changes, including increased rates of respiration, it is difficult to parse apart contributions arising from the production of H_2O_2 directly from Sod1 versus various metabolic sources that are affected by Sod1 expression, *e.g.* electron transport chain.

In light of the fact that vanishingly little Sod1 is required for defense against $O_2^{\bullet-}$ toxicity, the primary physiological role of Sod1 as a $O_2^{\bullet-}$ scavenger may need to be re-considered in yeast, and potentially other cell types and organisms; its role in redox signaling [31, 35], or non-redox related functions, *e.g.* Cu buffering [176-178] or as a transcription factor [147], may account for the function of most Sod1 in cells. An alternative rationale that may account for cells maintaining a high level of Sod1 is that it is required to protect against pathological conditions that transiently increase $O_2^{\bullet-}$ burdens. Indeed, Sod1 over-expression can protect against the oxidative stress associated with post-ischemic injury in mouse models [179]. In this context, our results from yeast suggest that in the absence of redox stress and $O_2^{\bullet-}$ toxicity, the majority of Sod1 is more vital for

functions unrelated to its role in superoxide scavenging. However, when cells are oxidatively stressed, larger amounts of Sod1 that are otherwise utilized for redox signaling or non-redox functions can "moonlight" as a $O_2^{\bullet-}$ scavenger.

Another interesting outcome of our study is that Sod1 localized to the IMS is sufficient to protect against cell-wide markers of $O_2^{\bullet-}$ toxicity. This result suggests that different pools of Sod1 may have very different physiological functions. For instance, IMS-localized Sod1 may be critical for protection against $O_2^{\bullet-}$ toxicity whereas extra-mitochondrial Sod1 may be more important for non-$O_2^{\bullet-}$ scavenging related functions, such as mediating H_2O_2-based redox signaling or acting as a transcription factor. The dual roles of Sod1 in redox signaling and protecting against $O_2^{\bullet-}$ toxicity in different locales may necessitate the existence of mechanisms to dynamically regulate the localization and/or activity/function of Sod1. Indeed, in human cell lines, it was recently found that acetylation of Sod1 at K122, which is in-part regulated by SIRT5, regulates the partitioning of Sod1 between the cytosol and mitochondrial IMS, which in-turn affects respiratory vs. fermentative energy metabolism [115]. In yeast and human cell lines, it was found that in response to H_2O_2, the cell cycle checkpoint regulating Mec1/ATM effector Dun1/Cds1 kinase phosphorylates Sod1 at S60 and S99 to trigger its nuclear import to regulate gene transcription [147]. In addition, it was recently demonstrated that Sod1 is reversibly phosphorylated at S39 in yeast or T40 in human cell lines by the nutrient sensing mTORC1 to regulate redox homeostasis and adaptation to changes in nutrient availability [113].

Why can IMS-localized Sod1 protect against cell-wide markers of $O_2^{\bullet-}$-toxicity? First, our data suggests that the source of matrix and extra-mitochondrial $O_2^{\bullet-}$ originates in the IMS. How then can $O_2^{\bullet-}$ in the IMS damage biomolecules in other compartments, including the mitochondrial matrix cytosol, vacuole, and nucleus? One possibility is that $O_2^{\bullet-}$ or $HO_2^{\bullet}$ in the IMS diffuses into the matrix and cytosol, possibly through membrane

channels [180], damaging Fe-S enzymes that reside in these locations [168]. The liberated labile Fe can then be bound and trafficked in a manner that enables it to catalyze deleterious redox reactions throughout the cell. Our results support prior observations that ROS derived from Complex III exerts its influence on extra-mitochondrial targets [181, 182].

Sod1 catalyzed $O_2^{\bullet-}$ disproportionation is paramount to its biological function. However, herein we propose that the majority of Sod1 in yeast, and possibly other cell types, is more vital as a source of H_2O_2 for redox signaling, and potentially other non-redox functions, than for scavenging $O_2^{\bullet-}$. The concentration and spatio-temporal distribution of $O_2^{\bullet-}$ encountered in various cells and organisms *in vivo* are still not well understood and will further define the relative roles of Sod1 in redox signaling and oxidative stress protection. Moreover, the identification of proteome-wide redox-targets of Sod1-derived H_2O_2 will be a new frontier in the cell biology of Sod1. Our results will have implications for understanding the basic redox biology of Sod1 and better inform the treatment of diseases in which Sod1 or redox homeostasis can be targeted, including certain cancers [31, 183], neurodegenerative disorders, *e.g.* amyotrophic lateral sclerosis (ALS) [184, 185], and aging [186, 187].

2.5. Methods

2.5.1. Chemicals, media components, and immunological reagents.

Dihydroethidium (Cat. # 50-850-563), FM-4-64 (Cat # T-3166), and Phen Green SK diacetate (Cat. # P-14313) was purchased from Thermo Fisher Scientific. Paraquat dichloride (Cat # 856177-1G) was purchased from Sigma-Aldrich. Yeast nitrogen base and SC dropout mixtures were purchased from Sunrise Science Products. The Yeast Mitochondria Isolation kit was purchased from Bio Vision (#Cat. K259-50). Rabbit polyclonal antibodies against GAPDH (Cat. # 89348-232) and GFP (Cat. # 89362-978) were purchased from VWR. Rabbit polyclonal antibody against PGK1 (Cat. #PA528612) and mouse monoclonal antibody against Porin (Cat. #459500) were purchased from Thermo Fisher and Invitrogen, respectively. A previously described rabbit polyclonal antibody against Sod1 was obtained from the laboratory of Valeria Culotta (Johns Hopkins University) [35].

*2.5.2. Yeast strains, plasmids, and growth***.**

S. cerevisiae strains used in this study were derived from BY4741 (*MAT*a, *his3*Δ1, *leu2*Δ0, *met15*Δ0, *ura3*Δ0). *sod1*::LEU2 and *sod1*::*kan*MX4 strains were generated by knocking out *SOD1* using the previously described deletion plasmids, pKS1[177] and pJAB002 [188].

The *GAL1* driven *SOD1* expression plasmid (pAR1026) was constructed by PCR amplification of the *SOD1* open reading frame from BY4741 genomic DNA with primers that introduced flanking 5' and 3' *SpeI* and *BamHI* sites, respectively. The *SOD1* amplicon was sub-cloned into the *SpeI* and *BamHI* sites of pRS316-*GAL1* [189] to generate

pAR1026. The *TEF1*-driven GFP-Yck1 expression construct (pAR113) was previously reported [35]. Expression constructs for wild type SOD1 (pRS415-SOD1) and IMS localized SCO2-SOD1 (pRS415-SCO2-SOD1), which are both driven by the native *SOD1* promoter, were previously described and were provided by the laboratory of Professor Dennis Thiele (Duke University) [172].

Yeast transformations were performed by the lithium acetate procedure[190]. Strains were maintained at 30 °C on either enriched yeast extract-peptone based medium supplemented with 2% glucose (YPD), or synthetic complete medium (SC) supplemented with 2% glucose and the appropriate drop-out mixture to maintain selection. For all experiments, cells were streaked from -80 °C glycerol stocks onto solid agar media plates and pre-cultured in an anaerobic chamber (Coy laboratories) maintained with an atmosphere of 95% N_2 and 5% H_2. Anaerobically grown cells required supplementing YPD or SC media with 15 mg/L of ergosterol and 0.5% Tween-80 (YPDE or SCE, respectively) [191].

For experiments involving the titration of *SOD1* using the *GAL1* driven *SOD1* expression plasmid, pAR1026, cells were cultured aerobically in SC-URA, with 2% raffinose and the indicated galactose concentrations. For typical experiments involving the IMS-targeted SCO2-SOD1 expression plasmid, cells were cultured aerobically in SC-LEU, with 2% raffinose. In all cases, cells were seeded at an OD_{600nm} ~ .01 and cultured for 14-17 hours to a density of OD_{600nm} ~ 1.0 at 30 °C in a shaking incubator (220 RPM). Following growth, cells were processed as described below for immunoblotting, enzyme assays, EPR spectroscopy, or measurements of labile Fe, superoxide, DNA damage, or vacuolar fragmentation. For all experiments, SOD1 activity and/or expression was assessed as described below. All experiments were conducted using biological replicates arising from duplicate or triplicate independent cultures of multiple clones. While the data reported in

the figures reflect biological replicates from single experimental trials, all of the data has been re-produced on multiple occasions in independent experimental trials.

2.5.3. Immunoblotting.

~2 x 10^8 cells were harvested, washed in ice-cold Milli-Q water, and lysed in two pellet volumes of lysis buffer (10 mM sodium phosphate, 50 mM sodium chloride, 5 mM EDTA, 1.0% Triton X-100, 1 mM PMSF and a protease inhibitor cocktail (GBiosciences) as described previously [192]. Lysis was achieved at 4 °C using one pellet volume of zirconium oxide beads and a bead beater (Bullet Blender, Next Advance) on a setting of 8 for 3 minutes[192]. Lysate protein concentrations were determined by the Bradford method (Bio-rad) and 14% tris-glycine gels (Invitrogen) were employed for SDS-PAGE[192]. Anti-GFP (1:4000), anti-GAPDH (1:4000) or anti-SOD1 (1:5000) polyclonal antibodies and a goat anti-rabbit secondary antibody conjugated to a 680 nm emitting fluorophore (Biotium) were used to probe for GFP-Yck1, GAPDH or Sod1 respectively. All gels were imaged on a LiCOR Odyssey Infrared imager [35, 165, 192].

2.5.4. Cell fractionation.

Mitochondria were isolated using the Yeast Mitochondria Isolation Kit (Bio Vision). For this purpose, *sod1*Δ cells expressing an empty vector (pRS415), SOD1 (pRS415-SOD1) or IMS localized SCO2-SOD1 (pRS415-SCO2-SOD1) were grown to a final OD_{600nm} = 1.0 in SC, 2% glucose media. ~4 x 10^{16} cells of each strain were harvested and washed in ice-cold Milli-Q prior to fractionation. After fractionation, the volume corresponding to one percent of whole lysate or cytosolic fraction and ten percent of mitochondrial fraction were loaded in the previously described gels for SDS-PAGE. The

samples were probed with anti-PGK1 (1:1000) and anti-SOD1 (1:5000) polyclonal antibodies and a goat anti-rabbit secondary antibody conjugated to a 680 nm emitting fluorophore (Biotium), in addition to anti-Porin (1:5000) monoclonal antibody and a goat anti-mouse secondary antibody conjugated to a 797nm emiting fluorophore (Thermo Fisher).

2.5.5. Enzyme assays.

SOD activity analysis was carried out by native PAGE and nitroblue tetrazolium staining as described previously [35, 193, 194] on exponential phase cultures grown to a final OD_{600nm} = 1.0 in SC, 2% raffinose media containing the indicated concentration of galactose. Yeast cells were washed with ultra-pure H_2O, resuspended in lysis buffer and lysed as described in the section on immunblotting. Protein samples (~10-30 µg) were separated in 14% native PAGE gels. Sod1 activity was visualized by staining gels with 2.43 mM nitro blue tetrazolium chloride (Sigma), 0.14 M riboflavin-50-phosphate (Sigma) and 28mM TEMED (Bio-Rad) for 60 min at room temperature in darkness. To visualize Sod1 activity, gels were rinsed with water twice and exposed to light.

For aconitase (Aco1p) and isopropylmalate isomerase (Leu1p) activity assays, cells were subjected to ZrO bead lysis in 50 mM MES, 100 mM KCl, 0.1% Triton X-100, pH 7.0 under a nitrogen atmosphere in a COY chamber. Aco1p and Leu1p activity was determined spectrophotometrically as described previously[165, 168] using a Biotek Synergy Mx multi-modal plate. The assay mixture contained 50–300 µg of lysate protein in 200 µL of a buffer containing 50 mM tris(hydroxymethyl) aminomethane (Tris)-HCl, pH 7.4, and 100 mM NaCl and supplemented with either 0.5 mM cis-aconitate (Aco1 activity) or 0.5 mM citraconitate (Leu1 activity). Activities were determined by monitoring the

disappearance of cis-aconitate (Aco1p) or citraconitate (Leu1p) at 240 or 235 nm, respectively, over the course of 5 minutes.

2.5.6. Superoxide measurements.

Superoxide levels were measured by monitoring the fluorescence of DHE stained cells (λ_{ex} = 485 nm, λ_{em} = 620 nm) similarly to what was described previously[35, 167]. Briefly, 1 x 10^7 cells were harvested from duplicate or triplicate cultures, resuspended and incubated in 500 µl of fresh media containing 50 µM DHE for 20 min in the dark, washed twice with PBS solution, and fluorescence recorded in a Biotek Synergy Mx multi-modal plate reader.

*2.5.7. Detection of labile Fe using EPR spectroscopy***.**

EPR detection of labile Fe in yeast was accomplished as described previously [158, 161, 195], but with the following modifications. 50 mL cultures of *sod1*Δ cells expressing pr^{GAL}-SOD1 seeded at a density of OD_{600nm} = .01 were grown in 250 mL Erlenmeyer flasks containing SC, 2% raffinose media with the indicated galactose concentration. Cultures were grown for 16 hours to an OD_{600nm} ~ 1. Cells were washed 2x with 10 mL of cold ultrapure H_2O and 1x with 10 mL cold 20 mM Tris-Cl, pH 7.4 on ice. Finally, the cells were resuspended in 500 µL of cold 20 mM Tris-Cl, pH 7.4, containing 10% glycerol and transferred into an EPR tube. The sample was flash frozen in liquid N_2 and stored at -80 °C until EPR measurements were performed. Spectra were recorded with a Bruker EMX X-band spectrometer equipped with an ESR900 continuous flow cryostat (Oxford Instruments, Concord, MA) at 70K. The parameters for EPR were as follows: center field,1,560 G; sweep width, 500 G; frequency 9.45 GHz; microwave power,

31 mW; attenuation, 10 dB; modulation amplitude, 20 G; modulation frequency, 100 kHz; receiver gain, 2· 105 ; sweep time, 20.97 s; time constant, 81.92 ms; resolution, 2,048 points; number of scans, 16. Fe(III) desferrioxamine (DFO) standards were prepared over a range of concentrations in 20 mM Tris HCl, 1 mM DFO, 10% glycerol, pH 7.4. The Fe(III) signal at *g* = 4.3 was analyzed with the Xenon software (Bruker) and used for quantitation of EPR-detectable iron levels. Calculation of cellular EPR-detectable Fe(III) was performed as described previously [195].

2.5.8. Detection of labile Fe with Phen Green SK.

Labile Fe was detected as described previously using Phen Green SK (λ_{ex} = 488 nm, λ_{em} = 530 nm), a fluorescent probe for divalent metals that is quenched upon Fe^{2+} binding [196-198]. 5 x 10^7 cells were resuspended in 300 µL of phosphate buffered saline (PBS). The cell suspension was incubated with 3 µL of a 2 mM Phen Green SK DMSO stock solution at 30 °C for 15 minutes in the dark. Cells were then washed with PBS, and split into 3 x 100 µL aliquots, and were treated with 1 µL of H_2O, 1 µL of a 200 mM aqueous stock solution of 1,10-phenantroline, a ferrous iron chelator, or treated with 1 µL of a 10 mM aqueous stock solution of ferrous ammonium sulfate, and incubated in the dark for 10 minutes, prior to recording fluorescence. Phen Green fluorescence was recorded in a Biotek Synergy Mx multi-modal plate reader. After subtracting the background fluorescence of unlabeled cells, the percentage of Phen Green bound to Fe^{2+} (% Bound) was calculated using the following formula:

$$\% \text{ Bound: } (F\text{-}F_{min}/F_{max}\text{-}F_{min})*100$$

where, F is Phen Green fluorescence intensity in the test sample, F_{min} is the Phen Green fluorescence intensity when it is not bound to Fe, and F_{max} is the Phen Green fluorescence intensity when it is saturated with Fe. F_{min} is determined by recording Phen Green fluorescence in cells incubated with the iron chelator, 1,10-phenantroline. F_{max} is determined by recording Phen Green fluorescence in cells incubated with ferrous ammonium sulfate.

2.5.9. Vacuolar fragmentation.

Vacuolar fragmentation was assessed as previously described [158]. Briefly, 2 x 10^7 cells were resuspended in 50µL of fresh growth media, typically SC media with 2% raffinose and appropriate galactose concentration. The cell suspension was incubated with 1µL of a 2 mM DMSO stock solution of FM4-64 at 30 °C for 20 minutes in the dark. The cells were then pelleted, washed with fresh media, and resuspended in 5 mL of fresh SC media with 2% raffinose and appropriate galactose concentration. The cells were cultured for an additional 1.5 hours at 30 °C, shaking at 220 RPM in the dark. The cells were then washed with PBS and resuspended in PBS to a density of 2 x 10^8 cells mL^{-1}. 3 µL of the cell suspension were placed on a glass slide and imaged using a Zeiss LSM 700 microscope equipped with a 63x, 1.4 numerical aperture oil objective, using the using the Texas Red channel. Approximately ~100 cells were counted from each culture condition in triplicate and scored for having either single vacuoles or multiple fragmented vacuoles as indicated in **Figure 2.1j**.

2.5.10. TUNEL assays.

TUNEL assays were conducted as previously described[147]. Yeast cells were fixed in 4% p-formaldehyde at room temperature for 30 minutes. The cells were then washed three times with PBS. The cell pellet was then re-suspended in PBS and digested with 300 µg / mL of Zymolyase 100T at 37 °C for 60 minutes. After 60 minutes, 10 µL of the cell suspension was applied to a clean glass slide and dried at 37 °C for 30 minutes. The slides were rinsed with PBS and incubated in a permeabilization solution (0.1% Triton X-100 and 0.1% sodium citrate) on ice for 2 min. The slides were then rinsed twice with PBS. The TUNEL reaction mixture (50 µl of enzyme solution and 450 µl of Label solution; *In Situ* Cell Death Detection Kit, Roche Diagnostics) was applied to the slides and incubated in the dark for 60 minutes. The cells labeled with fluorescein-dUTP were imaged using a Zeiss LSM 700 microscope equipped with a 63x, 1.4 numerical aperture oil objective. Approximately ~100 cells were counted from each culture condition in triplicate and scored for being either non-fluorescent or fluorescent using the FITC channel.

CHAPTER 3

Cu/Zn Superoxide Dismutase (Sod1) Regulates the Canonical Wnt Signaling Pathway

This chapter is adapted from the previously accepted work: Chandrasekharan, B., Montllor-Albalate, C., Colin, A., Jang, Y. LC., Reddi, A. R. “Cu/Zn-Superoxide Dismutase (Sod1) Regulates the Canonical Wnt Signaling Pathway” *BBRC*. (2020). The second author of this document, and author of this thesis dissertation, contributed to this work by conceiving, designing and performing the cell proliferation and antioxidant system expression experiments of the paper, making figures for such experiments and contributing to the writing of the manuscript with input from all authors.

3.1. Abstract

Cu/Zn Superoxide Dismutase (Sod1) catalyzes the disproportionation of cytotoxic superoxide radicals ($O_2^{\bullet-}$) into oxygen (O_2) and hydrogen peroxide (H_2O_2), a key signaling molecule. In *Saccharomyces cerevisiae*, we previously discovered that Sod1 participates in an H_2O_2-mediated redox signaling circuit that links nutrient availability to the control of energy metabolism. In response to glucose and O_2, Sod1-derived H_2O_2 stabilizes a pair of conserved plasma membrane kinases - yeast casein kinase 1 and 2 (Yck1/2) - that signal glycolytic growth and the repression of respiration. The Yck1/2 homolog in humans, casein kinase 1-γ (CK1γ), is an integral component of the Wingless and Int-1 (Wnt) signaling pathway, which is essential for regulating cell fate and proliferation in early development and adult tissue and is dysregulated in many cancers. Herein, we establish the conservation of the SOD1/YCK1 redox signaling axis in humans by finding that SOD1

regulates CK1γ expression in human embryonic kidney 293 (HEK293) cells and is required for canonical Wnt signaling and Wnt-dependent cell proliferation.

3.2. Introduction

Up to 1-2% of all molecular oxygen (O_2) consumed in cells is incompletely reduced to cytotoxic reactive oxygen species (ROS) such as superoxide ($O_2^{\bullet-}$), hydrogen peroxide (H_2O_2), and hydroxyl radicals ($^{\bullet}OH$) [199, 200]. As a consequence, a number of ROS scavenging enzymes evolved to defend against the toxicity of $O_2^{\bullet-}$, *e.g.*superoxide dismutases (SODs), and H_2O_2, *e.g.* catalases and peroxidases [144]. H_2O_2 is unique amongst the aforementioned ROS in that it is also a key signaling molecule [125, 126]. Peroxide-mediated oxidation of cysteine thiols to disulfides, sulfenic acid, or sulfinic acid on downstream targets can alter protein structure and function, leading to changes in cell physiology [30, 42, 201, 202]. However, the mechanisms underlying the transmission of peroxide-based signals in a cellular sea of H_2O_2 scavenging and detoxification systems is not well understood.

SODs, which detoxify $O_2^{\bullet-}$ by catalyzing its disproportionation into H_2O_2 and O_2, constitute a major enzymatic source of signaling peroxides. Most eukaryotes express two structurally unrelated intracellular SODs, a Mn-containing SOD (Sod2) that is confined to the mitochondrial matrix [145] and a Cu/Zn-containing SOD (Sod1) that is present in virtually every subcellular locale except the matrix [17]. Sod1 accounts for the majority of SOD activity, > 80% [165], and its importance in oxidative stress protection is underscored by reduced proliferation, decreased lifespan, and metabolic defects when *SOD1* is deleted in various cell lines and organisms [80, 124, 150-158, 160, 161].

Until recently, it was unclear what the relative contribution of SOD1 function was towards protecting against $O_2^{\bullet-}$ toxicity versus regulating H_2O_2-mediated signaling. $O_2^{\bullet-}$ is toxic because of its ability to oxidize and destroy Fe/S clusters in certain metabolic enzymes, which also releases cytotoxic iron that can catalyze deleterious redox reactions [26, 57, 122-124]. Most interestingly, using Baker's yeast as a model unicellular eukaryote, we found that only a small fraction (< 1%) of the total Sod1 pool is required to protect cells against cell-wide damage from $O_2^{\bullet-}$ [35, 81]. Rather, we found that much larger quantities of Sod1 are required to produce peroxides for the redox regulation of a nutrient-sensing pathway [81]. Based on these results, we proposed that the *primary* cellular function for bulk Sod1 is to act as a redox amplifier that provides bursts of signaling peroxides [81]. Indeed, Sod1-catalyzed $O_2^{\bullet-}$ disproportionation occurs with a 10^4 rate enhancement relative to the uncatalyzed reaction ($k^{SOD1} = 10^9\ M^{-1}\ s^{-1}$ vs. $k^{uncatalyzed} = 10^5\ M^{-1}\ s^{-1}$). In order to establish the role of Sod1 as a central mediator of peroxide signaling, we seek to identify new pathways and proteins that are regulated by Sod1. Moreover, we question if in mammalian cell lines, as observed in yeast, the bulk of Sod1 is required for redox signaling, i.e. CK1γ stabilization, and dispensable for oxidative protection.

To date, a small handful of proteins have been identified to be redox regulated by Sod1, including protein tyrosine phosphatases [31] and tyrosine kinase growth factor receptors [116]. In Baker's yeast, Sod1 was found to provide a source of H_2O_2 that stabilizes a pair of plasma membrane casein kinases, Yck1 and Yck2, that link extracellular glucose availability to repression of respiration and fermentative growth [35] (**Figure 3.1a**). The transcriptional effectors Mth1 and Std1 activate the expression of genes required for the metabolic adaptation to low glucose and enhances respiratory metabolism. Glucose binding to Snf3 and Rgt2, transmembrane glucose receptors, activates the peripheral membrane type I casein kinases, Yck1 and Yck2, which in turn

phosphorylate Mth1 and Std1 [203]. Mth1/Std1 phosphorylation induces its ubiquitination and proteasomal degradation by the Skp-Cullin-F-box (SCF) E3 ubiquitin ligase (UbL) Grr1. In the absence of glucose, Mth1/Std1 is not targeted for degradation and instead translocates to the nucleus to regulate gene expression. In the presence of O_2, a yeast NADPH oxidase (Yno1) catalyzes the formation $O_2^{\bullet-}$, which is converted to H_2O_2 by Sod1. Sod1-derived H_2O_2 stabilizes Yck1/2, which leads to glucose-mediated repression of respiration and fermentative growth. When Sod1 or $O_2^{\bullet-}$ is diminished, Yck1/2 is degraded, and respiratory metabolism is enhanced. Sod1 regulates Yck1 and Yck2 stability via the peroxide-dependent regulation of a still unknown post-translational modification (PTM) on conserved lysine (K) residues at the C-terminus of Yck1 and Yck2. Mutation of K^{383}, K^{386}, and K^{390} in Yck1 (K^{390}, K^{392}, and K^{397} in Yck2) to arginine (R) results in constitutively stable Yck1 that is not degraded in the absence of Sod1, O_2, or glucose.

The Yck1/2 homolog in humans, casein kinase 1-γ (CK1γ), is an integral component of the Wnt signaling pathway, which is essential for regulating cell fate and proliferation in early development and adult tissue and is dysregulated in many cancers [204]. The central component of the canonical Wnt pathway is the transcriptional effector β-catenin, which activates the expression of Wnt target genes in control of cell proliferation, differentiation, migration, adhesion, and energy metabolism. Just as yeast Yck1/2 link extracellular glucose availability to energy metabolism (**Figure 3.1a**), human CK1γ links extracellular signals from a family of Wnt proteins to control metabolism and physiology (**Figure 3.1b**). Wnt ligands bind to a heterodimeric receptor complex consisting of Frizzled (Frz) and low-density lipoprotein receptor-related proteins LRP5 and LRP6. This binding event activates CK1γ, which then phosphorylates LRP5/6, ultimately leading to the sequestration of the β-catenin destruction complex. With the destruction complex unavailable to target β-catenin for degradation, β-catenin is able to translocate to the

nucleus where it can activate Wnt-target genes (**Figure 3.1b**, **left**). In the absence of Wnt ligands, the β-catenin destruction complex phosphorylates β-catenin, which in turn leads to its ubiquitination and proteasomal degradation by the SCF UbL β-Transducin Repeat-Containing Protein (β-TrCP) (**Figure 3.1b**, **right**).

Having demonstrated previously that Sod1 regulates Yck1/2 expression and glucose signaling in yeast [35, 81], we sought to determine if Sod1 regulates CK1γ expression and Wnt signaling in mammalian cells. Moreover, we sought to understand if the observation that the bulk of Sod1 is required for Sod1-catalyzed H_2O_2 signaling, compared to a minuscule fraction required for oxidative stress protection is constant from yeast to humans. Herein, using RNA interference to silence *SOD1* in human embryonic kidney cell line (HEK293), we report that SOD1 regulates CK1γ expression and is required for canonical Wnt signaling and Wnt-dependent cell proliferation in mammalian cells and that, as observed in yeast, the vast majority of Sod1 is dispensable for oxidative stress protection, but required for redox signaling.

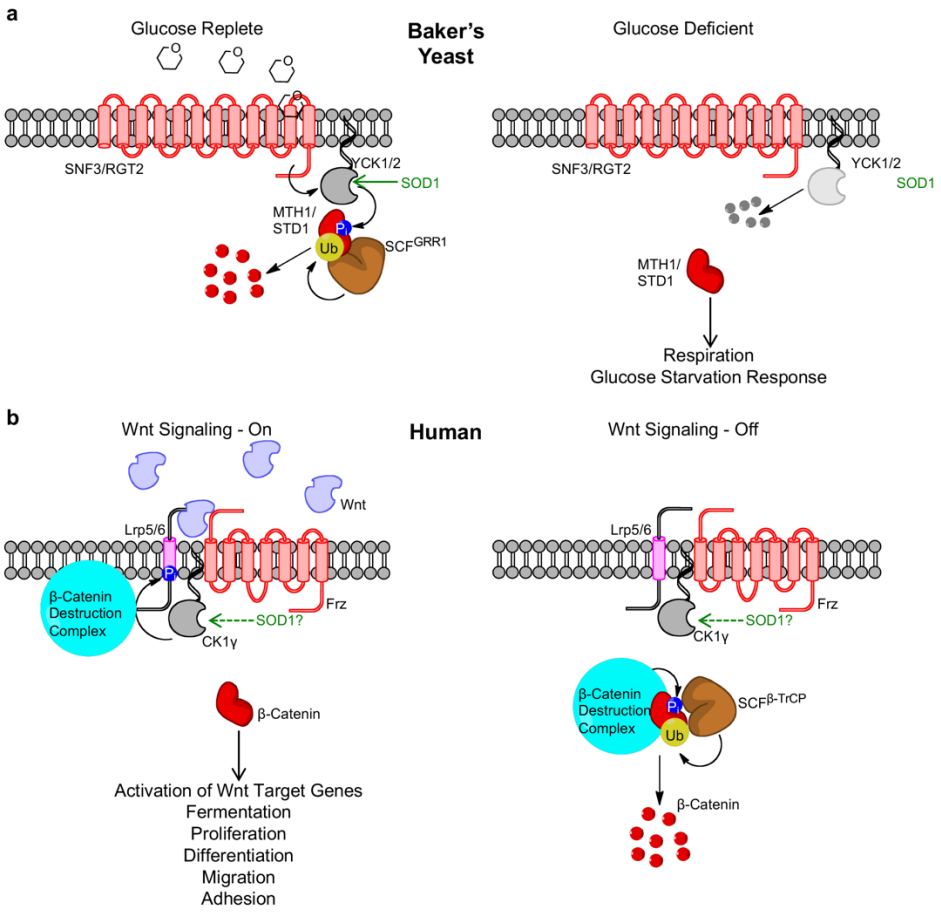

Figure 3.1. Comparison of (**a**) glucose sensing in Baker's yeast (*Saccharomyces cerivisaie*) and (**b**) Wnt signaling in humans, with an emphasis on the respective roles of Sod1 and plasma membrane casein kinase homologs, Yck1/Yck2 (yeast) and CK1γ (humans). See text for a detailed description of the two pathways.

3.3. Materials and Methods.

3.3.1. Chemicals, media components, and immunological reagents.

Dihydroethidium (Cat. # 50-850-563) was purchased from Thermo Fisher Scientific. Paraquat dichloride (Cat # 856177-1G) was purchased from Sigma-Aldrich. The

mammalian nuclear isolation kit was purchased from Thermo Fisher Scientific (Cat. #78833). Rabbit polyclonal antibodies against GAPDH (VWR; Cat. # 89348-232), PGK1 (Thermo Fisher; Cat. # PA528612), LRP6 (Cell Signaling; Catalog # 2560), phospho-β-catenin S33/S37/T41 (Cell Signaling; Catalog # 9561), β-catenin (Abcam; Cat # 6302), Phospho-LRP-6 T1479 (Abnova; Cat. # PAB12632) [205], Lamin A/C (Cell Signaling; Cat. # 2032S), CK1γ3 (Thermo Fisher; Cat # PA5-99838) [206], Prdx1 (Millipore Sigma; Cat. # HPA007730-100UL), Trx1 (Cell Signaling; Cat. # 2429), Gpx1 (Abcam; Cat. # ab22604), and Prdx-SO_3 (Abcam; Cat. # Ab16830), and mouse monoclonal antibodies against Porin (Invitrogen; Cat. #459500) and Prdx2: PRDX2 (Fisher Scientific; Cat. # LF-MA0144) were purchased from commercial sources as indicated. A previously described rabbit polyclonal antibody against Sod1 was obtained from the laboratory of Valeria Culotta (Johns Hopkins University) [35]. Goat α-rabbit (VWR; Cat # 89138-520) or α-mouse (VWR; Cat # 89138-516) secondary antibodies conjugated to a 680-nm emitting fluorophore were obtained from Biotium through VWR.

3.3.2. Cell culture, growth, gene silencing, Wnt stimulation, and nuclear fractionation.

Human embryonic kidney (HEK293) cells were obtained from (American Type Culture Collections. ATCC, Cat. # CRL-1573). Cells were cultured in Dulbecco's Minimal Essential Medium/ DMEM media (Thermo Fisher Scientific (Cat. # 3105328) containing Heat Inactivated Fetal Bovine Serum (HI-FBS, 10 %, VWR Cat # 89510-188), supplemented with L-glutamine in 5% CO2 and 37^0C with 1% antibiotics (Penicillin-Streptomycin). Cells were plated in 6 well plates for immunoblotting or qPCR experiments (0.25 - 0.3 million cells/ well), or on 13 mm coverslips in 24 well plates for immunostaining. SOD1 siRNA (Cat. # 4390824) and Control siRNA (Cat. # 4390843) were purchased from

(Thermo Fisher Scientific). SOD1 silencing was accomplished in reduced serum medium (Opti-MEM, Cat. # 11058021, Thermo Fischer Scientific) by transfection of SOD1 siRNA or scrambled control siRNA (for 72 hours) into 60-70% confluent HEK cellsusing Lipofectamine-2000 transfection reagent according to Manufacturer's protocols (Cat. # 11668019, Thermo Fischer Scientific).

Wnt conditioned media was produced by culturing L-Wnt-3A cells (ATCC, Cat. # CRL-2647) according to ATCC protocol, and media from L Cells (ATCC, Cat. # CRL-2648) was used as the corresponding negative control. Wnt stimulation was achieved by treating HEK293 cells with DMEM: Wnt3a conditioned media (1:1 v/v) for 3 hours.

3.3.3. Immunoblotting and SOD activity.

Immunoblotting was performed exactly as described previously with cells from 6-well dishes being harvested, washed in ice-cold Milli-Q water, and lysed in two pellet volumes of lysis buffer (10 mM sodium phosphate, 50 mM sodium chloride, 5 mM EDTA, 1.0% Triton X-100, 1 mM PMSF and a protease and phosphatase inhibitor cocktail (GBiosciences) [192]. For assessing peroxiredoxin oxidation, cell cultures were quenched with 10% trichloroacetic acid (TCA), followed by TCA-precipitating lysate protein and washing it in cold acetone. The dried pellet was resuspended in degassed resuspension buffer (6M urea, 10mM EDTA, 20mM Tris, 0.5%SDS, 10μM neocuproine, pH 8.5) containing 1mM PMSF and a protease inhibitor cocktail (GBiosciences) in an anaerobic chamber (Coy laboratories). Lysate protein concentrations were determined by the Pierce™ BCA protein assay kit (Thermo Scientific). SOD activity was measured using an in-gel assay based on native PAGE and nitroblue tetrazolium staining as described previously [35, 112, 193, 207].

3.3.4. Immunofluorescence.

HEK293 cells plated on coverslips and transfected with control or Sod1 siRNA (72 h), were fixed using 4% paraformaldehyde in phosphate buffered saline (PBS) for 30 min and blocked with 10% FBS for 1 hour. The coverslips were then incubated with the β-catenin antibody for 2 h, followed by Cy3-conjugated secondary antibody for 1 hour. 4′, 6-diamidino-2-phenylindole (DAPI,1:10,000 dilution, Sigma) was used for nuclear staining. The mounted coverslips were imaged using Zeiss LSM510 confocal microscopy to assess cytoplasmic versus nuclear localization of β-catenin. Results were expressed as percent localization relative to the total number of DAPI positive cells. At least 10 fields were imaged from each condition from 3 independent experiments.

3.3.5. qRT-PCR.

RNA was isolated from HEK293 cells using the RNAeasy kit (Qiagen). cDNA was synthesized from 1 ug of total RNA using iscript cDNA synthesis kit (Biorad). qRT-PCR was performed using SYBR Green PCR Master Mix (Biorad) and 7500 Real-Time PCR System (Applied Biosystems) using primers for β-catenin, Cyclin D1, c-myc, GAPDH, and SOD1.

3.4. Results.

3.4.1. Sod1 regulates the canonical Wnt signaling pathway.

In order to probe the role of Sod1 in the Wnt signaling pathway, we determined the effect of Sod1 silencing on CK1γ expression and its impact on Wnt pathway activation in HEK293 cells upon stimulation with the Wnt3a ligand (**Figure 3.1b**). There are three plasma membrane tethered CK1γ isoforms in humans: CK1γ1, CK1γ2, and CK1γ3. We chose to focus our efforts on Sod1-mediated regulation of CK1γ3 for the following reasons:

a. in HEK293 cells, CK1γ3 protein levels are ~4-fold higher than CK1γ2 and > 10-fold higher than CK1γ1, which is undetectable [208];
b. CK1γ3 (and CK1γ2) contains a conserved C-terminal K implicated in Sod1 and peroxide regulation of Yck1/Yck2 - K^{383} in Yck1 and K^{355} in CK1γ3 [35];
c. Sod1 regulates bovine CK1γ3 heterologously expressed in yeast [35].

SOD1 expression and activity is consistently reduced by ~60% using siRNA against SOD1 in HEK293 cells after 72 hours (**Figure 3.2a** and **3.2b**). This degree of *SOD1* silencing results in a ~40% decrease in CK1γ3 expression (**Figure 3.2a** and **3.2c**), as measured using a CK1γ3-specific antibody. These results are consistent with our previous studies in Baker's yeast that found that *sod1*Δ cells exhibited a marked loss in Yck1/2 expression and heterologously expressed bovine CK1γ3. It is important to note that *SOD1* silencing does not affect the expression of other cytosolic peroxide metabolizing enzymes, including peroxiredoxins 1 and 2 (**Figure A.1a-d**), thioredoxin 1 (**Figure A.1e** and **A.1f**), and glutathione peroxidase 1 (**Figure A.1e** and **A.1g**), thereby indicating that other antioxidant enzymes are not compensating for the loss of Sod1 function. Moreover, silencing of *SOD1* does not significantly impact steady-state peroxide

levels and oxidative stress as indicated by the lack of significant changes to peroxiredoxin oxidation (**Figure A.1h-j**).

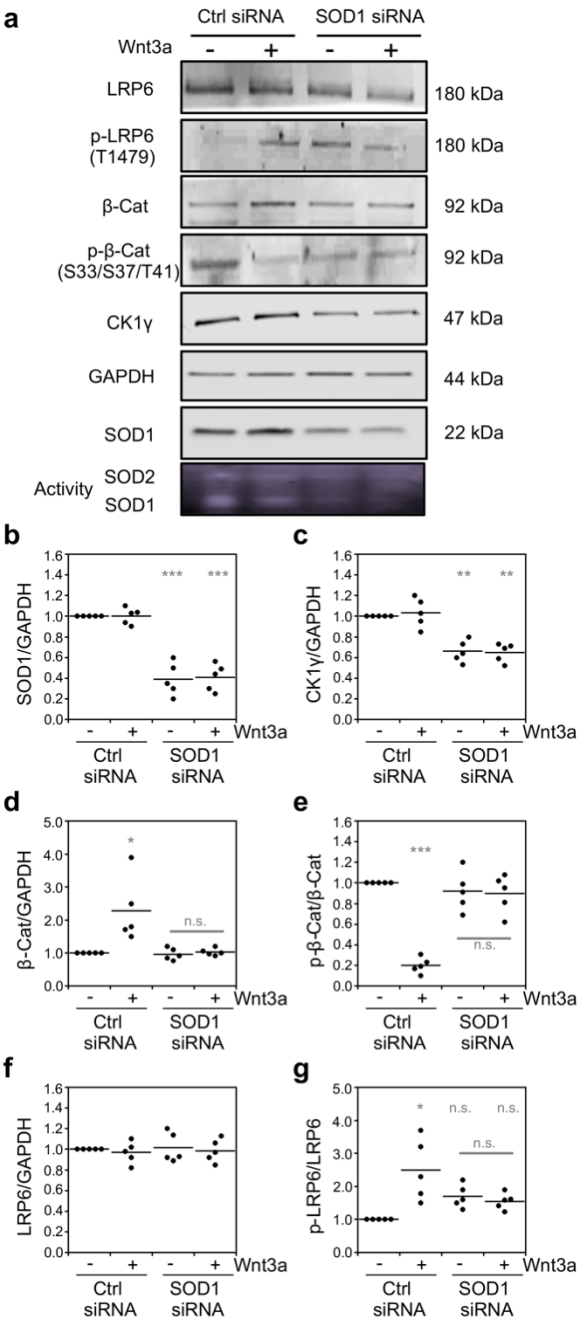

Figure 3.2. Sod1 is required for the Wnt3a-dependent activation of the canonical Wnt signaling pathway. (**a**) Representative immunoblots and SOD activity gel of Wnt signaling pathway markers in response to Wnt3a activation and/or silencing of Sod1 with siRNA. (**b**-**g**) Quantification of the normalized levels of (**b**) Sod1, (**c**) CK1γ3, (**d**) β-catenin (β-Cat), (**e**) phosphorylated β-catenin at residues S33, S37, and T41 (p-β-Cat), (**f**) LRP6, and (**g**) phosphorylated LRP6 at residue T1479 (p-LRP6) from five independent trials. p-LRP6 and p-β-Cat is normalized to total LRP6 or β-Cat, respectively. The statistical significance relative to – Wnt3a/Ctrl RNAi cells or for the indicated pairwise comparison is denoted by grey asterisks and determined by ordinary one-way ANOVA with the

Bonferroni multiple-comparison post-hoc test. * P < 0.01, ** P < 0.001, *** P < 0.0001, n.s. = not significant.

SOD1 silencing and the concomitant decrease in CK1γ3 expression resulted in a significant decrease in multiple markers of Wnt pathway activation (**Figure 3.1b**). Wnt3a binding to its cell surface receptor activates CK1γ, which in turn phosphorylates LRP6 at T1479, ultimately leading to sequestration of the β-catenin destruction complex [204]. As a consequence, cytosolic β-catenin cannot be phosphorylated at residues S33, S37, and T41, allowing it to escape proteasomal degradation and translocate to the nucleus to regulate gene expression. Accordingly, we find that Wnt3a stimulation results in an increase in LRP6 phosphorylation (**Figure 3.2a** and **3.2g**), a decrease in β-catenin phosphorylation (**Figure 3.2a** and **2e**), an increase in β-catenin stability (**Figure 3.2a** and **3**.**2d**), and increased nuclear β-catenin as measured by immunofluorescence (**Figure 3.3a** and **3.3b**) and subcellular fractionation (**Figure 3.3c** and **3.3d**). In contrast, Wnt3a stimulation in *SOD1* silenced cells <u>*does not*</u> increase LRP6 phosphorylation (**Figure 3.2a** and **3.2g**), decrease β-catenin phosphorylation (**Figure 3.2a** and **3.2e**), increase β-catenin stability (**Figure 3.2a** and **3.2d**), or increase nuclear localization of β-catenin (**Figure 3.3**). Thus, *in total*, Sod1 is required for Wnt-dependent activation of the canonical Wnt pathway.

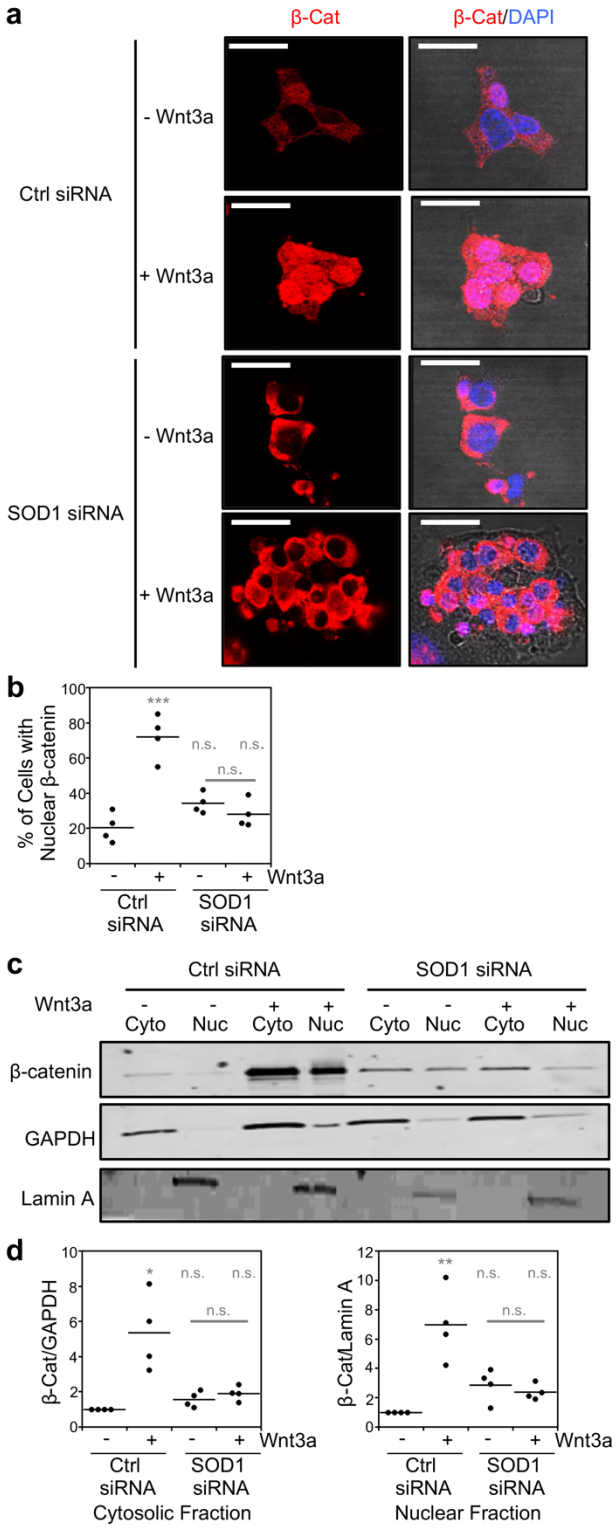

Figure 3.3. Sod1 is required for the Wnt3a-dependent nuclear localization of β-catenin. (**a**) Representative immunofluorescence of β-catenin localization relative to the nuclear marker, DAPI, in response to Wnt3a activation and/or silencing of Sod1 with

siRNA. Scale bar is 20 μm. (**b**) Quantification of β-catenin nuclear localization from four independent trials. ~200 cells were counted for each condition in each trial. (**c**) Representative immunoblots of β-catenin expression in cytosolic and nuclear fractions of HEK293 cells. (**d**) Quantification of the normalized levels of cytosolic and nuclear β-catenin (β-Cat) from four independent trials. Cytosolic β-Cat is normalized to the cytosolic marker GAPDH and nuclear β-Cat is normalized to the nuclear marker Lamin A. The statistical significance relative to – Wnt3a/Ctrl RNAi cells or for the indicated pairwise comparison is denoted by grey asterisks and determined by ordinary one-way ANOVA with the Bonferroni multiple-comparison post-hoc test. * $P < 0.01$, ** $P < 0.001$, *** $P < 0.0001$, n.s. = not significant.

3.4.2. Sod1 regulates the Wnt-dependent activation of Wnt target genes and cell proliferation.

We next determined if Sod1 impacts the expression of Wnt target genes and Wnt-dependent cell proliferation. Once in the nucleus, β-catenin associates with transcription factors from the T cell factor/lymphoid enhancer factor (TCF/LEF) family of transcription factors and drives transcription of hundreds of Wnt/β-catenin target genes. Using qRT-PCR, we determined if silencing SOD1 in Wnt stimulated cells altered the expression of Wnt/β-catenin target genes β-catenin, c-Myc, and Cyclin D1. Silencing SOD1 resulted in a 50% decrease in SOD1 mRNA (**Figure 3.4d**), consistent with the decrease in Sod1 polypeptide (**Figure 3.2a** and **3.2b**). Moreover, silencing SOD1 in Wnt3a stimulated cells reversed the Wnt-induced increase in expression of β-catenin (**Figure 3.4a**), c-Myc (**Figure 3.4b**), and Cyclin D1 (**Figure 3.4c**) mRNA as expected.

Given that Wnt/β-catenin target genes are associated with proliferative metabolism, we assessed if SOD1 silencing reversed Wnt-induced cell proliferation. Wnt stimulation results in a pronounced enhancement in cell proliferation by 48 hours (**Figure 3.4e**). However, in *SOD1* silenced cells, the Wnt-mediated stimulation in proliferation at 48 hours is completely reversed (**Figure 3.4e**). Notably, simply silencing SOD1 in the

absence of Wnt3a stimulation does not cause growth defects at any time point, indicating that the ~50% depletion in SOD1 does not result in overt oxidative stress. Altogether, our data support a role for SOD1 in regulating the Wnt signaling pathway.

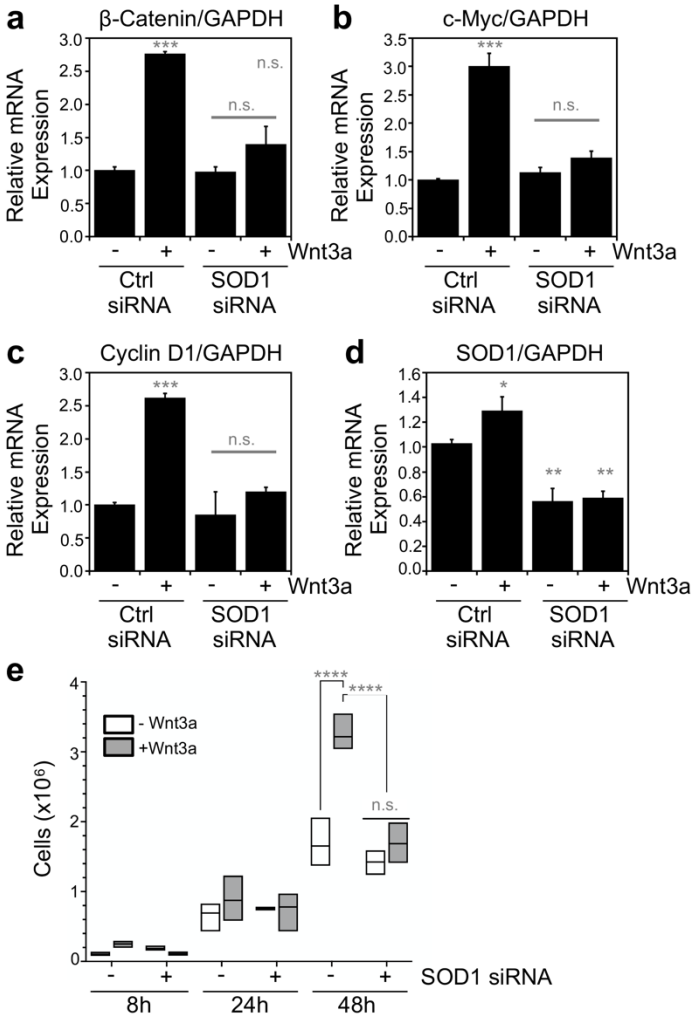

Figure 3.4. Sod1 regulates Wnt3a-dependent gene expression and HEK293 cell proliferation. (**a-d**) Normalized mRNA expression of (**a**) β-catenin, (**b**) c-Myc, (**c**) Cyclin D1, and (**d**) SOD1 relative to GAPDH as measured by qRT-PCR in response to Wnt3a activation and/or silencing of Sod1 with siRNA. The indicated values represent the mean ± s.d. from triplicate cultures. (**e**) Cell proliferation in response to Wnt3a activation and/or silencing of Sod1 with siRNA. The statistical significance relative to – Wnt3a/Ctrl RNAi cells or for the indicated pairwise comparison is denoted by grey asterisks and determined by ordinary one-way ANOVA with the Bonferroni multiple-comparison post-hoc test. * $P < 0.05$, ** $P < 0.01$, *** $P < 0.001$, **** $P < 0.0001$, n.s. = not significant.

3.5. Discussion

Wnt signaling critically regulates cell fate, proliferation, motility, and differentiation during development and in adult tissues. Dysregulation of the Wnt pathway is associated with many diseases, including various cancers and neurodegenerative disorders [209]. The plasma membrane casein kinases, Yck1/2 in yeast and CK1γ in humans, integrate extracellular ligand binding events to an intracellular signaling cascade that ultimately results in changes in gene expression and cell physiology (**Figure 3.1**). Herein, we report that SOD1 regulates CK1γ expression in human embryonic kidney 293 (HEK293) cells and is required for canonical Wnt signaling and Wnt-dependent gene expression and cell proliferation. The hardwiring of Yck1/CK1γ stability to Sod1 tightly links redox homeostasis and peroxide signaling to nutrient and cytokine sensing pathways in control of cell physiology and metabolism. Our findings have a number of implications for the redox regulation of the Wnt pathway, redox signaling, and Sod1 biology.

H_2O_2 has long been known to regulate Wnt signaling, albeit its effects are paradoxically associated with being both activating and inhibitory [210, 211]. For instance, supplementation with high doses of exogenous peroxide (~100 μM) was found to inhibit Wnt signaling in HEK293 cells [212] lines. On the other hand, it was also found that low doses of H_2O_2 rapidly stabilize β-catenin and increases the expression of Wnt target genes [213]. Thus, both physiological redox signaling and pathological oxidative stress have the potential to modulate Wnt signaling, with very different physiological consequences.

The activating effects of H_2O_2 were first ascribed to the redox regulation of nucleoredoxin (Nrx) mediated control of Dishevelled (Dvl) [211]. Dvl inhibits the GSK3β mediated phosphorylation of β-catenin in the β-catenin destruction complex, leading to the proteasomal degradation of β-catenin [214] (**Figure 3.1b**). Nrx is a thioredoxin-like enzyme that reduces oxidized thiols on target proteins. Reduced Nrx interacts with and

inhibits Dvl and this regulation is inhibited by treatment with H_2O_2 due to its ability to oxidize Nrx. The physiological source of peroxides for Wnt signaling is in part dependent on the NADPH oxidase, Nox1 [215]. Our finding that Sod1 regulates Yck1/CK1γ stability places an additional layer of redox control upstream of Dvl and the β-catenin destruction complex.

There may multiple physiological benefits for two-tiered regulatory control for peroxide signaling in a single pathway. Spatial and temporal control of peroxide signals acting on two separate targets would allow for a greater degree of pathway regulation and fine-tuning. Additionally, two separate targets of redox signaling, either through the upstream Sod1/CK1γ axis or the downstream Nrx-Dvl axis, would allow for Wnt-dependent or Wnt-independent peroxide control of β-catenin signaling, respectively. Also, since CK1γ functions in other pathways, including TGF-β signaling [216], Sod1/peroxide control of CK1γ would allow for the redox regulation of these other pathways while peroxide regulation of the Nrx-Dvl axis would ensure H_2O_2 maintains control of β-catenin signaling.

Our work continues to expand our understanding of the redox cell biology of Sod1. The canonical role for Sod1 is to detoxify superoxide radicals. However, we previously discovered that in *Saccharomyces cerevisiae*, < 1% of the total Sod1 pool is sufficient to protect against cell wide markers of superoxide toxicity [81]. Rather, much larger quantities of Sod1 are apparently required for redox signaling, and, in particular, control of Yck1/2 stability and nutrient sensing and signaling pathways [35, 81]. Thus, we proposed that the vast majority of Sod1 is required to provide a high localized flux of peroxide to control various redox signaling pathways rather than to combat superoxide stress [81]. Our studies in HEK293 cells are consistent with this hypothesis. Silencing of *SOD1* using RNA interference, which resulted in a ~50-80% decrease in Sod1 expression and activity, did not result in increased expression of antioxidant enzymes to account for loss of *SOD1*, including peroxiredoxin 1 and 2 (Prx1, 2), thioredoxin (Trx1) and glutathione peredoxidase

(GPx), or enhanced peroxiredoxin hyperoxidation (Prx-SO_3) (**Figure A.1**). This indicates that loss of the bulk of Sod1 does not have any effect on cellular oxidative stress status, suggesting that the vast majority of Sod1 is dispensable for oxidative stress protection in mammalian cell lines, analogous to yeast. Moreover, loss of ~60% Sod1 does not affect cell proliferation. A Sod1-dependent growth defect was only observed when cells were stimulated with Wnt3a, a condition requiring the Sod1-mediated redox control of Wnt signaling (**Figure 3.4e**).

In light of the totality of our studies in yeast [81] and human cell lines herein, we propose that many of the physiological defects associated with diminution of Sod1 expression or activity are tied to loss of peroxide signaling rather than superoxide toxicity. Consistent with this hypothesis, Gomez *et. al.* found that *SOD1* is essential for oncogene-driven mammary tumor formation but dispensable for normal development and proliferation [217]. While the authors suggested this was due to increased superoxide burden in tumor cells, we would argue that this is due to the requirement for SOD1-derived peroxide to signal proliferative growth and metabolism.

From a signaling perspective, Sod1 is most typically associated with integrating redox and nutrient/growth factor signaling to control proliferation and metabolism. For instance, Sod1-derived peroxides oxidatively inactivate cysteine dependent tyrosine phosphatases, which otherwise act to inhibit growth factor signaling pathways [31]. In another example, we previously found that SIRT5 can deacetylate Sod1 at K122, which enables Sod1 to translocate to the mitochondrial IMS and suppress respiratory metabolism [115]. Given that nutrient status can alter NAD^+ levels, the sirtuin SIRT5-dependent regulation of Sod1 may be a mechanism to link nutrient availability to energy metabolism and proliferation [115]. In addition, it was recently demonstrated that Sod1 is reversibly phosphorylated at S39 in yeast or T40 in human cell lines by the nutrient sensing mTORC1 to regulate redox homeostasis and adaptation to changes in nutrient availability

[113]. Thus, the growth and metabolic defects associated with inhibition of Sod1 activity or expression may be a consequence of suppressing peroxide-dependent pro-growth pathways. By extension, we posit that significant toxicity from superoxide only ensues when *SOD1* expression or activity is completely abolished, as in knockout models.

Altogether, our results have implications for understanding the basic redox biology of Sod1 and may better inform the treatment of diseases associated with aberrant Wnt signaling. Indeed, some cancers have a marked overexpression in CK1γ [216], providing the impetus to develop CK1γ inhibitors [218]. In addition, certain cancers, including head and neck, lung and breast cancers, exhibit elevated Wnt signaling and Sod1 expression [121, 217, 219-223], suggesting that there may be feed-forward mechanisms of Sod1-dependent Wnt pathway activation. Indeed, Wnt3a stimulation of HEK293 cells is associated with elevated Sod1 transcription (**Figure 3.4d**). In total, our results suggest that inhibiting Sod1 in cancers associated with elevated CK1γ and/or Wnt activation may be a fruitful therapeutic strategy.

CHAPTER 4

Sod1 Integrates Oxygen Availability to Redox Regulate NADPH Production and the Thiol Redoxome

This chapter is adapted from the previously submitted work: Montllor-Albalate, Kim, H., Jonke, A. P., Torres, M. P., Reddi, A. R. “Sod1 Integrates Oxygen Availability to Redox Regulate NADPH Production and the Thiol Redoxome”. The author of this document contributed to this work by conceiving, designing and performing all the experiments of the paper, except the mass spectrometry and bioinformatic analysis, making all figures, except the mass spectrometry figures, making all supplementary materials, and co-writing the manuscript with input from all authors.

The experiments and data analysis for the proteomics section of this chapter were performed by Hyojung Kim, a graduate student in the Reddi and Torres lab, with the help of Alex P. Jonke.

4.1. Abstract

Cu/Zn superoxide dismutase (Sod1) is a highly conserved and abundant antioxidant enzyme that detoxifies superoxide ($O_2^{\bullet -}$) by catalyzing its conversion to dioxygen (O_2) and hydrogen peroxide (H_2O_2). Using *Saccharomyces cerevisiae* and mammalian cells, we discovered that a major new aspect of the antioxidant function of Sod1 is to integrate O_2 availability to promote NADPH production. The mechanism involves Sod1-derived H_2O_2 oxidatively inactivating the glycolytic enzyme, glyceraldehyde phosphate dehydrogenase (GAPDH), which in turn re-routes carbohydrate flux to the oxidative phase of the pentose phosphate pathway (oxPPP) to generate NADPH. The

aerobic oxidation of GAPDH is exclusively dependent on and rate-limited by Sod1. Thus, Sod1 senses O_2 via $O_2^{\bullet-}$ to balance glycolytic and oxPPP flux, through control of GAPDH activity, for adaptation to life in air. Importantly, this new mechanism for Sod1 antioxidant activity requires the bulk of cellular Sod1, unlike for its role in protection against $O_2^{\bullet-}$ toxicity, which only requires < 1% of total Sod1. Using mass spectrometry, we identified proteome-wide targets of Sod1-dependent redox signaling, including numerous metabolic enzymes. Altogether, Sod1-derived H_2O_2 is important for antioxidant defense and a master regulator of metabolism and the thiol redoxome.

4.2. Introduction

Superoxide dismutases (SODs) are a highly conserved class of antioxidant enzymes that serve on the frontline of defense against reactive oxygen species (ROS). SODs, which detoxify $O_2^{\bullet-}$ by catalyzing its disproportionation into O_2 and H_2O_2, are unique amongst antioxidant enzymes in that they also produce a ROS byproduct. While much is known about the necessity of scavenging $O_2^{\bullet-}$, it is less clear what the physiological consequences of SOD-derived H_2O_2 are. Paradoxically, increased expression of Cu/Zn SOD (Sod1), which accounts for the majority of SOD activity in cells [224], is actually associated with reduced cellular H_2O_2 levels [225], suggesting there may be additional unknown mechanisms underlying Sod1 antioxidant activity.

The cytotoxicity of $O_2^{\bullet-}$ is largely due to its ability to oxidize and inactivate [4Fe-4S] cluster-containing enzymes, which results in defects in metabolic pathways that utilize [4Fe-4S] proteins and Fe toxicity due to its release from damaged Fe/S clusters [57, 122, 123, 226]. The released Fe can catalyze deleterious redox reactions, and, in particular, production of hydroxyl radicals ($^{\bullet}OH$) via Haber-Weiss and Fenton reactions, which indiscriminately oxidizes lipids, proteins, and nucleic acids [123, 124]. The importance of

Sod1 in oxidative stress protection is underscored by reduced proliferation, decreased lifespan, and numerous metabolic defects, including cancer, when *SOD1* is deleted in various cell lines and/or organisms [80, 82, 124, 156, 227]. It was previously proposed that Sod1 limits steady-state H_2O_2 levels because of its ability to prevent the $O_2^{\bullet-}$-mediated one-electron oxidation of Fe/S clusters, which results in the concomitant formation of H_2O_2 [225, 228, 229]. However, since vanishingly small amounts of Sod1, < 1% of total cellular Sod1, is sufficient to protect cells against $O_2^{\bullet-}$ toxicity, including oxidative inactivation of Fe/S enzymes [35, 112, 159], any changes in Sod1 expression is not expected to alter H_2O_2 arising from $O_2^{\bullet-}$ oxidation of Fe/S clusters. How then can Sod1, an enzyme that catalyzes H_2O_2 formation, act to reduce cellular H_2O_2 levels?

Two previously reported but unexplained metabolic defects in *sod1*Δ strains of *Saccharomyces cerevisiae* point to a potential role for Sod1 in regulating the production of NADPH, a key cellular reductant required for reductive biosynthesis and the reduction and regeneration of H_2O_2 scavenging thiol peroxidases [10] and catalases [11, 230]. Yeast strains lacking *SOD1* exhibit increased glucose consumption [170] and defects in the oxidative phase of the pentose phosphate pathway (oxPPP) [157], the primary source of NADPH. Inhibition of key rate-limiting enzymes in glycolysis, including phosphofructose kinase [231], glyceraldehyde phosphate dehydrogenase (GAPDH) [232, 233], and pyruvate kinase [234, 235], reduces glucose uptake [236-238] and increases the concentration of glucose-6-phosphate (G6P), a glycolytic intermediate that is also the substrate for the first enzyme in the oxPPP, G6P dehydrogenase (G6PDH), which in turn increases oxPPP flux and NADPH production [239-244]. Taken together, we surmised that Sod1 negatively regulates a rate determining enzyme in glycolysis, thereby accounting for the observed metabolic defects in glucose utilization and the oxPPP in *sod1*Δ cells [157, 170].

GAPDH, which catalyzes a rate-determining step in glycolysis [245, 246], is very abundant [247], and contains a H_2O_2-reactive catalytic Cys ($k \sim 10^2$-10^3 $M^{-1}s^{-1}$), represents a critical redox regulated node that can toggle flux between glycolysis and the oxPPP [241]. As such, we hypothesized that a novel aspect of the antioxidant activity of Sod1 is to oxidatively inactivate GAPDH using Sod1-catalyzed H_2O_2, which would in turn stimulate NADPH production via the oxPPP and enhance cellular peroxide scavenging by thiol peroxidases. This novel mechanism for Sod1 mediated antioxidant activity would explain a number of prior observations, including the findings that elevated Sod1 expression decreases peroxide levels and loss of *SOD1* increases glucose consumption and attenuates oxPPP activity. In addition, more generally, since Sod1-derived H_2O_2 has previously been implicated in the redox regulation of other enzymes, including protein tyrosine phosphatases [31] and casein kinases [35, 112], we also sought to identify proteome-wide redox targets of Sod1.

In the present report, we provide evidence highlighting a new antioxidant function for Sod1-derived H_2O_2 in integrating O_2 availability to control NADPH production to support aerobic growth and metabolism. The mechanism involves the conversion of O_2 to $O_2^{\bullet-}$ by mitochondrial respiration and an NADPH oxidase, followed by the Sod1-catalyzed conversion of $O_2^{\bullet-}$ to H_2O_2, which in turn oxidatively inactivates GAPDH. The inhibition of GAPDH serves to re-route metabolism from glycolysis to the oxPPP in order to maintain sufficient NADPH for metabolism in air. The aerobic oxidation of GAPDH is exclusively dependent on and rate-limited by Sod1, suggesting that it provides a privileged pool of peroxides to inactivate GAPDH under physiological conditions. Lastly, we revealed a larger network of cysteine-containing proteins that are oxidized in a Sod1-dependent manner using mass spectrometry-based redox proteomics approaches. Altogether, these results highlight a new mechanism for O_2 sensing and adaptation, reveal an important but previously unknown antioxidant role of Sod1 that goes beyond $O_2^{\bullet-}$ scavenging to include

the stimulation of aerobic NADPH production, and places Sod1 as a master regulator of proteome-wide thiol oxidation and multiple facets of metabolism.

4.3. Results

4.3.1. Sod1 regulates glycolysis.

In many eukaryotes, including *Saccharomyces cerevisiae*, glucose uptake negatively correlates with pO_2 [248-251]. Indeed, we find that batch cultures of WT yeast cells grown anaerobically consume more glucose per cell than aerobically grown cultures (**Figures 4.1A** and **4.1B**). Media glucose concentration is plotted versus cell density, rather than time, to correct for differences in growth rate (**Figure B.1A**). Consistent with previous studies [170], aerobic cultures of *sod1*Δ strains consume more glucose than WT cells (**Figures 4.1A** and **4.1B**). However, in the absence of oxygen, both WT and *sod1*Δ cells consume similar amounts of glucose (**Figures 4.1A** and **4.1B**).

Since defects in glycolytic enzymes, including hexokinase 2 or GAPDH, decrease glucose uptake [236, 237], we sought to determine if the increased glucose consumption of *sod1*Δ cells was associated with altered glycolytic flux. Intracellular cytosolic pH is an excellent reporter of glycolytic activity and can be monitored using the GFP-based ratiometric pH sensor, pHluorin. Glucose starved yeast exhibit an intracellular cytosolic pH of ~7.0. Upon exposure to glucose, there is a rapid decrease in cytosolic pH to a value of ~6.6 within 3 minutes, corresponding to proton release in phosphorylation reactions associated with hexokinase, phosphofructose kinase, and GAPDH (**Figures 4.1C** and **4.1D**, phase 1) [252]. The initial acidification is followed by a slower alkalization phase that brings the cytosolic pH up to ~7.3 over 15 minutes (**Figures 4.1C** and **4.1D**, phase 2), which is due to activation of Pma1, a cell surface H^+-ATPase that pumps H^+ into the

extracellular space [252]. In response to glucose, *sod1*Δ cells exhibit more rapid rates of intracellular acidification, indicating that glycolysis is more active compared to WT cells. Moreover, *sod1*Δ cells exhibit slightly diminished rates of re-alkalization, indicating that PMA1 is less active in response to glucose. Indeed, prior work found that *sod1*Δ cells exhibit a defect in PMA1 activity [35, 253]. To rule out that the intracellular acidification phase is unaffected by PMA1-dependent re-alkalization, glucose-dependent changes in intracellular pH were monitored in a strain expressing a hypomorphic allele of PMA1, *pma1-tap*, containing a C-terminal tandem affinity purification (TAP)-tag (**Figure B.1B**). In *pma1-tap* cells, the rate of glucose-induced acidification is similar to WT cells (**Figure 4.1D**, Phase 1), but there is a significant decrease in the rate of re-alkalization (**Figure 4.1D,** Phase 2). Taken together, the data demonstrate that Sod1 negatively regulates glucose uptake and glycolytic activity.

4.3.2. Extra-mitochondrial Sod1 regulates GAPDH oxidation and activity.

We hypothesized that Sod1-derived H_2O_2 may negatively regulate glucose uptake and glycolytic activity through the oxidative inactivation of GAPDH, which catalyzes a rate-determining step in glycolysis and contains a peroxide-sensitive active site Cys [232]. *Saccharomyces cerevisiae* encodes three GAPDH isoforms, *TDH1*, *TDH2*, and *TDH3*, with *TDH3* being the most highly expressed in log phase cultures, accounting for > 50% of total cellular GAPDH [192]. Yeast GAPDH has only two cysteines, catalytic C150 and C154, which sensitizes C150 to oxidation by H_2O_2 (**Figure 4.1E**). In order to probe the Sod1-dependence of GAPDH oxidation, we employed a thiol alkylation assay that exploits the reactivity of methoxypolyethylene glycol maleimide (mPEG-mal) with reduced but not oxidized thiols [254]. The extent of GAPDH labeling with mPEG-mal, which is 5 kDa, is assessed by determining the changes in electrophoretic mobility of PEGylated GAPDH,

corresponding to single and double labeled GAPDH at reduced C150 and/or C154 (**Figures 4.1F, 4.1G** and **B.1C**). Thus, the fraction of GAPDH oxidized *in vivo* can be determined by quantifying the ratio of the intensity of unlabeled GAPDH (oxidized GAPDH) to total GAPDH (**Figures B.1D** and **B.1F-B.1M)**. The mPEG-mal approach was validated by treating cells with H_2O_2 and observing a 2-fold increase in GAPDH oxidation (**Figure B.1D** and **B.1E**). Moreover, the identity of the specific sites of mPEG-mal labeling was confirmed by observing that a yeast strain expressing a single allele of $Tdh3^{C154S}$ was found to have only two GAPDH proteoforms corresponding to single and unlabeled GAPDH (**Figure B.1N**).

To determine if Sod1 oxidizes GAPDH *in vivo*, we analyzed GAPDH PEGylation in *sod1*Δ cells expressing empty vector (EV) (*sod1*Δ + EV) or WT *SOD1* (*sod1*Δ + *SOD1*). Interestingly, *sod1*Δ + EV cells exhibit an increase in mPEG-mal labeling compared to *sod1*Δ + *SOD1* cells (**Figures 4.1G**-**1I**), indicating that GAPDH is more oxidized in cells expressing *SOD1*. Over 4-independent trials, we found that cells expressing *SOD1* exhibit a ~2-fold increase in GAPDH oxidation compared to cells not expressing *SOD1* (**Figure 4.1H**). Due to variations in the absolute levels of GAPDH oxidation across multiple trials (**Figure 4.1H**), we also chose to normalize oxidation levels to *SOD1* expressing cells within each trial (**Figure 4.1I**). Such an analysis accounts for trial-to-trial variation in GAPDH oxidation and increases the statistical significance of the results between various strains.

We next evaluated the effect of Sod1-mediated GAPDH oxidation on GAPDH catalytic activity. GAPDH catalyzes the oxidative phosphorylation of GAP to 1,3 BPG and requires Cys^{150} for activity. GAPDH activity is 3-fold greater in cells lacking *SOD1* (*sod1*Δ + EV*)* (**Figures B.1J**, **B.1O** and **B.1P**), which correlates with the 2-fold decrease in GAPDH oxidation relative to *SOD1* expressing cells (**Figures 4.1G** and **4.1I**).

Notably, Sod1-mediated GAPDH oxidation is not dependent on the carbon source. In yeast, glucose represses mitochondrial respiration and promotes fermentation. Galactose is a fermentable carbon source that alleviates respiration repression, resulting in more mitochondrial respiratory activity [35]. The absolute (**Figure B.1R**) and relative (**Figure 4.1L**) amounts of GAPDH oxidation in *sod1*Δ + EV and *sod1*Δ + *SOD1* cells cultured in 2% galactose is similar to cells cultured in 2% glucose. (**Figures 4.1K, 4.1L, B.1Q** and **B.1R)**.

We next evaluated the effect of Sod1 localization on GAPDH oxidation. Sod1 is primarily cytosolic but is also present in the mitochondrial IMS. *sod1*Δ cells expressing an IMS-targeted allele of Sod1, Sco2-SOD1 [35, 112, 255], exhibit comparable GAPDH oxidation to *sod1*Δ + EV cells, both of which are significantly lower than cells expressing WT *SOD1* (**Figures 4.1M, 4.1N** and **B.1S**). Altogether, these results indicate that extramitochondrial Sod1-derived H_2O_2 oxidizes GAPDH and decreases its catalytic activity, thereby explaining the previous observations that *sod1*Δ cells exhibit increased glucose uptake (**Figures 4.1A** and **4.1B**) and glycolytic activity (**Figures 4.1C** and **4.1D**).

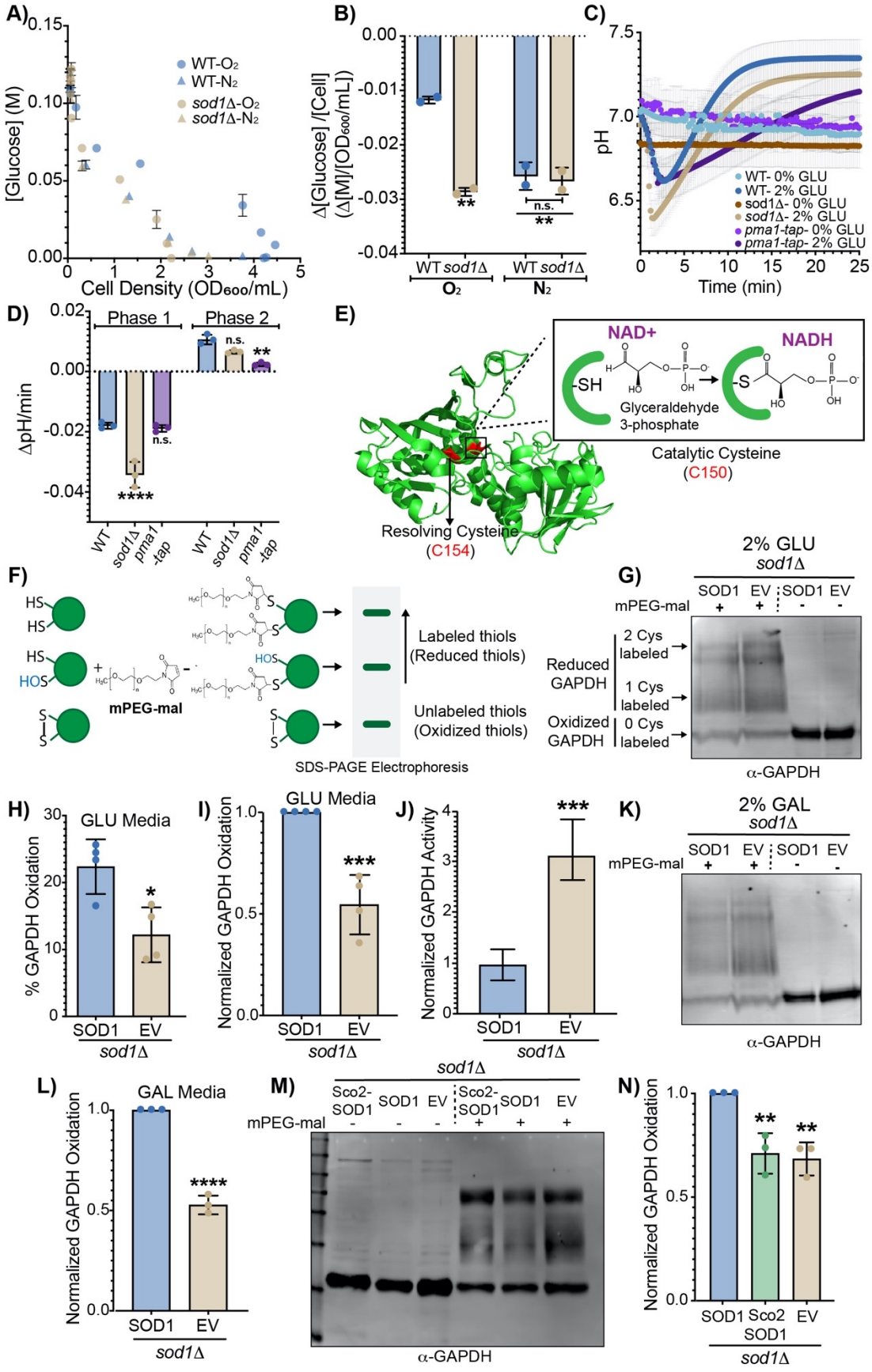
A)
[Glucose] (M)
Cell Density (OD600/mL)
WT-O2
WT-N2
sod1Δ-O2
sod1Δ-N2
B)
Δ[Glucose] /[Cell]
(Δ[M]/[OD600/mL])
WT sod1Δ
O2
WT sod1Δ
N2
n.s.
C)
pH
Time (min)
WT- 0% GLU
WT- 2% GLU
sod1Δ- 0% GLU
sod1Δ- 2% GLU
pma1-tap- 0% GLU
pma1-tap- 2% GLU
D)
ΔpH/min
Phase 1
Phase 2
WT
sod1Δ
pma1-tap
E)
NAD+
NADH
-SH
Glyceraldehyde 3-phosphate
Catalytic Cysteine (C150)
Resolving Cysteine (C154)
F)
mPEG-mal
Labeled thiols (Reduced thiols)
Unlabeled thiols (Oxidized thiols)
SDS-PAGE Electrophoresis
G)
2% GLU
sod1Δ
SOD1
EV
mPEG-mal
Reduced GAPDH
2 Cys labeled
1 Cys labeled
Oxidized GAPDH
0 Cys labeled
α-GAPDH
H)
GLU Media
% GAPDH Oxidation
SOD1
EV
sod1Δ
I)
GLU Media
Normalized GAPDH Oxidation
J)
Normalized GAPDH Activity
K)
2% GAL
sod1Δ
α-GAPDH
L)
GAL Media
Normalized GAPDH Oxidation
M)
sod1Δ
Sco2-SOD1
mPEG-mal
α-GAPDH
N)
Normalized GAPDH Oxidation
SOD1
Sco2 SOD1
EV

Figure 4.1. Cytosolic Sod1 regulates glycolysis via the redox regulation of GAPDH.
(A-B) Extracellular glucose measurements as a function of culture density for WT and *sod1*Δ cells grown aerobically (O_2) or anaerobically (N_2) (**A**) and glucose consumption per cell as derived from the slope of the linear regions of the plot (**B**). The data represent the average ± SD from two biological replicates (See also Figure B.1A).
(C-D) Time-resolved intracellular pH measurements of glucose starved cells upon pulsing WT, *sod1*Δ, or *pma1*-tap cells expressing a GFP-based pH sensor, pHluorin, with 2% or 0% glucose (GLU) (**C**). The cytosolic acidification rate, a proxy for glycolytic activity (Phase 1), and the rate of re-alkalization of the cytosol, a proxy for Pma1 activity (Phase 2), is shown for the indicated strains (**D**). The data represent the average ± SD from triplicate cultures. See also Figure B.1B.
(E) The structure of *Saccharomyces cerevisiae* GAPDH, Tdh3 (PDB file 4IQ8), with catalytic Cys_{150} and resolving Cys_{154} represented in red, and a depiction of the Cys_{150} thioester covalent intermediate with glyceraldehyde-3-phosphate.
(F-I) Analysis of Sod1-dependent GAPDH oxidation as assessed by labelling GAPDH with thiol reactive methoxypolyethylene glycol maleimide (mPEG-mal). **(F)** Schematic representation of all possible redox-dependent GAPDH (green spheres) Cys-mPEG-mal adducts and their respective electrophoretic mobilities. (**G**) Representative immunoblot analysis of GAPDH-mPEG-mal adducts in *sod1*Δ cells expressing yeast Sod1 (SOD1) or empty vector (EV) cultured in 2% GLU. (**H**) % GAPDH oxidation, as assessed by quantifying the ratio of mPEG-mal labelled GAPDH to total GAPDH, in the indicated strains from multiple trials. (**I**) Relative GAPDH oxidation in the indicated strains as assessed by normalizing to the % GAPDH oxidation of *SOD1* expressing cells from each trial. Data represents the average ± SD from 4 independent trials.
(J) Measurements of GAPDH enzymatic activity in *sod1*Δ cells expressing SOD1 or EV. Data represents the average ± SD from quadruplicate cultures. See also Figures B.1O-P.
(K-L) Assessment of GAPDH oxidation in *sod1*Δ cells expressing yeast Sod1 (SOD1) or empty vector (EV) cultured in 2% galactose (GAL). Representative immunoblot analysis of GAPDH-mPEG-mal adducts (**K**) and normalized GAPDH oxidation from multiple trials (**L**). Data represents the average ± SD from 3 independent trials. See also Figures B.1Q and B.1R.
(M-N) Assessment of GAPDH oxidation in *sod1*Δ cells expressing yeast Sod1 (SOD1), mitochondrial IMS targeted Sod1 (Sco2-SOD1), or empty vector (EV). Representative immunoblot analysis of GAPDH-mPEG-mal adducts (**M**) and normalized GAPDH oxidation from multiple trials (**L**) in the indicated strains. Data represents the average ± SD from 3 independent trials. See also Figure B.1S.
The statistical significance is indicated by asterisks using two-tailed Student's t-tests for pairwise comparisons (panels **H**, **I**, **J**, and **L**) or by one-way ANOVA for multiple comparisons with Dunett's post-hoc test (panels **B**, **D** and **N**); *p<0.05, **p<0.01, ***p>0.001, ****p<0.0001, n.s.= not significant.

4.3.3. Yno1 and mitochondrial respiration are sources of superoxide for GAPDH oxidation.

Sod1 requires a superoxide source to catalyze peroxide production for the control of GAPDH oxidation and activity. As with higher eukaryotes, two primary sources of superoxide in yeast include mitochondrial respiration and the yeast NADPH oxidase, Yno1 [256]. Both sources contribute towards GAPDH oxidation as respiration deficient *rho*^{0} and *yno1*Δ cells exhibit a ~3-fold lower degree of GAPDH oxidation relative to WT cells and phenocopy the *sod1*Δ mutant (**Figures 4.2A**, **4.2B** and **B.2A**). Furthermore, overexpression of Yno1 on a galactose-inducible promoter (pYES-YNO1, 3%GAL), which resulted in a ~30% increase in DHE-detectable superoxide (**Figure B.2B**), promoted GAPDH oxidation by 2-fold as compared to cells expressing empty vector (pYES2-EV, 0 and 3%GAL) or that were cultured in non-inducing media (pYES2-YNO1, 0%GAL) (**Figures 4.2C**, **4.2D** and **B.2C**). In total, these results indicate that both Yno1 and mitochondrial respiration are sources of the superoxide substrate required by Sod1 to drive the H_2O_2 dependent oxidation of GAPDH.

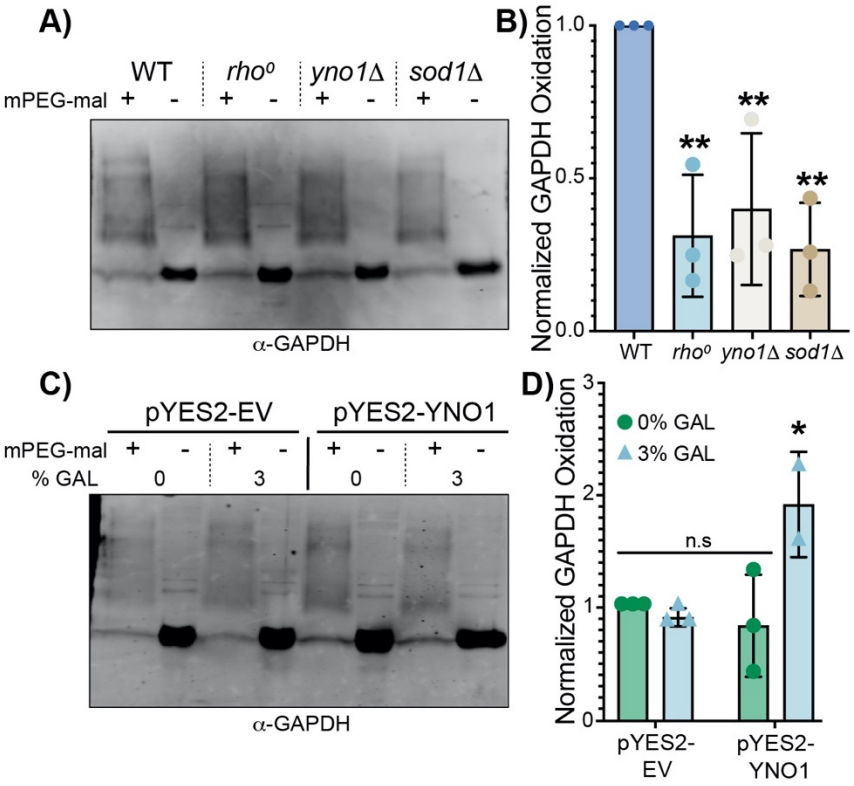

Figure 4.2. Yno1 and mitochondrial respiration are sources of superoxide for GAPDH oxidation.

(**A**-**B**) Representative immunoblot analysis of GAPDH oxidation as assessed by mPEG-mal labeling of GAPDH in WT, *rho*^{0}, *yno1*Δ and *sod1*Δ cells cultured in 2% GLU **(A)** and normalized GAPDH oxidation from multiple trials (**B**). Data represents the average ± SD from 3 independent trials. See also Figure B.2A.

(**C**-**D**) Representative immunoblot analysis of GAPDH oxidation as assessed by mPEG-mal labeling of GAPDH in WT cells expressing GAL1-driven *YNO1* (pYES2-YNO1) or empty vector (pYES2-EV) cultured in 2% raffinose, supplemented with non-inducing (0%) or inducing (3%) GAL concentrations and (**C**) the normalized GAPDH oxidation from multiple trials (**D**). Data represents the average ± SD from 3 independent cultures. See also Figures B.2B-B.2C.

The statistical significance relative to WT (panel **B**) or pYES2-EV 0%GAL (panel **D**) is indicated by asterisks using ordinary one-way ANOVA or two-way ANOVA with Dunett's post-hoc test for the indicated pairwise comparisons in panel **B** and **D**, respectively; *p<0.05, **p<0.01, ***p>0.001, ****p<0.0001, n.s.= not significant.

4.3.4. O_2 dependent GAPDH oxidation is exclusively dependent on and rate limited by SOD1.

All metabolic sources of superoxide and peroxide are ultimately derived from O_2. We therefore sought to determine if Sod1 is the sole enzymatic adapter that links oxygen availability to the control of GAPDH oxidation and if GAPDH oxidation is rate-limited by Sod1. Towards this end, we first asked if Sod1 mediates O_2-dependent GAPDH oxidation. Since WT Sod1 is transcriptionally and post-translationally down-regulated in response to hypoxia and anoxia (Brown et al., 2004; Leitch et al., 2009; Leitch et al., 2012; White et al., 2009), we utilized *sod1*Δ cells expressing *ADH1*-driven $Sod1^{P144S}$, which is a mutant previously engineered to constitutively express mature enzymatically active Sod1 even in the absence of O_2 [35, 188]. Indeed, the $Sod1^{P144S}$ mutant is enzymatically active in lysates derived from both aerobic and anaerobic cultures, whereas WT Sod1 is only fully active in lysates derived from aerobically cultured cells (**Figures 4.3A** and **4.3B**). *sod1*Δ cells expressing WT or $Sod1^{P144S}$ exhibit a nearly 2-fold decrease in GAPDH oxidation when cultured anaerobically, consistent with the requirement for O_2 as the metabolic origin of superoxide and peroxide (**Figures 4.3C**, **4.3D** and **B.2D**). However, remarkably, the O_2-dependence of GAPDH oxidation is completely lost in cells lacking *SOD1*. Furthermore, we determined that the oxidation of GAPDH is rate limited by Sod1, finding that GAL-regulated titration of Sod1 levels results in a dose-dependent increase in GAPDH oxidation (**Figures 4.3E**, **4.3F** and **B.2E**). Altogether, these results indicate that the aerobic oxidation of GAPDH is exclusively dependent on and rate limited by Sod1.

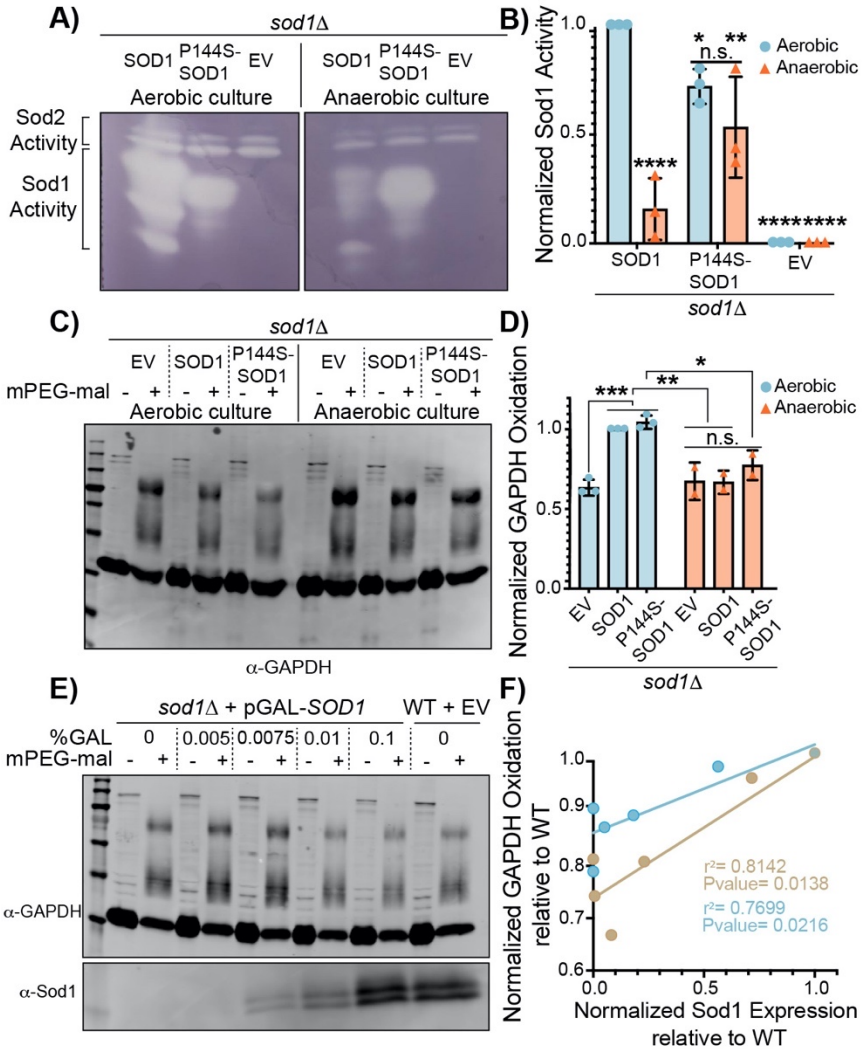

Figure 4.3. O_2 dependent GAPDH oxidation is exclusively dependent on and rate limited by Sod1.

(A-D) Assessment of the Sod1-dependence on the aerobic oxidation of GAPDH. (**A**) Representative SOD activity gel to assess aerobic and anaerobic Sod1 maturation in *sod1*Δ cells expressing empty vector, WT SOD1, or the P144S *sod1* mutant and (**B**) normalized levels of mature Sod1 from multiple trials. Data represents the average ± SD from 3 independent cultures. (**C**) Representative immunoblot analysis of GAPDH oxidation as assessed by mPEG-mal labeling of GAPDH in aerobic or anaerobic *sod1*Δ cells expressing empty vector, WT SOD1, or the P144S *sod1* mutant and (**D**) the normalized GAPDH oxidation from multiple trials. Data represents the average ± SD from two or three independent trials. See also Figure B.2D.

(**E-F**) Representative immunoblot analysis of GAPDH oxidation in WT or *sod1*Δ cells expressing GAL-driven *SOD1* cultured with increasing concentrations of galactose (GAL) (0%, 0.005%, 0.0075%, 0.01% and 0.1% GAL) and (**E**) the positive correlation between Sod1 expression and GAPDH oxidation from two independent trials (**F**). Sod1 expression and GAPDH oxidation were normalized to that of the WT cells and the linear regression

analysis of the two trials gives coefficients of determination (r^2) of .81 and .77, with p-values of .01 and .02, respectively. See also Figure B.2E.
The statistical significance relative to the aerobic SOD1 expressing cells is indicated by asterisks using 2-way ANOVA for multiple comparisons with Dunett's or Bonferroni post-hoc test for the indicated pairwise comparisons in panel **B** and **D**, respectively; *p<0.05, **p<0.01, ***p>0.001, ****p<0.0001, n.s.= not significant.

4.3.5. Sod1-mediated oxidative inactivation of GAPDH results in increased NADPH production and oxidative stress resistance.

We next determined if the Sod1-dependent oxidative inactivation of GAPDH results in re-routing of glycolytic metabolism towards oxPPP to produce NADPH and increase resistance to oxidative stress. Titration of Sod1 expression using a GAL-driven *SOD1* allele results in both a dose dependent increase in GAPDH oxidation as well as NADPH levels (**Figures 4.4A**-**4C** and **B.3A**-**B.3F**). Control experiments in which GAL is titrated into cells expressing a non-GAL-driven *SOD1* allele indicate that GAL alone does not alter NADPH levels (**Figure B.3G**). Moreover, *tdh3*Δ cells, which express ~60% less GAPDH than WT cells, exhibit increased NADPH levels, consistent with our finding that oxidative inactivation of GAPDH increases NADPH (**Figures 4.4D**-**4**.**4F**).

Since NADPH is required for the reduction and regeneration of numerous cellular antioxidant systems, we also determined if the alterations in Sod1-mediated NADPH production correlated with the oxidation state of Tsa1, a yeast peroxiredoxin important for oxidant defense and redox signaling that is maintained in a reduced state using reducing equivalents from NADPH. Consistent with a role for NADPH in maintaining reduced Tsa1, *zwf1*Δ cells lacking glucose-6-phosphate dehydrogenase (G6PD), which catalyzes the first committed step of the oxPPP, exhibit decreased NADPH levels and elevated Tsa1 oxidation as assessed by immunoblotting using an antibody that recognizes sulfinic acid oxidized peroxiredoxins (Prx-SO_3) (**Figure 4.4G**-**4**.**4I**). Titration of Sod1 using a GAL-

regulated promoter results in a dose dependent decrease in Tsa1 oxidation, consistent with the role of Sod1 in promoting NADPH production due to oxidative inactivation of GAPDH (**Figure 4.4J** and **4.4K**). In order to determine if the oxidative inactivation of GAPDH by Sod1 provides a physiological benefit for cells, we measured the aerobic growth and oxidative stress resistance of cells expressing low and high levels of GAPDH. Although WT and *tdh3*Δ cells have similar aerobic and anaerobic growth rates in 2% GLU (**Figure 4.4L**), when cultured in 2% GAL, a fermentable carbon source that promotes respiration in yeast, *tdh3*Δ cells have a marked enhancement in growth rate compared to WT cells (**Fig. 4.4M**). Moreover, *tdh3*Δ cells exhibit a modest, but significant, resistance to peroxide stress (**Figure 4.4N**). Altogether, the enhanced aerobic fitness and peroxide tolerance of cells depleted of GAPDH is consistent with a beneficial role for the Sod1-mediated inactivation of GAPDH.

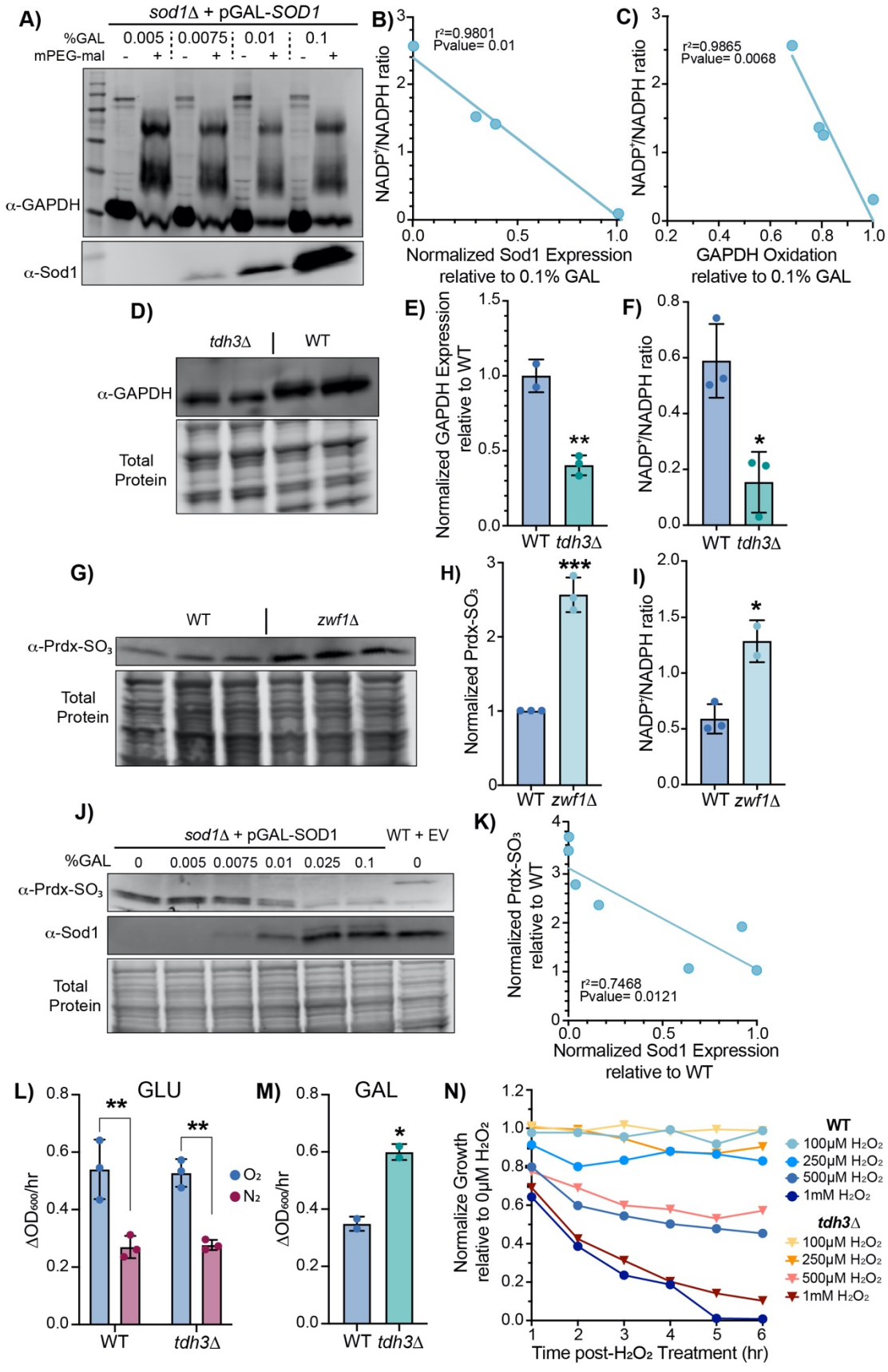
A)
sod1Δ + pGAL-SOD1
%GAL 0.005 0.0075 0.01 0.1
mPEG-mal - + - + - + - +
α-GAPDH
α-Sod1
B)
r²=0.9801
Pvalue= 0.01
NADP+/NADPH ratio
Normalized Sod1 Expression relative to 0.1% GAL
C)
r²=0.9865
Pvalue= 0.0068
NADP+/NADPH ratio
GAPDH Oxidation relative to 0.1% GAL
D)
tdh3Δ | WT
α-GAPDH
Total Protein
E)
Normalized GAPDH Expression relative to WT
WT tdh3Δ
F)
NADP+/NADPH ratio
WT tdh3Δ
G)
WT | zwf1Δ
α-Prdx-SO3
Total Protein
H)
Normalized Prdx-SO3
WT zwf1Δ
I)
NADP+/NADPH ratio
WT zwf1Δ
J)
sod1Δ + pGAL-SOD1
WT + EV
%GAL 0 0.005 0.0075 0.01 0.025 0.1 0
α-Prdx-SO3
α-Sod1
Total Protein
K)
Normalized Prdx-SO3 relative to WT
r²=0.7468
Pvalue= 0.0121
Normalized Sod1 Expression relative to WT
L)
GLU
ΔOD600/hr
O2
N2
WT tdh3Δ
M)
GAL
ΔOD600/hr
WT tdh3Δ
N)
Normalize Growth relative to 0μM H2O2
Time post-H2O2 Treatment (hr)
WT
100μM H2O2
250μM H2O2
500μM H2O2
1mM H2O2
tdh3Δ
100μM H2O2
250μM H2O2
500μM H2O2
1mM H2O2

Figure 4.4. Sod1-mediated oxidative inactivation of GAPDH results in increased NADPH production and resistance to oxidative stress.

(A-C) Sod1 expression positively correlates with GAPDH oxidation and NADPH production. (**A**) Immunoblot analysis of GAPDH oxidation as assessed by mPEG-mal labeling of GAPDH in *sod1*Δ cells expressing GAL-driven *SOD1* cultured with increasing concentrations of galactose (GAL) (0.005%, 0.0075%, 0.01% and 0.1% GAL). See also Figure B.3A (**B**-**C**) The NADP+/NADPH ratio inversely correlates with normalized Sod1 expression (**B**) and normalized GAPDH oxidation (**C**). The linear regression analysis in panels **B** and **C** gives coefficient of determinations (r^2) of .98 and .99 and p-values of .01 and .007, respectively. See also Figures B.3B-B.3H.

(D-F) Depletion of intracellular GAPDH decreases the NADP+/NADPH ratio. (**D**) Representative immunoblot analysis of GAPDH expression in WT and *tdh3*Δ cells and (**E**) normalized GAPDH expression from multiple trials. (**F**) Measurements of the NADP+/NADPH ratio in WT and *tdh3*Δ. Data represents the average ± SD from triplicate cultures.

(**G**-**I**) Ablation of glucose-6-phosphate dehydrogenase (Zwf1) increases peroxiredoxin oxidation (Prdx-SO_3) and the NADP/NADPH ratio. Representative immunoblot analysis of Prdx-SO_3 (**G**), normalized Prdx-SO_3 levels from replicates, and NADP+/NADPH ratios from WT and *zwf1*Δ cells. Data represents the average ± SD from triplicate cultures.

(**J**-**K**) Sod1 expression inversely correlates with Prdx-SO_3. (**J**) Representative immunoblot analysis of peroxiredoxin oxidation (Prdx-SO_3) and Sod1 expression in WT or *sod1*Δ cells expressing GAL-driven *SOD1* cultured with increasing concentrations of galactose (GAL) (0%, 0.005%, 0.0075%, 0.01%, 0.025%, and 0.1% GAL). (**K**) Sod1 expression inversely correlates with Prdx oxidation, with a linear regression analysis giving a coefficient of determination (r^2) of 0.75 and a p-value of .01.

(**L**-**N**) Aerobic and anerobic growth rates in 2%Glucose media (**L**), aerobic growth rate in 2%GAL media (**M**) and peroxide sensitivity of WT and *tdh3*Δ cells (**N**). Data represent the average ± SD from triplicate cultures.

The statistical significance relative to WT is indicated by asterisks using two-tailed Student's t-test for pairwise comparisons in panels **E**, **F**, **H**, and **I**; *p<0.05, ***p>0.001.

4.3.6. SOD1 regulates GAPDH oxidation in human cells.

Both Sod1 and GAPDH are highly conserved from yeast to humans. To establish the conservation of the Sod1-GAPDH redox-signaling axis, we employed human embryonic kidney HEK293 cells. It is worth noting that human GAPDH has an additional peroxide reactive Cys, which would result in 3 PEGylated proteoforms, corresponding to triple-, double-, and single-labeled GAPDH in immunoblots (**Figures B.4A**-**B.4C**). As expected, cells treated with H_2O_2 exhibited less mPEG-mal labelling, indicating a larger fraction of oxidized GAPDH compared to non-treated cells (**Figure B.4B**). To determine if Sod1 promoted GAPDH oxidation, we depleted Sod1 in HEK293 cells using small interfering RNA against Sod1 (siSOD1) or scrambled control RNAi (siCTRL). Across various trials, we consistently observed a depletion of ~60-80% of Sod1 (**Figures 4.5A** and **4.5B)** and a corresponding decrease in GAPDH oxidation (**Figures 4.5C**, **4.5D**, **B.4C** and **B.4D**). The extent to which Sod1 promotes GAPDH oxidation ranges from ~7 to 16%, which is comparable to the contribution observed from exogenous peroxide treatment (**Figure B.4B**). Moreover, as with yeast, we find that Sod1 expression levels across multiple trials positively correlate with GAPDH oxidation (**Figure 4.5E**). The correlation coefficient (r^2) from a linear regression analysis is 0.7605, with p = .0022. Notably, the y-intercept of the linear regression is close to 0, indicating that in the complete absence of Sod1, GAPDH oxidation is expected to be ~0% (**Figure 4.5E**). Furthermore, cell lines that overexpress Sod1, such as the breast cancer cell line MCF7 [257], exhibit a nearly 3-fold increase in GAPDH oxidation compared to HEK293 cells (**Figure B.4E** and **B.4F**). Altogether, these results indicate that Sod1-mediated oxidation of GAPDH is conserved in humans.

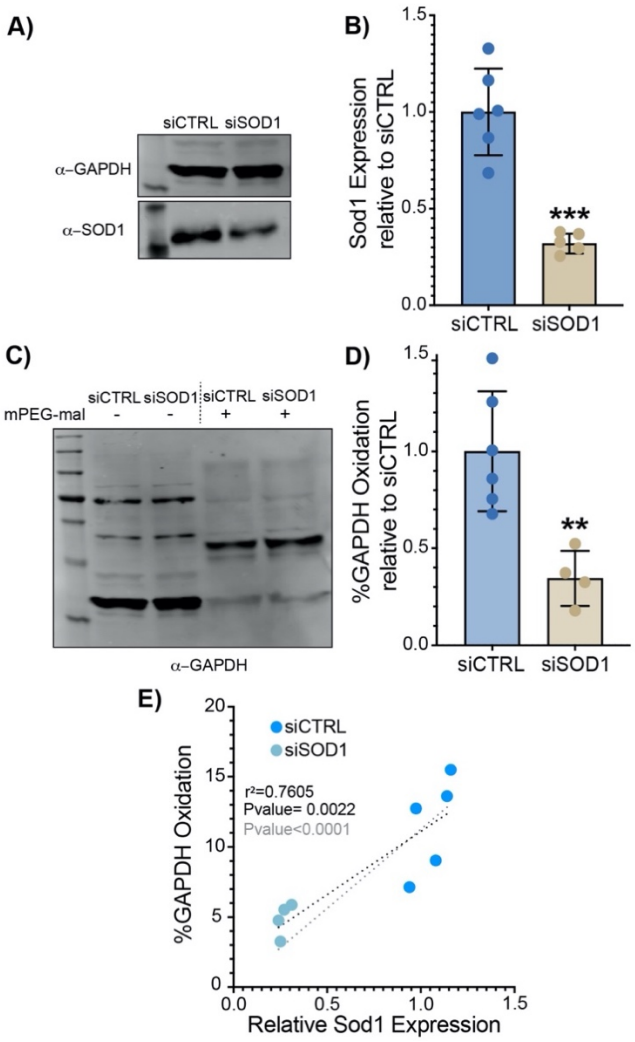

Figure 4.5. Sod1-mediated GAPDH oxidation is conserved in human cells.
(A-B) Representative immunoblot analysis of Sod1 and GAPDH from human embryonic kidney HEK293 cells that have *SOD1* silenced with small interfering RNA_i (siSOD1) or control scrambled RNA_i (siCTRL) (**A)** and normalized ratios of Sod1/GAPDH expression from multiple trials (**B**). Data represents individual values from five or six biological replicates.
(C-D) Representative immunoblot analysis of GAPDH oxidation as assessed by mPEG-mal labeling of HEK293 cells with silenced (siSOD1) or unsilenced (siCTRL) Sod1 **(C)** and normalized GAPDH oxidation from multiple trials (**D**). Data represents the average ± SD from five or six biological replicates. See also Figures B.4C-B.4D.
(E) The correlation between %GAPDH oxidation and relative Sod1 expression, as assessed by measuring the ratio of Sod1/GAPDH levels, from the multiple trials depicted in panel **D**. A linear regression analysis gives a coefficient of determination (r^2) of .76 and a p-value of 0.002 (black line). If the x and y-intercept of the linear regression is fixed at 0% oxidation and no Sod1 expression (gray line), the correlation remains significant ($p<0.0001$).
In panels **B** and **D**, the statistical significance relative to siCTRL is indicated by asterisks using two-tailed Student's t-test for pairwise comparison; *p<0.05, **p<0.01, ***p>0.001, ****p<0.0001, n.s.= not significant.

4.3.7. Redox proteomics identifies additional putative targets of Sod1 redox regulation.

Many non-biased proteome-wide studies in the literature have used a combination of thiol alkylating agents with mass reporters, such as iodoTMT [258], to identify cysteine thiolates in proteins that are susceptible to oxidation upon treatment with exogenous H_2O_2 [233, 259-261]. Though these studies are instrumental to understand potential redox targets, there is still a necessity to understand the degree to which the identified protein thiols are oxidizable under physiological levels of H_2O_2, without requiring the addition of exogenous oxidants that may yield a physiologically irrelevant degree of thiol oxidation. Recent studies, however, have significantly contributed towards how we perceive the physiologically relevant protein thiol oxidation cell and tissue-wide [262]. Still, until now, there isn't any body of work that gauged the effect of intracellular sources of peroxide. Given that Sod1 is the main source of intracellular peroxide, is widely distributed throughout the cell and is highly abundant, it may redox regulate a broad variety of substrates cell-wide, besides GAPDH. Therefore, in order to further understand the implication of Sod1-derived peroxide in redox signaling, in collaboration with the Torres Lab, we executed a non-biased proteome-wide approach. For this purpose, we used iodoacetyl tandem mass tag (iodo-TMT^{TM}) reagents (Thermo Scientific) in combination with single isoptope labeling with amino acids in cell culture (SILAC) in wild type (WT) and *sod1*Δ yeast cells. Iodo-TMT, which consist of a mass reporter, a mass normalizer and a iodoacetyl cysteine reactive group, selectively labels and enable duplex to sixplex mass spectrometry quantitation of free thiols in cysteines of target proteins from complex biological samples due to the six different mass reporters (126-131 Da) [263]. The combination of SILAC and iodo-TMT, enables the identification of Sod1-dependent changes in protein expression and reversible cysteine oxidation before and after DTT treatment between strains, respectively.

Briefly, *lys1*Δ (WT) and *lys1*Δ *sod1*Δ (*sod1*Δ) yeast cultures are grown in media containing heavy and light lysine, respectively. Growth is stopped by adding trichloroacetic acid (TCA) to the culture followed by TCA lysis, which at its low pH prevents oxygen from reacting with the free sulfhydryl groups in cysteine residues and favors a real "snapshot" of the protein redox status *in vivo* [264]. After lysis and protein quantification, equal amounts of protein lysate from both samples are mixed using a 1 to 1 ratio. Proteins are first labelled with iodoTMT^{126} (**Figure 4.6A**, iodo-TMT1), which will covalently label the reduced sulfhydryl in thiols from cysteine residues in proteins. Next, the oxidized thiols, yielding a disulfide bond or sulfenic acid, are reduced using the reducing agent dithiothreitol (DTT) followed by labeling of the newly formed free sulfhydryl with iodoTMT^{129} (**Figure 4.6A**, iodo-TMT2). After labelling, the proteins are fractionated using high pH reverse phase liquid chromatography (RPLC) and subsequently analyzed *via* liquid chromatography coupled to tandem mass spectrometry (LC-MS-MS) (**Figure 4.6A)**. Protein lysis, labeling, mass spectrometry and data analysis was executed by *Hyojung Kim*, with the help of *Alex P. Jonkee* in the Torres lab. For this study, we used three biological replicates, and three different pairs of iodo-TMT reporters, allowing statistical analysis of our results. In total, 4,409 unique proteins (**Figure 4.6B**) were confidently detected and quantified, revealing proteins that undergo significant changes in abundance, cysteine oxidation, or both when cells are lacking *SOD1* (**Figure 4.6C**).

Protein expression of each protein is analyzed *via* SILAC, whereby each peptide corresponding to WT or *sod1*Δ, can be distinguished by a mass shift, which allows quantitation of the same peptide, and its corresponding protein, in each strain. The protein expression difference between both strains is calculated using the following formula; Protein expression difference = $\log_2$ (*sod1*Δ_{light}/WT_{heavy}). From the 4,409 proteins detected, ~9% of these (373) exhibit significant differences between the two strains. Concretely, of

these, 114 (30.6%) are significantly less expressed in *sod1*Δ, in contrast to 259 (69.4%) that exhibit a significant increase in *sod1*Δ cells (**Figure 4.6B**, **4.6C** and **4.6D**). The changes in protein expression reflect known metabolic defects associated with loss of *SOD1*, including alleviation of glucose repression, increased mitochondrial mass, induction of the iron starvation and antioxidant responses, and diminished plasma membrane casein kinase expression (**Figure 4.6E)**.

Besides protein quantification with SILAC, the peptides that contain a cysteine residue, release a TMT reporter ion that enables the quantification of the cysteine oxidation percentage in each strain (oxidation difference= *sod1*Δ%Ox – WT%Ox). As a consequence, this study reveals the effect of *SOD1* expression on cell-wide cysteine redox status. In particular, a total of 2,077 cysteine residues were confidently detected ranging in oxidation extent from 1 to 100% and a median level of 28.9% across all sites measured (**Figure 4.6B**). Approximately 5% of the quantified cysteine sites (99 sites, 96 proteins) undergo significant changes in oxidation between WT and *sod1*Δ cells, and of these, we found that 65% exhibit reduced oxidation levels in the absence of *SOD1* (left) (**Figure 4.6F**). This suggests that Sod1-catalyzed H_2O_2 oxidizes and potentially regulates a wide array of proteins. It is intriguing, however, that most of the cysteine thiolates that are oxidized in a Sod1-dependent manner, unlike in GAPDH, are not catalytic cysteines. It is feasible that Sod1 redox regulates cysteine residues located in allosteric sites of some proteins, ultimately affecting protein activity, or cysteine residues involved in protein-protein interactions, which may interfere/facilitate key interactions for signaling cascades. Therefore, future work is required to understand the effect of Sod1-catalyzed H_2O_2 on the non-catalytic cysteines of the identified proteins. Besides, the enhanced oxidation observed in some cysteine residues in *sod1*Δ compared to WT cells (**Figure 4.6F**, right), may be due to oxidative stress caused by the lack of *sod1*Δ. However, we are most interested in the proteins that exhibit increased cysteine oxidation in WT cells, which

encompass potential targets of Sod1 metabolism (**Figure 4.6F**, left) that will be further studied in detail.

Our non-biased proteome wide study addresses this need to elucidate how a key intracellular source of peroxide, namely Sod1, contributes towards redox signaling cell-wide; and to identify the proteins that are redox regulated under oxidative stress, such as it encountered when cells lack *SOD1*. The role of Sod1 on cell-wide redox signaling can be dual; on one hand it acts as a direct source of peroxide that directly oxidizes a target cysteine thiolate, and, on the other hand, it may promote redox signaling by supporting the regeneration of antioxidant systems involved in redox relays, such as peroxiredoxins. Moreover, the combination of SILAC with iodo-TMT reports changes in cysteine oxidation between WT and *sod1*Δ cells, and shifts in protein expression, which also provides information on the transcriptional and translational adaptations that cells devoid of *SOD1* undergo. For instance, we observe that cells lacking *SOD1*, which are more oxidatively stressed, express more antioxidant enzymes, as expected (**Figure 4.6G**). This study identifies redox targets of a physiological endogenous source of H_2O_2 and supports Sod1 as a master regulator of the thiol redoxome.

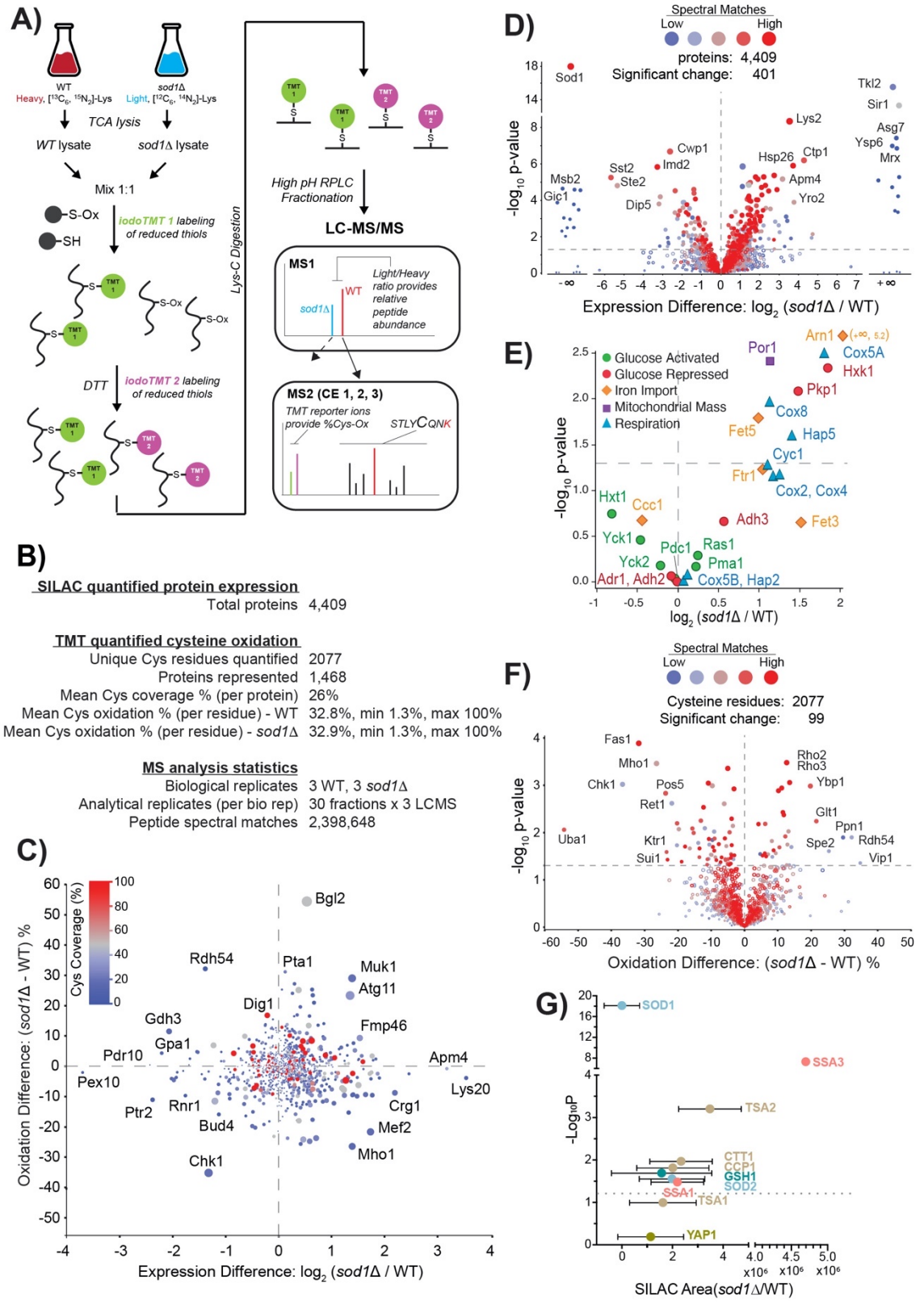

Figure 4.6. Redox proteomics identifies additional putative targets of Sod1 redox regulation. (A) SILAC-TMT redox proteomics workflow. SILAC labels distinguish the

cellular origin of each peptide. Cysteine-reactive and isobaric iodoTMT reporters, undetectable during the first MS stage (MS1) and released during peptide fragmentation in MS2, enable unique cysteine %oxidation calculation in WT and *sod1*Δ cells. **(B)** Data obtained from the proteome wide mass spectrometry study, including protein expression and cysteine oxidation data. **(C)** Plot of aggregated average cysteine oxidation difference relative to protein expression difference in *sod1*Δ versus WT cells. Points near the origin (0,0) undergo less change in relative abundance and cysteine oxidation compared to points further from the origin. Cysteine coverage indicates the fraction of cysteine residues detected for each protein. **(D)** Volcano plot of $-Log_{10}$(P-value) relative to protein expression difference [Log_2(*sod1*Δ/WT)] calculated from aggregate SILAC data. Proteins above $-Log_{10}$(P-value) 1.3 are significantly different in abundance between the two strains ($p<0.05$). Positive and negative values of log_2(*sod1*Δ/WT) indicate proteins that are more expressed in *sod1*Δ and WT, respectively. Proteins with a single detected label are indicated as +/- infinity. **(E)** Volcano plot of $-Log_{10}$(P-value) relative to protein expression difference [$\%Ox_{sod1D}$ - $\%Ox_{WT}$] calculated from iodoTMT data aggregated at the cysteine level. $-Log_{10}$(P-value) of 1.3 or above indicate significantly different Cysteine oxidation between the two strains ($p<0.05$). **(F)** Subset of data from D, showing expression change for proteins associated with bioprocesses functionally associated with loss of *SOD1*. **(G)** Subset of data from D, showing expression change for proteins associated with antioxidant responses, overexpressed when cells are devoid of *SOD1*.

4.4. Discussion.

Life in air necessitates that cells sense and detoxify ROS generated from aerobic metabolism. As a consequence, a number of enzymatic antioxidant defenses evolved to combat ROS, including $O_2^{\bullet-}$-scavenging SODs and H_2O_2-scavenging thiol peroxidases and catalases. SODs are unusual “antioxidants” in that they catalyze the production of one ROS, H_2O_2, as a byproduct of detoxifying another ROS, $O_2^{\bullet-}$. Rather curiously, prior studies found that increased expression of Sod1 reduces cellular H_2O_2 levels [225], hinting at additional unknown mechanisms underlying Sod1 antioxidant activity. Herein, we sought to understand if there were physiological roles for Sod1-derivied H_2O_2 in redox regulating antioxidant defenses and the thiol proteome. Indeed, we identified a novel redox circuit in which Sod1 senses the availability of O_2 via metabolically produced $O_2^{\bullet-}$ radicals and catalyzes the production of H_2O_2 that oxidatively inactivates GAPDH. GAPDH

inactivation in turn promotes flux through the oxPPP to generate the NADPH required for aerobic metabolism and antioxidant defenses [239, 240]. Moreover, using mass spectrometry-based redox proteomics approaches, we identified a larger network of proteins whose redox state, like GAPDH, is sensitive to Sod1 levels. Altogether, our results highlight a new mechanism for the antioxidant activity of Sod1 – namely that Sod1-derived H_2O_2 can stimulate NADPH production – and place Sod1 as a master regulator of the cellular redox landscape through two potential mechanisms; either by providing a direct source of thiol oxidizing H_2O_2 or by altering the NADPH/NADP+ redox balance through the Sod1/GAPDH signaling axis (**Figure 4.7**).

GAPDH catalyzes a rate determining step of glycolysis and is amongst the most abundant peroxide reactive enzymes in eukaryotes [232]. Prior to our work, the oxidative inactivation of GAPDH and subsequent increase in NADPH via the PPP to combat redox stress was exclusively associated with high concentrations of exogenous oxidants [233, 239-242, 265]. Our studies found that endogenous H_2O_2, specifically derived from Sod1, is responsible for the aerobic oxidation of GAPDH (**Figure 4.3D**). These results indicate that only a highly localized and privileged pool of peroxide is capable of physiological GAPDH oxidation and control of glycolytic flux. As GAPDH and Sod1 are amongst the most abundant soluble proteins in cells, we propose that there may be transient interactions between there proteins that facilitate Sod1-dependent GAPDH oxidation. While we could not detect the co-immunoprecipitation (Co-IP) of endogenous Sod1 and Tdh3 from yeast cells, we did observe that purified recombinant bovine Sod1 and yeast Tdh3 do interact as assessed by co-IP (data not shown). By extension, we suggest that signaling H_2O_2 is channeled between Sod1 and down-stream targets via protein-protein interactions, rather than through diffusion. This model for Sod1-based redox signaling complements other paradigms of peroxide signaling such as the transfer of oxidizing equivalents through thiol-disulfide exchange [51] or the “flood-gate” effect, which posits

that a burst of H_2O_2 inactivates antioxidants like peroxiredoxins so that sufficient peroxide may diffuse far enough to transmit redox signals [52].

The aerobic oxidation of GAPDH is rate limited by Sod1 (**Figure 4.3E** and **4.3F**), suggesting that the oxidative inactivation of GAPDH and glycolytic flux may be dynamically regulated by Sod1 expression, maturation, which itself is O_2 dependent, its interactions with GAPDH, or post translational modifications (PTMs) that regulate Sod1 localization and/or activity [105, 113-115]. With respect to Sod1 PTMs, it is tempting to speculate that the O_2 sensing redox circuit we identified herein may be integrally linked to the nutrient sensing TOR pathway. TOR-dependent phosphorylation at Ser38 in yeast (Thr39 in humans) suppresses Sod1 activity in response to nutrient abundance to promote cell growth, whereas starvation promotes Sod1 activity [113]. TOR/Sod1 signaling may be coupled to the redox regulation of GAPDH and glycolytic flux, thereby providing a means to integrate oxygen and nutrient availability to control metabolism. With respect to Sod1 expression, since many cancer cells over-express Sod1, it is conceivable that the Sod1/GAPDH signaling axis promotes cancer cell survival and drug resistance due to its potentiation of NAPDH production via the PPP [266]. Thus, our work also sheds new light on the benefits of anti-Sod1 therapeutic interventions [113, 117, 120, 121, 217]. Indeed, we find that the breast cancer MCF-7 cell line exhibits greater levels of GAPDH oxidation relative to HEK293 cells, correlating with its higher levels of Sod1 expression.

The integration of O_2 availability through the Sod1/GAPDH redox signaling axis is dependent on key sources of $O_2^{\bullet-}$, including the yeast NADPH oxidase Yno1 and mitochondrial respiration (**Figure 4.2**). Given that Sod1 and GAPDH are primarily cytosolic enzymes, it is not surprising that we found Yno1, which is localized at the ER membrane and produces $O_2^{\bullet-}$ on the cytosolic side, is required for transducing O_2 availability to the $O_2^{\bullet-}$ signal required for Sod1/GAPDH signaling [256]. Indeed, Yno1 was previously found to regulate Sod1-mediated redox regulation of yeast casein kinase Yck1/2 signaling, which

also occurs in the cytosol in proximity to the plasma membrane. However, it was rather surprising to find that mitochondrial respiration, as assessed in a respiratory incompetent yeast mutant lacking mitochondrial DNA, could also contribute $O_2^{\bullet-}$ for Sod1 mediated GAPDH oxidation in the cytosol. Complex I (missing in *S. cerevisiae*) and III are the primary sources of electron leakage from the electron transport chain and produce $O_2^{\bullet-}$ in the mitochondrial IMS [135]. Yet, IMS targeted Sod1 does not mediate GAPDH oxidation (**Figure 4.1M** and **4.1N**). Thus, IMS $O_2^{\bullet-}$, which is charged and membrane impermeable, must exit the mitochondria for Sod1/GAPDH signaling via voltage-dependent anion channels (VDACs) [180] or as membrane-permeable neutral hydroperoxyl radicals ($HO_2^{\bullet}$). Our results highlight how mitochondrial respiration may be an important sensor for O_2, providing a source of $O_2^{\bullet-}$ that can act as a retrograde signal to control extra-mitochondrial metabolism for adaptation to increasing pO_2. The current study complements prior work that found mitochondrial respiration is a key source of ROS required for adaption to hypoxia via HIF signaling [267].

The 10^4-rate enhancement of Sod1-catalyzed $O_2^{\bullet-}$ disproportionation relative to the uncatalyzed reaction suggests that Sod1 acts as a redox amplifier that provides a localized burst of H_2O_2 within the vicinity of Sod1 for specific redox signaling events. Indeed, the O_2-dependent redox regulation of GAPDH and casein kinase signaling are exclusively dependent on Sod1. These findings prompted us to determine if other redox targets of Sod1 exist. Indeed, mass spectrometry-based redox proteomics identified a number of proteins that, like GAPDH, are more oxidized in the presence of Sod1. Interestingly, enzymes associated with pathways orthogonal to glycolysis and the PPP, namely involved in amino acid biosynthesis, were prominently enriched over other groups (**Figures 4.6H**), and suggest that Sod1-dependent growth control may also be modulated through additional targets within these pathways that may have evolved Sod1-sensitive cysteine oxidation sites. On the other hand, all but one of these proteins (Nbp35) are

oxidized at Cys residues not associated with a direct role in catalysis or function, raising the possibility that oxidation of such sites may function allosterically. For instance, the E1 ubiquitin activating enzyme Uba1 is differentially oxidized at C447 (**Table B.1J**), which is immediately adjacent to the ATP binding site, and the cysteine desulfurase Nfs1 is differentially oxidized at C199, which is adjacent to the site of pyridoxal phosphate cofactor attachment. Future work will probe the functional consequences of Sod1-dependent protein oxidation. We also identified proteins that are more oxidized in *sod1*Δ cells, which we interpret as arising due to oxidative stress associated with the loss of GAPDH/Sod1 signaling and the concomitant decrease in NADPH levels and/or $O_2^{\bullet -}$ toxicity. It is worth noting that although past redox proteomics studies revealed much about potential targets of redox regulation, they typically involved treatment with exogenous oxidants mimicking pathological stress levels outside the physiological range [233, 258, 259, 261, 268]. Our study is notable in that we have identified redox targets of a physiological endogenous source of H_2O_2.

To what degree does Sod1 regulate thiol oxidation in animal models? A recent elegant redox proteomics study from Couchani and co-workers, termed “Oximouse”, describes tissue specific protein thiol oxidation in a mouse model [269]. Since active Sod1 requires the formation of an intramolecular disulfide bond between Cys 147 and Cys 56, we plotted % Sod1-Cys147 oxidation as a proxy for mature active Sod1 against overall average Cys oxidation in each tissue and found a statistically significant linear correlation (r^2 = 53; p = .04) (**Figure B.5A**). To determine if this correlation between active Sod1 and overall thiol oxidation was unique to Sod1, we also plotted tissue Cys oxidation against the oxidation of active site Cys residues in other peroxide metabolizing enzymes, including peroxiredoxins 1 and 5 (PRDX1, PRDX5) or glutaredoxin 3 (GLRX3). Unlike Sod1, the activity of these other enzymes, as assessed by their active site oxidation, do not significantly correlate with overall Cys oxidation (**Figure B.5B-B.5F**). Moreover, we also

found that the oxidation of other enzymes known to be redox regulated by Sod1, including tyrosine phosphatases PTP1N (PTP1B in humans) and PTPN11 [270, 271] and a GTPase involved in vesicular protein transport from the ER to the Golgi, Rab1α [272] (**Figures B.5G-B.5I**), exhibit a linear correlation between active Sod1 and their active site oxidation. Notably, there is no correlation with PRDX1 Cys oxidation, which is typically associated with the transmission of oxidizing equivalents to regulate redox signaling [51] (**Figures B.5J-B.5L**). Together, the data we extracted from the Oximouse study supports our principal findings from yeast that Sod1-derived peroxide regulates proteome-wide thiol oxidation.

Our studies have also finally explained a mystery regarding the role of Sod1 in antioxidant defense. Prior to the current work, the primary role of Sod1 in antioxidant defense was thought to be $O_2^{\bullet-}$ scavenging. However, we previously found that the vast majority of Sod1, > 99%, was dispensable for protection against cell wide markers of $O_2^{\bullet-}$ toxicity [112]. We surmised that exceedingly low amounts of Sod1 were sufficient to protect against $O_2^{\bullet-}$ because the targets of $O_2^{\bullet-}$ toxicity are limited in scope, primarily Fe-S cofactor containing proteins. Indeed, all $O_2^{\bullet-}$-related toxicity phenotypes arise from diminished activity of Fe-S enzymes and iron toxicity due to iron release from damaged clusters. Our work indicates that a broader role for Sod1 in oxidant defense is to promote the production of NADPH via the GAPDH/Sod1 signaling axis. As a major cellular reductant for numerous antioxidant systems, NADPH offers more expansive protection against redox stress than just defending against $O_2^{\bullet-}$. Since GAPDH and Sod1 are amongst the most ancient and highly conserved enzymes in aerobic life, we propose that this new reported function of Sod1 to produce NADPH via GAPDH oxidation was a key requirement for O_2 sensing and integration for adaptation to life in air.

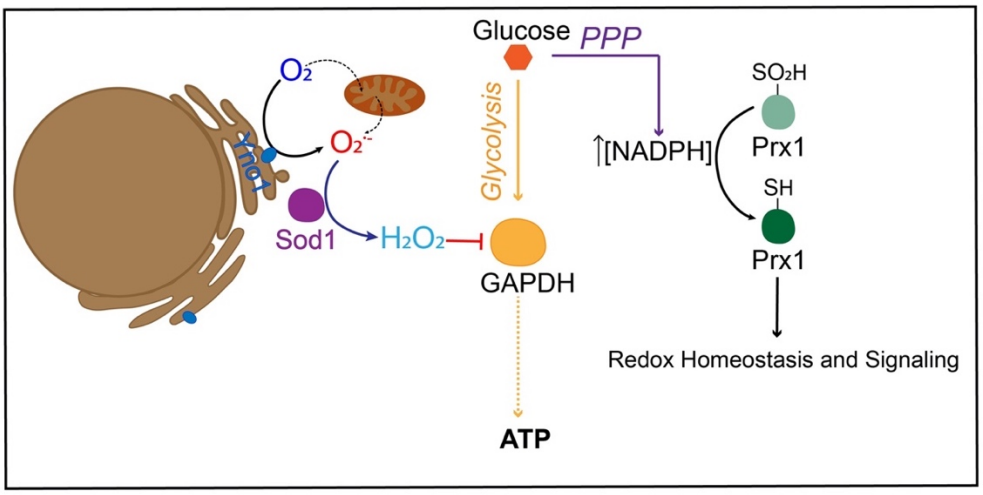

Figure 4.7. Proposed model for how Sod1 integrates O_2 availability to regulate GAPDH oxidation and balance flux between glycolysis and the PPP.

4.5. Methods

4.5.1. Chemicals, media components and immunological reagents.

Dihydroethidium (Cat. # 50-850-563) was purchased from Thermo Fisher Scientific. Methoxypolyethylene glycol maleimide, 5kDa (Cat. # 63187) was purchased from Sigma Aldrich. SC and YPD dropout mixtures were purchased from Sunrise Science Products and VWR, respectively. The yeast GAPDH activity assay kit (Cat. # K680-100) and the NADP/NADPH quantification kit (Cat. #K347-100) were purchased from Bio Vision. Rabbit polyclonal antibody (Cat. # G4595) and mouse monoclonal antibody against GAPDH (Cat. # G8795) were purchased from Sigma Aldrich. Rabbit polyclonal antibody against Peroxiredoxin-SO_3 (Cat. # ab16830) was purchased from Abcam. Goat Anti-Rabbit (Cat. #89138-520) and anti-mouse CF680 (Cat. # 20067) secondary antibody were purchased from Biotium. Goat anti-rabbit DyLight 800 secondary antibody was purchased

from Thermo Fischer Scientific (Cat. # SA5-35571). A previously described rabbit polyclonal antibody against Sod1 was obtained from the laboratory of Valeria Culotta (Johns Hopkins University)[35]. Revert™ 700 Total protein stain kit for protein normalization was purchased from (LI-COR).

4.5.2. Yeast strains, plasmids, and growth.

S. cerevisiae strains used in this study were derived from BY4741 (MATa, his3Δ1, leu2Δ0, met15Δ0, ura3Δ0). sod1::*KANMX4* strains were generated by knocking out *SOD1* using the previously described deletion plasmid pJAB002 [188]. Expression constructs for wild type *SOD1* (pRS415-*SOD1*) and IMS localized SCO2-*SOD1* (pRS415-SCO2-*SOD1*), which are both driven by the native SOD1 promoter, were previously described and were provided by the laboratory of Professor Dennis Thiele (Duke University) [255].

The previously described *GAL1* driven *SOD1* expression plasmid (pAR1026) [112] was constructed by PCR amplification of the *SOD1* open reading frame from BY4741 genomic DNA with primers that introduced flanking 5′ and 3′ *SpeI* and *BamHI* sites, respectively. The *SOD1* amplicon was sub-cloned into the *SpeI* and sites of pRS316-*GAL1* [189] to generate pAR1026.

The ADH driven SOD1 expression construct (pCMA002) was constructed by PCR amplification of the *SOD1* open reading frame from *BY4741* genomic DNA using plasmids that introduced 5’ and 3’ flanking regions with the *BamHI* and *XhoI* restriction sites, respectively. The *SOD1* amplicon was cloned into the *BamHI* and *XhoI* cloning sites of p415ADH to generate pCMA002. The plasmid expressing *CCS1*-independent SOD1 mutant (pCMA010, p415ADH-*SOD1*-P144S) was generated using site directed mutagenesis on the pCMA002 plasmid (**Table B.1**).

Expression constructs for Yno1 (p416YES2-*YNO1*) or EV (p416YES2-EV), which are driven by a strong galactose inducible promoter were previously described and were provided by the laboratory of Michael Breitenbach (University of Salzburg) [256]. These constructs were cloned in the previously described sod1::kanMX4 strain expressing wild type *SOD1* (pRS415-*SOD1*).

A previously described 3Δ (312) TDH3 strain (BY4742 Δtdh3::*kanMX4* Δtdh1::*natNT2* Δtdh2::*hphNT1* + pDP8) expressing wild type *TDH3* (pDP8, p415TEF-TDH3) was provided by the laboratory of Tobias P. Dick (dkfz) [232]. The resolving cysteine TDH3 mutant (p415TEF-*TDH3*-C154S) was generated via site directed mutagenesis (**Table B.1**).

Yeast transformations were performed by the lithium acetate procedure [273]. Strains were maintained at 30 °C on either enriched yeast extract-peptone based medium supplemented with 2% glucose (YPD), or synthetic complete medium (SC) supplemented with 2% glucose and the appropriate drop-out mixture to maintain selection. For all experiments, cells were streaked from -80 °C glycerol stocks onto solid agar media plates and pre-cultured in an anaerobic chamber (Coy laboratories) maintained with an atmosphere of 95% N2 and 5% H2. Anaerobically grown cells required supplementing SC media with 15mg/L of ergosterol and 0.5% Tween-80 (SCE) [274].

For typical experiments involving the IMS-targeted SCO2-*SOD1* expression plasmid, cells were cultured aerobically in SC-LEU, with 2% glucose. In all cases, cells were seeded at an OD_{600nm} ~ .01 and cultured for 14-17 hours to a density of OD_{600nm} ~ 1.0 at 30 °C in a shaking incubator (220 RPM). Following growth, cells were processed as described below for immunoblotting and enzyme assays. For experiments involving the *CCS1*-independent mutant *SOD1*-P144S, cells were cultured aerobically or anaerobically in previously degassed SCE-LEU with 2% glucose. Anaerobic cultures were seeded at an OD_{600nm}~ .08 and cultured for 14-17 hours to a density of OD_{600nm} ~ 1.0 at 30 °C shaking

in the anaerobic chamber (200 RPM). For this experiments, Sod1 activity and/or expression was assessed as described below. For experiments involving the titration of *YNO1* and *SOD1* using the GAL-driven *YNO1 and SOD1* expression plasmids, cells were cultured aerobically in SC-URA with 2% raffinose and the indicated galactose concentrations.

Human embryonic kidney HEK293 cells were obtained from the laboratory of Loren D. Williams (Georgia Institute of Technology). Cells were cultured in Dulbecco Modified Eagle's Medium (DMEM, VWR), with 4.5g/L glucose and without L-Glutamine or Sodium Pyruvate, supplemented with 10% fetal bovine serum (FBS). *SOD1* silencing was accomplished using 50μM SOD1 silencer (Ambion, Cat. # 4390824) or scrambled control (Ambion, #Cat AM4611). Cells were transfected in Opti-MEM (Fisher) with Lipofectamine 2000 (Invitrogen) for 72h. MCF7 cells were cultured in DMEM without Phenol Red or L-glutamine (VWR).

All experiments were conducted using biological replicates arising from duplicate, triplicate or more independent cultures of multiple clones. All of the data has re-produced on multiple occasions in independent experimental trials.

4.5.3. TCA precipitation and thiol alkylation with mPEG-mal in yeast cultures.

10 mL aerobic or anaerobic overnight yeast cultures were quenched at a density of OD_{600nm} mL^{-1} ~ 1 by adding cold 100% trichloroacetic acid (TCA) to a final concentration of 10% (v/v). The TCA-stopped cultures were incubated on ice for 1h before pelleting and washing in 20%TCA. The final pellet was stored at -80ºC. For experiments involving H_2O_2 treatment, H_2O_2 was added to a final concentration of 1 mM to yeast cultures and incubated for 2 minutes while shaking prior to TCA precipitation.

Pellets were thawed on ice and lysed at 4ºC in TCA lysis buffer (12.5% v/v TCA in 1 mM Tris-HCl, pH = 8.0, 25mM NH_4Ac,1mM Na_2EDTA pH 8.0) using half pellet volume of zirconium oxide beads and a beat beater on a setting of 8 for 3 minutes, twice (Bullet Blender, Next Advance) [192]. The TCA lysate was transferred to a fresh tube by poking a hole 45º from the cap using a hot needle and pelleted, washed in cold acetone (-20ºC) and dried. The dried pellet was resuspended in 200 µL degassed resuspension buffer (6M urea, 10mM EDTA, 20mM Tris, 0.5% w/v SDS, 10µM neocuproine, pH 8.5) containing 1mM PMSF and a protease inhibitor cocktail (GBiosciences) in the anaerobic chamber (Coy laboratories). Lysate protein concentrations were determined by the Pierce™ BCA protein assay kit (Thermo Scientific).

Alkylation of free thiols was accomplished by diluting the lysate to a protein concentration of 0.18 µg/µL in resuspension buffer with 7.5 mM mPEG-mal (dissolved in DMSO) or DMSO and incubated for 1h shaking in the anaerobic chamber protected from exposure to light. The excess mPEG-mal was discarded using PD SpinTrap G-25 columns (GE Healthcare) and the resulting lysates were electrophoretically separated by SDS-PAGE in 14% tris-glycine gels (Invitrogen). Anti-GAPDH (1:4000) polyclonal rabbit antibody and a goat secondary antibody conjugated to a 680nm emitting fluorophore were used to visualize GAPDH in the immunoblot. All gels were imaged on a LiCOR Odyssey Infrared imager. Immunoblot quantitation was conducted using the LIC-COR Odyssey imager software (Image Studio Lite). %GAPDH oxidation was calculated dividing the intensity of the bottom band (unlabeled oxidized GAPDH) by both top and bottom bands (total detected GAPDH, labeled plus unlabeled).

4.5.4. Enzyme assays.

SOD activity analysis was performed by native PAGE and nitroblue tetrazolium staining as described previously [35, 112, 193, 207] on exponential phase aerobic and anaerobic cultures grown to a density of OD_{600nm} ~ 1.0 in degassed SCE-LEU, 2% glucose media. Yeast cells were washed in ultrapure H_2O, resuspended in cold (4ºC) lysis buffer (10mM sodium phosphate, 50 mM sodium chloride, 5 mM EDTA, 0.1% Triton X-100, 1 mM PMSF and protease inhibitor cocktail). Lysis was achieved at 4ºC using half pellet volume of zirconium oxide beads and a beat beater as described before [112]. Lysate protein concentrations were quantified by the Bradford method (Bio-Rad) and 15 µg of each protein sample was loaded and separated in 14% native PAGE gels. Sod1 activity was visualized by staining the gel with SOD activity staining solution (2.43 mM nitro blue tetrazolium chloride, Sigma, 0.14M riboflavin-50-phosphate, Sigma, 45mM dipotassium phosphate buffer, 4.5mM monopotassium phosphate buffer) with 28mM TEMED (Bio-Rad) for 60 minutes at room temperature in darkness. After the incubation, gels were rinsed with water twice and exposed to light.

GAPDH activity was measured using the GAPDH activity assay kit (Bio vision) according to the manufacturer's specifications. For this purpose, *sod1*Δ cells expressing an empty vector (pRS415) or SOD1 (pRS415-SOD1) were grown in 10mL SC-LEU 2% glucose cultures to a density of OD_{600nm}=1.0. Cells pellets were washed in ultrapure water and lysed in cold degassed lysis buffer as described for the SOD activity analysis. Increasing concentrations of protein lysate within a linear detection range were diluted in assay buffer to a final volume of 50 µL and mixed with 50 µL of reaction mix. Activities were monitored by spectrophotometrically measuring the generation of 1,3-bisphosphoglycerate (BPG) at 450 nm over the course of 60 minutes using a Biotek Synergy Mx multi-modal plate reader.

ATPase activity was assayed in membrane fractions with or without a 5 min preincubation with 50 mM vanadate. ATPase activity was determined by quantitating the phosphate released during vanadate-sensitive ATP hydrolysis by molybdate reactivity [275], and activity was normalized to WT cells.

4.5.5. NADPH measurements.

NADP/NADPH ratio measurements were conducted using the NADPH kit (Bio vision) according to the manufacturer's specifications. Briefly, yeast 10 mL cultures were split in half after reaching an OD_{600}/mL~1.0, and 5 OD_{600} were TCA precipitated, as previously described, to assess peroxiredoxin oxidation (Prdx-SO_3) and the other 5 OD_{600} were harvested and lysed in the NADP/NADPH extraction buffer provided by the manufacturer. Half the lysate was incubated on ice to assess total [NADP] and [NADPH], and the other half was heated for 30 minutes at 60ºC in a heat block to assess [NADPH]. Increasing concentrations of protein lysate within a linear detection range were diluted in assay buffer to a final volume of 50µL and mixed with 100µL of reaction mix and 10µL of Developer. NADPH was monitored after 1h incubation every 20 minutes for 4h at 450nm using Biotek Synergy Mx multi-modal plate reader.

4.5.6. Superoxide measurements.

Superoxide levels were measured by monitoring the fluorescence of DHE stained cells (λex =485 nm, λem =620 nm) as previously described [112]. Briefly, 1 x10^7 cells were harvested from triplicate cultures, resuspended and incubated in 500µL filter-sterilized 1xPBS solution containing 50µM DHE for 20 minutes at 30ºC in the dark, washed twice in 1xPBS. The fluorescence was recorded in a Biotek Synergy Mx multi-modal plate reader.

4.5.7. Growth test.

Growth tests of WT and *tdh3*Δ aerobic and anaerobic cultures were performed growing three biological replicates anaerobically overnight and diluting each biological replicate to 0.15 OD_{600}/mL in duplicate 10mL cultures the next morning. Each replicate was cultured aerobically or anaerobically for 12h. OD_{600}/mL readings were taken every hour or 2h from aerobic and anaerobic cultures, respectively, using a UV/vis spectrophotometer (Agilent). For peroxide sensitivity tests, WT and *tdh3*Δ aerobic cultures were grown overnight and diluted to 0.15 OD_{600}/mL with increasing concentrations of H_2O_2 (0, 100μM, 250μM, 500μM, 1mM). Readings were taken every hour using a UV/vis spectrophotometer (Cary 60, Agilent).

4.5.8. HEK293 and MCF7 TCA precipitation and thiol alkylation with mPEG-mal.

For assessing Sod1-dependent GAPDH oxidation in HEK293 cells, cells were silenced by adding 50μM SOD1 silencer (Ambion, Cat. # 4390824) or scrambled control and Lipofectamine 2000 (Invitrogen) in Optimem to cells seeded in 6 well plates and incubated for 72h. GAPDH oxidation was assessed by lysing cells via TCA precipitation 72h-post transfection where 100% cold TCA was added to the collected cell suspension to a final concentration of 10% and incubated for 1h on ice. After TCA lysis, cells were pelleted and washed in cold acetone and dried. Dried pellet resuspension, thiol alkylation and immunoblotting were carried out as described in the section on TCA precipitation and thiol alkylation in yeast cultures, using a concentration of 0.5μg/μL lysate protein for thiol alkylation.

SOD1 silencing was assessed via immunoblotting from the cell lysates used for mPEG-mal labeling using a Sod1 a polyclonal rabbit antibody (1:1000) and a goat secondary antibody conjugated to a 680nm emitting fluorophore. GAPDH was used as the loading control and was visualized using a GAPDH mouse monoclonal antibody (1:4000) and a goat antibody conjugated to an 800nm emitting fluorophore. Silencing efficiency was calculated by normalizing Sod1 expression (measured normalizing the Sod1 band intensity to the GAPDH band intensity) from siSOD1 or siCTRL treated cells to the average Sod1 expression value from siCTRL treated cells.

For assessing GAPDH oxidation via exogenous peroxide addition, ~10^5 cells were seeded in a 6-well plate in a reduced-serum media (Optimem, Gibco), grown for 24h and treated with 100μM H_2O_2 dissolved in Optimem (37ºC) for 2 minutes prior to cell harvesting and TCA lysis. As a control, cells were incubated with 2mL Optimem containing the same volume in H_2O.

For assessing GAPDH oxidation in MCF-7 cells, cells were seeded in a 6 well plate and harvested and lysed via TCA precipitation 24h after the cells were seeded, as previously described.

4.5.9. Quantification and Statistical analysis.

Data and statistical analysis were performed using GraphPad Prism, Pymol and Studio Lite software. P values were calculated using two-tailed Student's t-test for pairwise comparisons, One-way Anova and Dunett's post-Hoc test for multiple comparisons or Two-way Anova for multiple comparisons with more than one variable. The P value for linear regression analysis was calculated using GraphPad Prism.

4.5.10. SILAC labeling and cell lysis.

Three biological replicates were analyzed each for WT and *sod1*Δ cells. For each replicate, *lys1*Δ and *lys1*Δ *SOD1::KANMX4* single colonies were inoculated in 3mL starter cultures and grown to saturation in synthetic complete (SC). The following day, starter cultures were diluted to ~0.1 OD_{600} in 10mL dropout SC media to reach 0.8 OD_{600}/mL and then seeded at an OD_{600} 0.0075 in 50mL SC media containing heavy (WT) or light (*sod1*Δ) lysine, respectively. Culture growth was stopped after ~10 doublings by adding 100% cold TCA to a final concentration of 10%. The cells were incubated on ice in 10%TCA for 1h and pelleted for 10 minutes at 4,000 rpm, 4ºC. The cell pellets were then washed in 20% TCA and pelleted for 10 minutes at 16,000 G, 4ºC. After discarding the supernatant, the pellets were stored at -80ºC.

To prepare extracts, the SILAC-labelled cell pellets were separately thawed on ice and resuspended in 20% TCA followed by vortexing with glass beads for 10 min at 4 °C. Lysates were transferred to new centrifuge tubes followed by centrifugation at 16,000 × g for 10 min at 4 °C. Pellets were washed with ice cold acetone followed by centrifugation at 16,000 × g for 5 min at 4 °C. Pellets were resuspended in freshly prepared 6 M urea, 200 mM Tris pH 8.0, 2% SDS, 10 mM EDTA, 10 µM neocuproine. Protein concentrations for both WT and sod1Δ resuspensions were determined by DC protein assay (Bio-Rad Laboratories) and mixed equivalently generating 400 µg total.

4.5.11. iodoTMT labeling.

The combined SILAC-labeled protein samples (heavy/light) were labeled using iodoTMT sixplex Isobaric Label Reagent Set (Thermo Scientific) according to the

manufacturer specifications. Each bio-replicate was labeled with two different iodoTMT labels (either 126/129, 127/130, or 128/131). For pre-reduction iodoTMT-labeling, each replicate was labeled overnight followed by removal of unreacted TMT label by chloroform-methanol precipitation as previously described [276]. Following the first labeling reaction, oxidized thiols were reduced in 50 mM DTT at 37 °C for 1 hr followed by excess DTT removal by chloroform-methanol precipitation. Post-reduction iodoTMT-labeling was carried out as before with overnight incubation followed by the unreacted TMT label reagent removal. Each replicate was washed with ice cold acetone followed by resuspension in 100 mM Tris pH 8.0, 1 M ABC, 6 M urea and incubation at 37 °C for 1 hr. Lys-C protease (Thermo) was added to each replicate (1:20; enzyme:protein) followed by overnight incubation at 37 °C with shaking at 600 rpm.

4.5.12. High pH RPLC fractionation.

SILAC-TMT labeled peptides were pre-fractionated by high pH reverse phase liquid chromatography using an Agilent 1100 HPLC system with Gemini C18 reverse phase column (2 × 150 mm, 5 µM, 110 Å; Phenomenex Inc.) with solvents A (10 mM ammonium formate) and B (10 mM ammonium formate in 90% acetonitrile) adjusted to pH 10 using ammonium hydroxide. A gradient method (from 0% to 70% B in 150 min, then from 70% to 0% in 20 min) was applied at a flow rate of 100 µl/min. Fractions were collected every 5 min and frozen at -80 °C followed by lyophilization by CentriVap.

4.5.13. LCMS.

Peptide fractions were analyzed by LCMS using a Q-Exactive Plus orbitrap mass spectrometer equipped with Dionex UltiMate 3000 LC system (Thermo). The lyophilized

fractions were resuspended in 0.1% FA in 5% ACN and loaded onto a trap column, 75 µm I.D. x 2 cm, packed with Acclaim PepMap100 C18, 3 µm, 100Å (set of 2) nanoViper and resolved through an analytical column, 75 µm I.D. x 15 cm, packed with Acclaim PepMap RSLC C18, 2 µm, 100Å, nanoViper at a flow rate of 0.3 µl/min with a gradient solvent A (0.1% FA in 2% ACN) and a gradient solvent B (0.1% FA in 90% ACN) for 150 minutes. MS analysis was conducted in a data dependent manner with full scans in the range from 200 to 1800 m/z using an Orbitrap mass analyzer at a mass resolution of 70,000. The top fifteen most intense precursor ions were selected for MS2 with the isolation window of 4 m/z. Isolated precursors were fragmented by high energy collisional dissociation (HCD) with normalized collision energies (NCE) of 28, 31, and 33 for each analytical replicate. This led to the acquisition of 3 analytical replicates for each bio replicate for a grand total of 9 detection attempts per peptide fraction.

4.5.14. MS data analysis.

For SILAC data evaluation for protein expression, a total of 33,289 proteins of 3 biological replicates with 3 different NCEs of 28, 31, and 33 analyzed by PD 2.0 (**Table A.2K**). Of these, 32,630 proteins were further evaluated excluding transposable elements. Protein SILAC ratios (*sod1*Δ_{Light} / WT_{Heavy}) were calculated as the ratio of integrated MS1 peak areas for light and heavy peptides. Statistical significance in the difference between WT and *sod1*Δ data were determined using Response Screening (JMP 15.0) wherein up to 9 average responses per protein per yeast strain (18 total) were possible. Cases in which only one channel of a SILAC pair was present (heavy or light) were processed separately are reported as +/- infinite change in protein abundance.

For iodoTMT data evaluation a total of 307,894 peptides represented by 2,398,648 PSMs were identified using PD 2.0 (**Table A.2L**). Of these, 35,476 unique peptides (259,936 PSMs) corresponded to iodoTMT-labeled cysteine-containing peptides, again with transposable elements excluded. These data were processed at the peptide level to calculate percent cysteine oxidation level by dividing the reporter ion signal of TMT2 by the sum of signals from TMT1 and TMT2, producing an oxidation percentage for WT_{Heavy} and *sod1*Δ_{Light} peptide isoforms. Statistical significance in the difference between WT and *sod1*Δ data were again determined using Response Screening (JMP 15.0) for oxidation percentages measured between the two strains wherein up to 9 average responses per protein per yeast strain (18 total) were possible. Cases in which only one SILAC peptide was present were processed separately. To examine overall differential oxidation levels of proteins, the cysteine coverage of a protein (# detected Cys / # total Cys in a protein) was calculated using the non-redundant UniProt Yeast (*BY4741*) proteome database. Custom scripts necessary to organize data in the context of cysteine native position and to determine relative cysteine detection coverage per protein were written in Perl 5.3.

4.5.15. Bioinformatics.

SILAC-iodoTMT proteomics data were further analyzed using PANTHER, an ontology-based database equipped with data analysis tools. GO enrichment of biological processes, molecular functions, and cellular components was performed for proteins with greater than +1 or less than -1 $\log_2$ SILAC ratio ($sod1\Delta_{Light}$ / WT_{Heavy}), representing differential protein abundance. Separately, similar GO enrichment analysis was performed for proteins with observed TMT-labeled cysteine residues falling greater than 5% (or 10%) or less than -5% (or -10%) differential oxidation (*sod1*Δ – WT). Enriched terms with

statistical significance above the 95% confidence level were considered further. GO enrichment bins were defined by first identifying GO terms with fold enrichment values that were statistical outliers (>90th percentile), which resulted in well-defined bins reported in Figures 6E, 6H and Tables S5B, S5H. The mean fold enrichment for the GO Terms embedded with each bin was reported to allow comparison of fold enrichment values within each bin.

Evaluation of cysteine oxidation site bio-process outliers (Figure 6I, 6J, S6A, and Table S5I) was performed as follows. First, SGD GO analysis and EBI QuickGO were utilized to generate the list of bio-process GO terms for proteins undergoing statistically significant changes in oxidation (99 proteins in total). Second, GO terms were searched individually by AmiGO 2 to retrieve proteins in each of the GO terms filtered by *S. cerevisiae* S288C (see Figure S6). Third, the resulting list was filtered against proteins where cysteine oxidation in WT and sod1D cells could be quantified, and then further filtered to retrieve bio-processes in which any of the 99 significant ox changers were found to be a statistical outlier from other cysteine residues in the bio-process. Outlier responses of any cysteine oxidation change were highlighted by determining the distribution of observed responses within the bio-process. Outliers defined by this process were used to highlight specific proteins shown in Figures 6I and 6J.

Pathway analysis of significant ox changers was further analyzed via the Kyoto Encyclopedia of Genes and Genomes (KEGG) Brite and Pathway analysis tools (see Figure 6G; Tables S5F, S5G). Identification of functional cysteine residues was achieved using UniProt curated data with restriction to “Binding Site”, “Active Site”, “DNA Binding”, or “Metal Binding”.

CHAPTER 5

CONCLUSIONS AND FUTURE DIRECTIONS

5.1. Conclusions

My thesis work challenges how we have perceived Sod1 in biology. It shows that the function of the bulk of Sod1 is not superoxide protection, as previously thought, since only a minuscule fraction is needed for that purpose, but to promote peroxide-based redox signaling relays cell-wide. Given that Sod1 is the most prominent source of H_2O_2 in most organisms and human cell types and is widely distributed throughout the cell it facilitates localized redox signaling relays. Our proteome-wide mass spectrometry data suggests that a large fraction of the identified Sod1-redox regulated proteins corresponds to metabolic enzymes and places Sod1 as a master regulator of metabolism and redox signaling. This forces us to re-direct most of the previous conclusions and hypothesis towards a new direction.

The presented work suggests that Sod1 is a key cellular component that drives cell adaptation to oxygen by turning on certain pathways when cells are exposed to increasing pO_2, *via* H_2O_2 generation from O_2-dependent $O_2^{\cdot-}$ generation, including promoting generation of NADPH redox equivalents to sustain all antioxidant systems in the cell. Until now, the phenotypes observed with cells devoid of Sod1 or expressing inactive Sod1 mutants have been associated with damaging effects of superoxide build-up [183]. But is it just that? Our work defies this assumption and suggests that the damaging effects of lacking Sod1 is not mere superoxide build-up, but the lack of the key element that integrates oxygen availability to sustain adequate NADPH levels that maintain antioxidant systems that protect from a wide variety of reactive oxygen species,

not just superoxide. Besides, the perturbation of physiologic Sod1-driven redox relays may further contribute to the damaging effects of lacking Sod1. It turns out, we may have had a reductionist perception of Sod1 until now.

Recently Sod1 has been regarded as an important therapeutic target for cancer treatment. There has been more than one reported Sod1 inhibitor that effectively arrests cancer cell growth and promotes apoptosis. But why does Sod1 inhibition have such "conventional" effects? There is not still a clear answer, however, it is suggested that it may be due to superoxide toxicity associated with the lack Sod1. Our new findings indicate that it may be because the regeneration of cell-wide antioxidant systems is impaired, contributing to higher ROS levels that can trigger apoptosis. Moreover, it is conceivable that the role Sod1 plays in redox signaling may also have an effect in proliferation. For instance, it is known that Sod1-catalyzed H_2O_2 promotes the activation of the epidermal growth factor receptor (EGFR) by inducing its dimerization and further prolongs its activity by redox inactivating the protein tyrosine phosphatase that inhibits it [116]. This particular pathway, along with many soon-to be discovered Sod1 redox-regulated pathways, might be significant in promoting cancer cell tumorigenesis. Moreover, the role of Sod1 in glucose sensing *via* CK1γ stabilization may additionally support cancer cell proliferation, given the heavy reliance of cancer cells in glucose and fermentative metabolism for growth [35, 277]. Regarding the role of Sod1 on CK1γ stabilization, given that CK1γ is a key factor in the Wnt signaling pathway, we also found that Sod1 is necessary for canonical Wnt signaling, a pathway that many cancer cells rely on for carcinogenesis. Hence, Sod1 is required for many signal-stimulated prooncogenic pathways and to boost cell antioxidant capacity, posing it as a pivotal factor to support tumorigenesis and cancer cell survival. However, although this dissertation covers the identification of many Sod1 sponsored pathways, that support cancer progression and other diseases, we are still far from

understanding the complete contribution of Sod1. Therefore, there is a necessity to further explore the role of Sod1 in cell motility, proliferation and epidermal to mesenchymal transition (EMT) [278], a key mechanism for metastasis, to understand the role Sod1 plays in carcinogenesis and why it has such potential as a target for cancer treatment.

This novel perspective on the role of Sod1 should be applied to study other Sod1 related diseases, such as familial amyotrophic lateral sclerosis (FALS), and diseases that are potentially associated with Sod1, such as metabolic diseases. Additionally, Sod1 should be taken in account as a key element in a wide array of redox signaling pathways necessary for cell physiology and pathology.

5.2. Future Directions

The work presented on this thesis, has been just the inception of re-framing the role of Sod1 in biology. The next steps of the work presented would involve investigation on how Sod1 regulates the most relevant proteins identified in the mass spectrometry study. Understanding how Sod1 regulates these proteins will further expand the horizons on the role of Sod1 in redox signaling and would contribute towards elucidating novel signaling networks. For instance, understanding how Sod1 regulates Uba1, the E1 ligase required for protein ubiquitination, would shed light on potential redox regulation of protein degradation pathways, which may ultimately help identify the pathway by which Sod1 promotes yeast casein kinase 1 (Yck1) stabilization.

Future work may also encompass repeating the mass spectrometry study in different human cell lines to identify potential Sod1-dependent redox regulated pathways that are conserved across phylogeny, which would help unveil novel significant networks for life in air, and potentially additional Sod1-dependent oxygen sensing mechanisms.

Additionally, it would be interesting to explore the different requirements for Sod1 in cancer cell lines that overexpress Sod1 under normoxia and anoxia. Understanding the requirement for Sod1 when oxygen is scarce *versus* when it is abundant, would aid to further understand the role of Sod1 in cell biology and cancer under different pO_2. In addition to that, it would be compelling to study to which extent the ability of Sod1 to promote NADPH production has an effect in carcinogenesis. The Sod1-driven NADPH generation may be tightly regulated by the allosteric inhibition of G6PD by NADPH when the levels of NAPDH are sufficient to maintain a physiologic reducing potential. This negative feedback loop may act to prevent further re-routing towards the PPP, conferring an additional level of complexity and regulation to this pathway. Given that cancer cells rely on glycolysis, understanding whether this is just for rapid energy requirements and to have cellular building blocks; or if it is also because they rely heavily on Sod1-dependent re-routing from glycolysis to the oxidative phase of the pentose phosphate pathway to generate NADPH, would shed light on the implications of our newly discovered pathway in disease. Additionally, it would further suggest that Sod1 inhibitors may be significant for the treatment of certain cancers.

APPENDIX A

SUPPLEMENTARY INFORMATION FOR CHAPTER 3

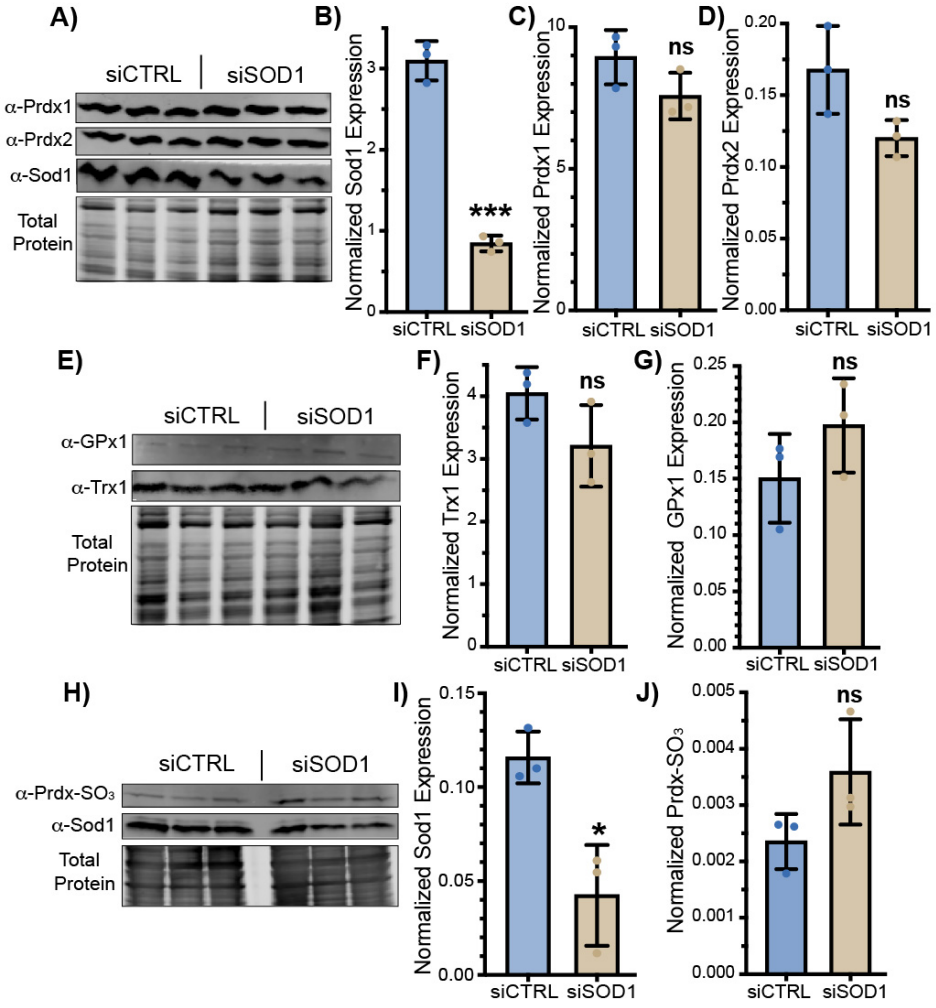

Figure A.1. Sod1 silencing does not affect the expression of other cytosolic peroxide metabolizing enzymes or peroxiredoxin oxidation. (**a**) Immunoblots of peroxiredoxins Prdx1 and Prdx2 and Sod1 in response to silencing of *SOD1* with siRNA. (**b-d**) Quantification of the normalized levels of (**b**) Sod1, (**c**) Prdx1, and (**d**) Prdx2. (**e**) Immunoblots of glutathione peroxidase Gpx1 and thioredoxin Trx1 in response to silencing of *SOD1* with siRNA. (**f-g**) Quantification of the normalized levels of (**f**) Trx1 and (**g**) Gpx1. (**h**) Immunoblots of sulfenic acid oxidized peroxiredoxin (Prdx-SO_3) and Sod1 in response to silencing of *SOD1* with siRNA. (**i-j**) Quantification of the normalized levels of (**i**) Sod1 and (**j**) Prdx-SO_3. Expression of the indicated proteins is normalized to total protein as assessed by the Revert stain from Licor. The statistical significance is assessed using an unpaired student's t-test, where: *p < 0.05, ***p < 0.001, and n.s. = not significant.

APPENDIX B

SUPPLEMENTARY INFORMATION FOR CHAPTER 4

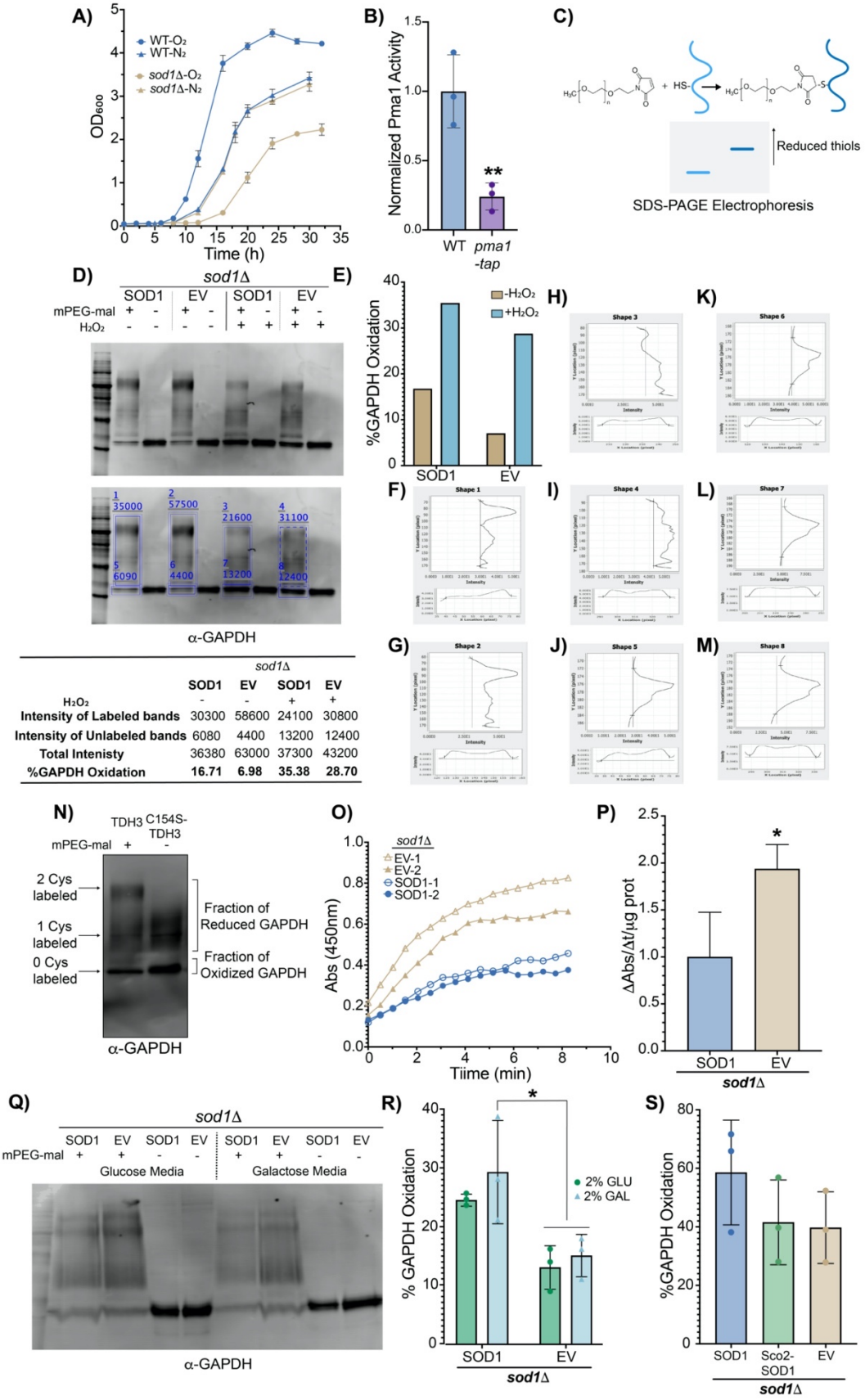

	sod1Δ			
	SOD1	EV	SOD1	EV
H_2O_2	-	-	+	+
Intensity of Labeled bands	30300	58600	24100	30800
Intensity of Unlabeled bands	6080	4400	13200	12400
Total Intenisty	36380	63000	37300	43200
%GAPDH Oxidation	**16.71**	**6.98**	**35.38**	**28.70**

Figure B.1. Development and validation of key strains, reagents, and techniques to establish Sod1-dependent GAPDH oxidation; related to Figure 4.1.
(A) Aerobic (O_2) and anerobic growth (N_2) of WT and *sod1*Δ cells. Data represent the average ± SD from duplicate cultures.
(B) Normalized Pma1 activity in WT cells and cells expressing a hypomorphic allele of *PMA1* (*pma1-tap*). Data represent the average ± SD from triplicate cultures and is normalized to the average activity of WT cells.
(C) Schematic representation of Cys-mPEG-mal adducts upon covalent modification with methoxypolyethylene glycol maleimide (mPEG-mal) and the corresponding electrophoretic shift.
(D) Representative immunoblot analysis of GAPDH-mPEG-mal adducts in *sod1*Δ cells expressing yeast Sod1 (SOD1) or empty vector (EV) cultured in 2% GLU and treated with 1mM H_2O_2 (+ H_2O_2) or H_2O (- H_2O_2) for three minutes prior to treatment with mPEG-mal. Immunoblot quantitation was conducted using the LIC-COR Odyssey imager software (Image Studio Lite) (middle), yielding the values exhibited in the blue squares and the bottom table. The percentage of GAPDH oxidation is displayed in the bottom table and obtained dividing the intensity of unlabeled bands by the sum of the intensity of labeled and unlabeled bands.
(E) % GAPDH oxidation, as assessed by quantifying the ratio of mPEG-mal labelled GAPDH to total GAPDH, in the indicated strains.
(F to M) Peak profiles (Y location, top; X location, bottom) corresponding to the blue shapes displayed in panel D (middle) used to identify the intensity of the immunoblot bands accounting for background. The quantitation is performed using the Studio Lite software.
(N) Representative immunoblot analysis of GAPDH-mPEG-mal adducts in *tdh1*Δ*tdh2*Δ*tdh3*Δ cells expressing yeast GAPDH (TDH3, left) or C154S-TDH3 (right). The arrows indicate the TDH3 or TDH3-C154S-mPEG-mal adducts.
(O-P) Measurements of time-dependent (**O)** or average (**P**) GAPDH enzymatic activity in *sod1*Δ cells expressing SOD1 (blue) or EV (gold). Data represents the average ± SD from 2 (**O**) and 4 (**P**) independent trials.
(Q-R) Assessment of GAPDH oxidation in *sod1*Δ cells expressing yeast Sod1 (SOD1) or empty vector (EV) cultured in 2% glucose (GLU) or 2% galactose (GAL). Representative immunoblot analysis of GAPDH-mPEG-mal adducts (**Q**) and absolute %GAPDH oxidation from multiple trials (**R**) in the indicated strains. Data represents the average ± SD from 3
(S) Assessment of GAPDH oxidation in *sod1*Δ cells expressing yeast Sod1 (SOD1), mitochondrial IMS targeted Sod1 (Sco2-SOD1), or empty vector (EV).
The statistical significance is indicated by asterisks using two-tailed Student's t-test pairwise comparison (panels B and P) or two-way ANOVA for multiple comparisons with Dunett's post-hoc test for the indicated pairwise comparison (panel R). *p<0.05, **p<0.01, ***p>0.001, ****p<0.0001, n.s.= not significant.

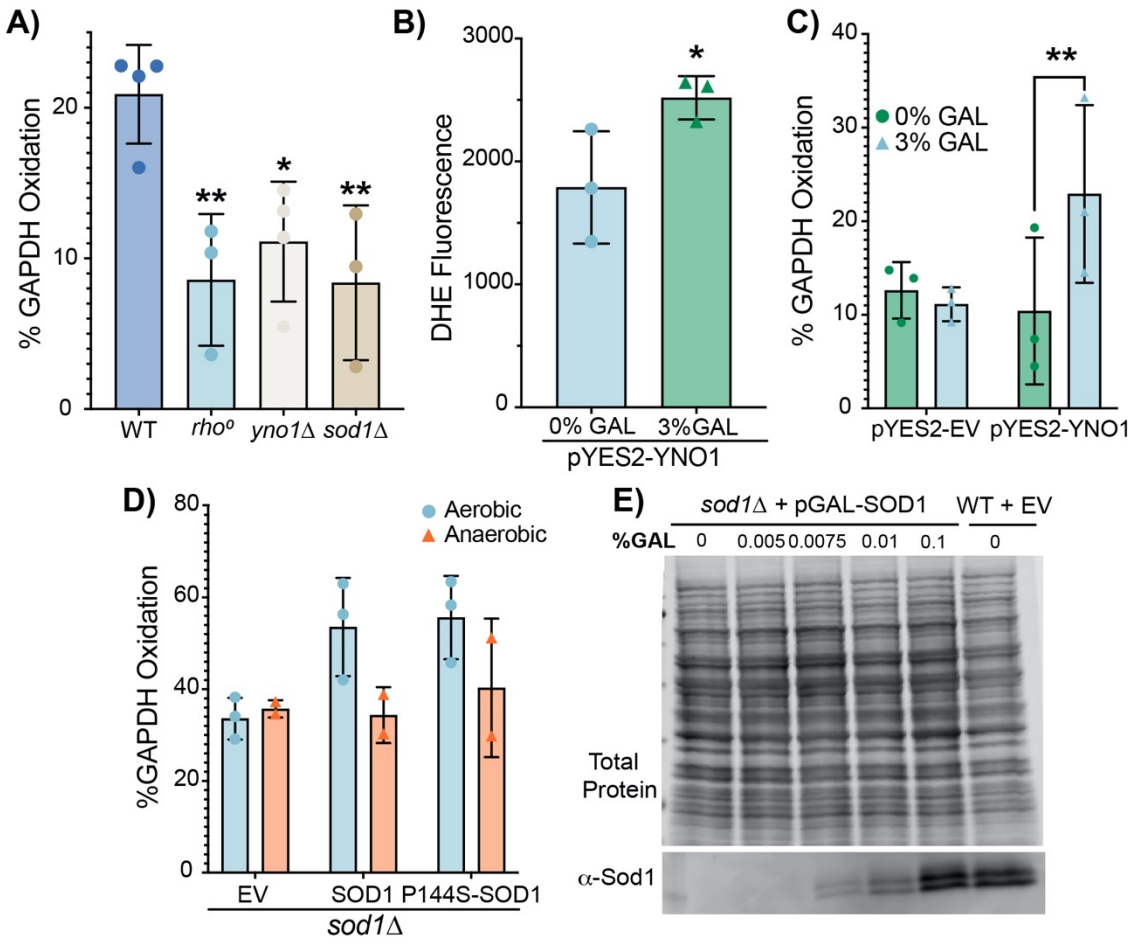

Figure B.2. The effect of Yno1, respiration, O_2, and Sod1 expression on % GAPDH oxidation; related to Figures 4.2 and 4.3.

(A) % GAPDH oxidation assessed by mPEG-mal labeling of GAPDH in WT, *rho*^{0}, *yno1*Δ and *sod1*Δ cells cultured in 2% GLU (Fig. 2A) from multiple trials. Data represents the average ± SD from 3 independent trials.

(**B-C**) DHE-detectable superoxide (**B**) and percentage GAPDH oxidation (**C**) in in WT cells expressing GAL1-driven *YNO1* (pYES2-YNO1) or empty vector (pYES2-EV) cultured in 2% raffinose, supplemented with non-inducing (0%) or inducing (3%) GAL concentrations from multiple trials. Data represents the average ± SD from 3 independent cultures.

(**D**) Assessment of the Sod1-dependence on the aerobic oxidation of GAPDH. Percentage GAPDH oxidation in aerobic or anaerobic *sod1*Δ cells expressing empty vector, WT SOD1, or the P144S SOD1 mutant (Fig. 3.3C). Data represents the average ± SD from two or three independent trials.

(**E**) Representative immunoblot of Sod1 from *sod1*Δ cells expressing *GAL1* driven *SOD1* or WT cells transformed with empty vector (EV) cultured in the indicated concentrations of galactose (GAL).

The statistical significance is indicated by asterisks using two-tailed Student's t-test pairwise comparison (panel B), one-way ANOVA for multiple comparisons with Dunett's post-hoc test for the indicated pairwise comparison (panel A) or two-way ANOVA for multiple comparisons with Dunett's post-hoc test for the indicated pairwise comparison (panel C and D). *p<0.05, **p<0.01, ***p>0.001, ****p<0.0001, n.s.= not significant.

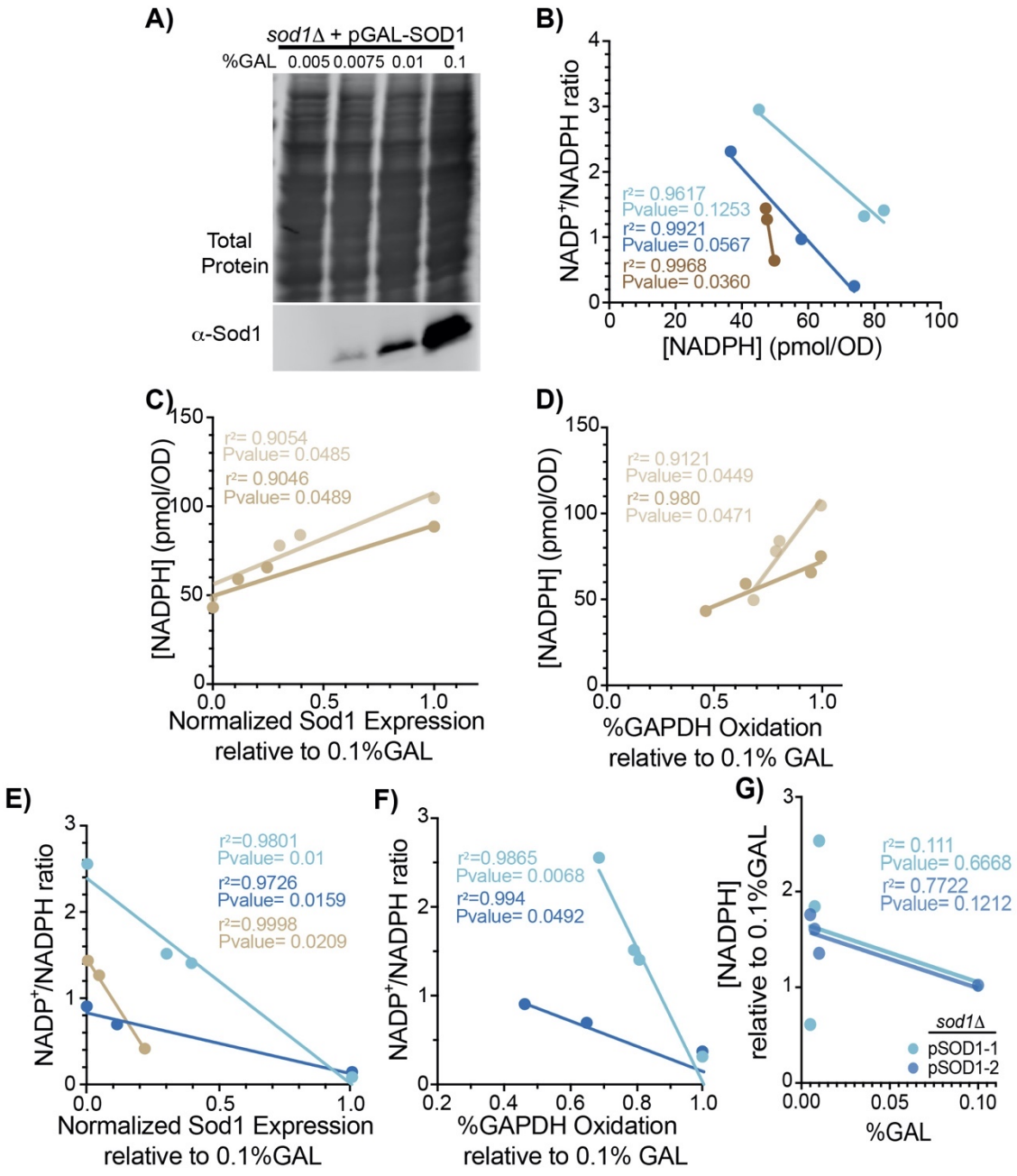

Figure B.3. Titration of Sod1 results in a dose-dependent increase of [NADPH] and NADP$^+$/NADPH ratio; related to Figure 4.4.

(A) Immunoblot analysis of Sod1 expression and total protein quantification in *sod1*Δ cells expressing GAL-driven *SOD1* cultured with increasing concentrations of galactose (GAL) (0.005%, 0.0075%, 0.01% and 0.1% GAL).

(B) The NADP+/NADPH ratio inversely correlates with cellular [NADPH]. The linear regression analysis in three independent trials gives coefficient of determinations (r^2) of .96, .992 and .9968 and p-values of .12, .057 and .0036, respectively.

(**C-D**) The [NADPH] correlates with normalized Sod1 expression (**C**) and normalized GAPDH oxidation (**D**). Each color indicates two individual trials used for both correlation

with Sod1 expression and GAPDH oxidation. The linear regression analysis in panel **C** gives coefficient of determinations (r^2) of .9054 and .9046 and p-values of .0485 and .0489, respectively. The linear regression analysis in panel **D** gives coefficient of determinations (r^2) of .9121 and .98 and p-values of .0449 and .0471, respectively.
(**E-F**) The NADP+/NADPH ratio correlates with normalized Sod1 expression (**E**) and normalized GAPDH oxidation (**F**). Each color indicates individual trials used for both correlation with Sod1 expression and GAPDH oxidation. The linear regression analysis in panel **E** gives coefficient of determinations (r^2) of .9801, .9726 and .998 and p-values of .01, .0159 and .0209, respectively. The linear regression analysis in panel **F** gives coefficient of determinations (r^2) of .9865 and .994 and p-values of .0068 and .0492, respectively.
(**G**) Increasing concentrations of GAL do not positively correlate with [NADPH] in *sod1*Δ cells expressing a non-GAL regulated allele of yeast *SOD1* (p*ADH1*-SOD1). The linear regression analysis in panel **G** gives coefficient of determinations (r^2) of .11 and .772 and p-values of .067 and .12, respectively.

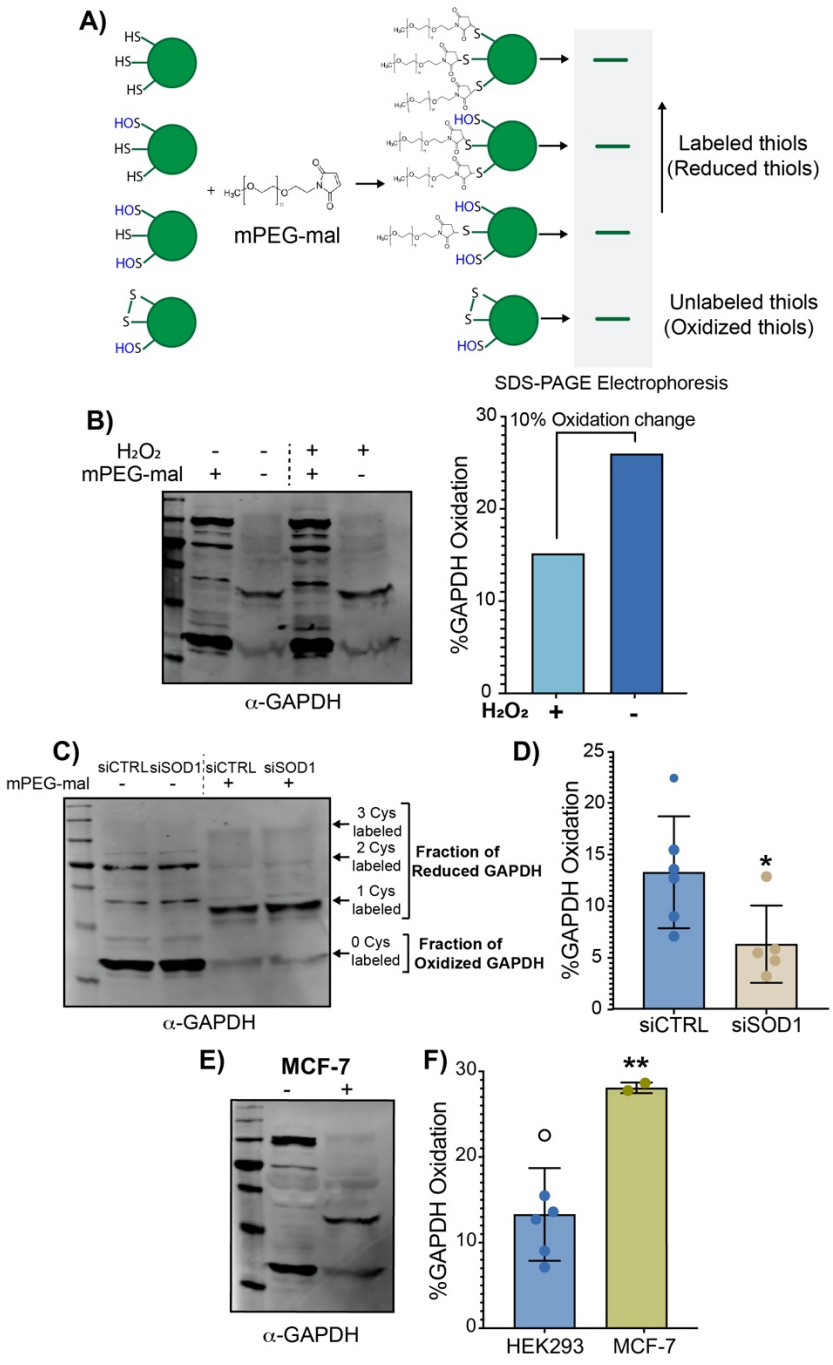

Figure B.4. Validation of H_2O_2 and Sod1-mediated GAPDH oxidation in human cell lines; related to Figure 4.5.

(A) Schematic representation of all possible redox-dependent GAPDH (green spheres) Cys-mPEG-mal adducts and their respective electrophoretic mobilities.

(B) Representative immunoblot analysis of GAPDH oxidation as assessed by mPEG-mal labeling from human embryonic kidney HEK293 cells that have been treated with 100μM 100μM H_2O_2 (+H_2O_2) or H_2O (-H_2O_2) and the %GAPDH oxidation (bar graph).

(C-D) Representative immunoblot analysis of GAPDH oxidation as assessed by mPEG-mal labeling of HEK293 cells with silenced (siSOD1) or unsilenced (siCTRL) *SOD1* **(C)**

and % GAPDH oxidation from multiple trials (**D**). Data represents the average ± SD from five or six biological replicates.
(E-F) Representative immunoblot analysis of GAPDH oxidation as assessed by mPEG-mal labeling of MCF-7 cells **(C)** and % GAPDH oxidation from multiple trials compared to HEK293 cells (**D**). Data represents the average ± SD from two and six biological replicates. The statistical significance relative to siCTRL or HEK293 cells is indicated by asterisks using two-tailed Student's t-test for pairwise comparison. *p<0.05, **p<0.01, ***p>0.001, ****p<0.0001, n.s.= not significant.

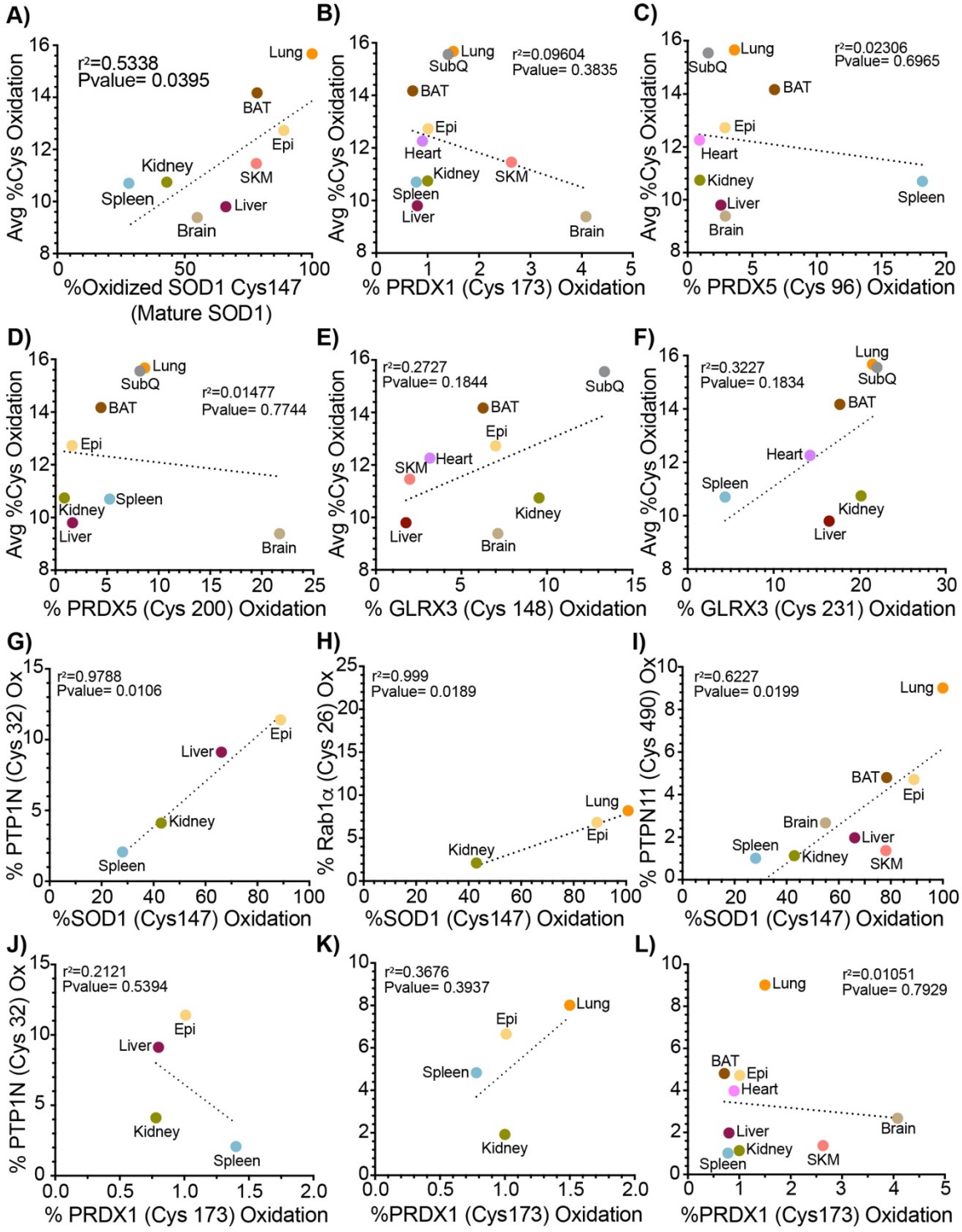

Figure B.5. Sod1 maturation correlates with overall and specific protein percentage cysteine oxidation in mice tissues quantified in the Oximouse study.
(A - F) The correlation between the average of percentage cysteine oxidation (Y axis) and Sod1 Cys147 **(A)**, Peroxiredoxin 1 (PRDX1) Cys173 **(B)**, Peroxiredoxin 5 (PRDX5) Cys96 **(C)**, Peroxiredoxin 5 (PRDX5) Cys200 **(D)**, Glutaredoxin 3 (GLRX3) Cys148 **(E)** and Glutaredoxin 3 (GLRX3) Cys231 **(F)** percentage cysteine oxidation (X axis) form individual

tissues is represented as an XY graph. A linear regression analysis gives a coefficient of determination (r^2) of .5538, 0.09604, 0.02306, 0.01477, 0.02727 and 0.3227, respectively, and a p-value of 0.0395, 0.3835,0.6965, 0.7744, 0.1844 and 0.1834, respectively.

(G - L) Sod1 Cys147 oxidation correlates with oxidation of PTP1N (Tyrosine-protein phosphatase non-receptor type I) Cys32, mouse homolog of PTP1B (protein tyrosine phosphatase 1B) **(G)**, Rab1α Cys26 **(H)** and PTPN11 (Tyrosine-protein phosphatase non-receptor type 11) Cys490 **(I)**. **(J** to **L)** PRDX1 Cys173 oxidation does not correlate with oxidation of PTP1N Cys32, mouse homolog of PTP1B **(J)**, Rab1α Cys26 **(K)** and PTPN11 Cys490 **(L).** A linear regression analysis gives a coefficient of determination (r^2) of 0.9788, 0.0999, 0.6227, 0.2121, 0.3676 and 0.01051, respectively, and a p-value of 0.0106, 0.0189, 0.0199, 0.5394, 0.3937 and 0.7929, respectively.

Tissue identity is indicated using distinctive colors and labels. Lung (orange), BAT (brown adipose tissue, brown), Epi (epididymal fat, yellow), SKM (skeletal muscle, coral), liver (dark red), heart (pink), spleen (light blue), kidney (dark green), brain (gold), SubQ (subcutaneous fat, gray).

The statistical significance is calculated using linear regression analysis. The Pearson's correlation coefficient (r) and p-value for each correlation are described in each graph, where $p<0.05$ corresponds to a significant correlation.

Primer name	Sequence	Description
prCMA009	5’ GAAGACTGGTAATGCCGGTCCAAGATCTGCCTGTGGTGTCATTG 3’	Site-directed mutagenesis of *SOD1* (*SOD1-P144S*). Forward primer
prCMA010	5’ CAATGACACCACAGGCAGATCTTGGACCGGCATTACCAGTCTTC 3’	Site-directed mutagenesis of *SOD1* (*SOD1-P144S*). Reverse primer
prCMA003	5’ GCTTCTTGTACCACCAACTCTTTGGCTCCATTGG 3’	Site-directed mutagenesis of *TDH3* (*TDH3-C154S*). Forward primer
prCMA004	5’ GCTTCTTGTACCACCAACGCTTTGGCTCCATTGG 3’	Site-directed mutagenesis of *TDH3* (*TDH3-C154S*). Reverse primer
prCMA017	5’ CAAATAAAACATAATGGATCCATAATGGTTCAAGCAGTCG 3’	Amplify *SOD1* to subclone in pCMA002. Forward primer (*BamHI* restriction site)
prCMA018	5’ CAAGTATATTCTCGAGAACATTAGTTGGTTAGACAC 3’	Amplify *SOD1* to subclone in pCMA002. Reverse primer (*XhoI* restriction site)

Table B.1. Primers used to generate the strains in Chapter 3

REFERENCES

1. Imlay, J. and S. Linn, *DNA damage and oxygen radical toxicity.* Science, 1988. **240**: p. 1302-1309.
2. Sturtz, L.A. and V.C. Culotta, *Superoxide dismutase null mutants of the bakers yeast Saccharomyces cerevisiae.* Meths. Enzymol., 2002. **349**: p. 167-72.
3. Murphy, Michael P., *How mitochondria produce reactive oxygen species.* Biochemical Journal, 2009. **417**(1): p. 1-13.
4. Chen, K., et al., *Regulation of ROS signal transduction by NADPH oxidase 4 localization.* J Cell Biol, 2008. **181**(7): p. 1129-39.
5. Fridovich, I., *Superoxide anion radical (O2/-??), superoxide dismutases, and related matters*. 1997. p. 18515-18517.
6. Okado-Matsumoto, A. and I. Fridovich, *Subcellular distribution of superoxide dismutases (SOD) in rat liver: Cu,Zn-SOD in mitochondria.* J. Biol. Chem., 2001. **276**(42): p. 38388-93.
7. Sturtz, L.A., et al., *A fraction of yeast Cu,Zn-superoxide dismutase and its metallochaperone, CCS, localize to the intermembrane space of mitochondria. A physiological role for SOD1 in guarding against mitochondrial oxidative damage.* Journal of Biological Chemistry, 2001. **276**(41): p. 38084-38089.
8. Rhee, S.G., et al., *Peroxiredoxin functions as a peroxidase and a regulator and sensor of local peroxides.* J Biol Chem, 2012. **287**(7): p. 4403-10.
9. Franco, R., et al., *The central role of glutathione in the pathophysiology of human diseases*. 2007. p. 234-258.
10. Poole, L.B., A. Hall, and K.J. Nelson, *Overview of peroxiredoxins in oxidant defense and redox regulation.* Current protocols in toxicology, 2011. **49**(1): p. 7.9. 1-7.9. 15.
11. Kirkman, H.N. and G.F. Gaetani, *Catalase: a tetrameric enzyme with four tightly bound molecules of NADPH.* Proceedings of the national academy of sciences, 1984. **81**(14): p. 4343-4347.
12. Imlay, J.A., *Cellular defenses against superoxide and hydrogen peroxide.* Annu. Rev. Biochem., 2008. **77**: p. 755-76.
13. Gerschman, R., *Oxygen poisoning and x-irradiation: a mechanism in common*, in *Glutathione*. 1954, Elsevier. p. 288-291.
14. Commoner, B., J. Townsend, and G.E. Pake, *Free radicals in biological materials.* Nature, 1954. **174**(4432): p. 689-691.
15. Harraan, D., *Aging: a theory based on free radical and radiation chemistry.* 1955.
16. Fridovich, I. and P. Handler, *Xanthine oxidase V. Differential inhibition of the reduction of various electron acceptors.* Journal of Biological Chemistry, 1962. **237**(3): p. 916-921.
17. McCord, J.M. and I. Fridovich, *Superoxide dismutase: An enzymic function for erythrocuprein (hemocuprein).* J. Biol. Chem., 1969. **244**: p. 6049-6055.
18. Loschen, G., L. Flohe, and B. Chance, *Respiratory chain linked H2O2 production in pigeon heart mitochondria.* FEBS letters, 1971. **18**(2): p. 261-264.

19. NOHL, H. and D. HEGNER, *Do mitochondria produce oxygen radicals in vivo?* European Journal of Biochemistry, 1978. **82**(2): p. 563-567.
20. Halliwell, B. and J.M.C. Gutteridge, *Free Radicals in Biology and Medicine*. 4 ed. 2007: Oxford Biosciences. 851.
21. Winterbourn, C.C., *Reconciling the chemistry and biology of reactive oxygen species.* Nature chemical biology, 2008. **4**(5): p. 278-286.
22. Imlay, J. and I. Fridovich, *Assay of metabolic superoxide production in Escherichia coli.* J. Biol. Chem., 1991. **266**: p. 6957-6955.
23. Turrens, J.F., et al., *The effect of hyperoxia on superoxide production by lung submitochondrial particles.* Archives of biochemistry and biophysics, 1982. **217**(2): p. 401-410.
24. Hoffman, D.L., J.D. Salter, and P.S. Brookes, *Response of mitochondrial reactive oxygen species generation to steady-state oxygen tension: implications for hypoxic cell signaling.* American Journal of Physiology-Heart and Circulatory Physiology, 2007. **292**(1): p. H101-H108.
25. Boveris, A. and B. Chance, *The mitochondrial generation of hydrogen peroxide. General properties and effect of hyperbaric oxygen.* Biochem J, 1973. **134**(3): p. 707-16.
26. Imlay, J.A., *Pathways of oxidative damage.* Annu Rev Microbiol, 2003. **57**: p. 395-418.
27. Holmström, K.M. and T. Finkel, *Cellular mechanisms and physiological consequences of redox-dependent signalling.* Nature reviews Molecular cell biology, 2014. **15**(6): p. 411-421.
28. Bienert, G.P., J.K. Schjoerring, and T.P. Jahn, *Membrane transport of hydrogen peroxide.* Biochimica et Biophysica Acta (BBA)-Biomembranes, 2006. **1758**(8): p. 994-1003.
29. Bienert, G.P., et al., *Specific aquaporins facilitate the diffusion of hydrogen peroxide across membranes.* Journal of Biological Chemistry, 2007. **282**(2): p. 1183-1192.
30. Paulsen, C.E., et al., *Peroxide-dependent sulfenylation of the EGFR catalytic site enhances kinase activity.* Nat Chem Biol, 2011. **8**(1): p. 57-64.
31. Juarez, J.C., et al., *Superoxide dismutase 1 (SOD1) is essential for H2O2-mediated oxidation and inactivation of phosphatases in growth factor signaling.* Proc. Natl. Acad. Sci. U. S. A., 2008. **105**(20): p. 7147-52.
32. Nakashima, I., et al., *Redox-linked signal transduction pathways for protein tyrosine kinase activation.* Antioxidants and Redox Signaling, 2002. **4**(3): p. 517-531.
33. Keyes, J.D., et al., *Endogenous, regulatory cysteine sulfenylation of ERK kinases in response to proliferative signals.* Free Radical Biology and Medicine, 2017.
34. Corcoran, A. and T.G. Cotter, *Redox regulation of protein kinases.* The FEBS journal, 2013. **280**(9): p. 1944-1965.
35. Reddi, A.R. and V.C. Culotta, *SOD1 integrates signals from oxygen and glucose to repress respiration.* Cell, 2013. **152**(1-2): p. 224-35.

36. Sobotta, M.C., et al., *Peroxiredoxin-2 and STAT3 form a redox relay for H 2 O 2 signaling.* Nature chemical biology, 2015. **11**(1): p. 64-70.
37. Delaunay, A., et al., *A thiol peroxidase is an H2O2 receptor and redox-transducer in gene activation.* Cell, 2002. **111**(4): p. 471-481.
38. Ahn, S.-G. and D.J. Thiele, *Redox regulation of mammalian heat shock factor 1 is essential for Hsp gene activation and protection from stress.* Genes & development, 2003. **17**(4): p. 516-528.
39. Cai, H., *Hydrogen peroxide regulation of endothelial function: origins, mechanisms, and consequences.* Cardiovascular research, 2005. **68**(1): p. 26-36.
40. Boudreau, H.E., et al., *Nox4 involvement in TGF-beta and SMAD3-driven induction of the epithelial-to-mesenchymal transition and migration of breast epithelial cells.* Free Radical Biology and Medicine, 2012. **53**(7): p. 1489-1499.
41. Niethammer, P., et al., *A tissue-scale gradient of hydrogen peroxide mediates rapid wound detection in zebrafish.* Nature, 2009. **459**(7249): p. 996-999.
42. Sies, H., *Hydrogen peroxide as a central redox signaling molecule in physiological oxidative stress: Oxidative eustress.* Redox Biol, 2017. **11**: p. 613-619.
43. Stone, J.R. and S. Yang, *Hydrogen peroxide: a signaling messenger.* Antioxidants & redox signaling, 2006. **8**(3-4): p. 243-270.
44. Sarsour, E.H., A.L. Kalen, and P.C. Goswami, *Manganese superoxide dismutase regulates a redox cycle within the cell cycle.* Antioxidants & redox signaling, 2014. **20**(10): p. 1618-1627.
45. Niki, E., *Oxidative stress and antioxidants: Distress or eustress?* Free Radical Biology and Medicine, 2018. **124**: p. 564.
46. Selye, H., *Stress without distress*, in *Psychopathology of human adaptation*. 1976, Springer. p. 137-146.
47. Lushchak, V.I., *Free radicals, reactive oxygen species, oxidative stress and its classification.* Chemico-biological interactions, 2014. **224**: p. 164-175.
48. Winterbourn, C.C. and A.V. Peskin, *Kinetic approaches to measuring peroxiredoxin reactivity.* Molecules and cells, 2016. **39**(1): p. 26.
49. Winterbourn, C.C. and M.B. Hampton, *Thiol chemistry and specificity in redox signaling.* Free Radic Biol Med, 2008. **45**(5): p. 549-61.
50. Gutscher, M., et al., *Proximity-based protein thiol oxidation by H2O2-scavenging peroxidases.* Journal of Biological Chemistry, 2009. **284**(46): p. 31532-31540.
51. Stöcker, S., et al., *A role for 2-Cys peroxiredoxins in facilitating cytosolic protein thiol oxidation.* Nature chemical biology, 2018. **14**(2): p. 148.
52. Wood, Z.A., L.B. Poole, and P.A. Karplus, *Peroxiredoxin evolution and the regulation of hydrogen peroxide signaling.* Science, 2003. **300**(5619): p. 650-3.
53. Bedard, K. and K.H. Krause, *The NOX family of ROS-generating NADPH oxidases: physiology and pathophysiology.* Physiol Rev, 2007. **87**(1): p. 245-313.
54. Block, K. and Y. Gorin, *Aiding and abetting roles of NOX oxidases in cellular transformation.* Nat Rev Cancer, 2012. **12**(9): p. 627-37.
55. Jiang, F., Y. Zhang, and G.J. Dusting, *NADPH oxidase-mediated redox signaling: roles in cellular stress response, stress tolerance, and tissue repair.* Pharmacological Reviews, 2011. **63**(1): p. 218-242.

56. Fisher, A.B., *Redox signaling across cell membranes.* Antioxid Redox Signal, 2009. **11**(6): p. 1349-56.
57. Wang, Y., et al., *Superoxide dismutases: Dual roles in controlling ROS damage and regulating ROS signaling.* J Cell Biol, 2018. **217**(6): p. 1915-1928.
58. Antonyuk, S.V., et al., *The structure of human extracellular copper–zinc superoxide dismutase at 1.7 Å resolution: insights into heparin and collagen binding.* Journal of molecular biology, 2009. **388**(2): p. 310-326.
59. Marklund, S.L., *Extracellular superoxide dismutase in human tissues and human cell lines.* The Journal of clinical investigation, 1984. **74**(4): p. 1398-1403.
60. Marklund, S.L., *Product of extracellular-superoxide dismutase catalysis.* FEBS letters, 1985. **184**(2): p. 237-239.
61. Kang, Y., et al., *Structures of native and Fe-substituted SOD2 from Saccharomyces cerevisiae.* Acta Cryst. Sec. F, 2011.
62. Yang, M., et al., *The effects of mitochondrial iron homeostasis on cofactor specificity of superoxide dismutase 2.* EMBO J., 2006. **25**: p. 1775-83.
63. Naranuntarat, A., et al., *The interaction of mitochondrial iron with manganese superoxide dismutase.* J Biol Chem, 2009. **284**(34): p. 22633-40.
64. He, C., et al., *SOD2 acetylation on lysine 68 promotes stem cell reprogramming in breast cancer.* Proceedings of the National Academy of Sciences, 2019. **116**(47): p. 23534-23541.
65. Zhu, Y., et al., *Lysine 68 acetylation directs MnSOD as a tetrameric detoxification complex versus a monomeric tumor promoter.* Nature communications, 2019. **10**(1): p. 1-15.
66. Smith, M.W. and R.F. Doolittle, *A comparison of evolutionary rates of the two major kinds of superoxide dismutase.* Journal of molecular evolution, 1992. **34**(2): p. 175-184.
67. Perry, J., et al., *The structural biochemistry of the superoxide dismutases.* Biochimica et Biophysica Acta (BBA)-Proteins and Proteomics, 2010. **1804**(2): p. 245-262.
68. Kwasigroch, J.M., et al., *SODa: an Mn/Fe superoxide dismutase prediction and design server.* BMC Bioinformatics, 2008. **9**: p. 257.
69. Lancaster, V.L., et al., *A cambialistic superoxide dismutase in the thermophilic photosynthetic bacterium Chloroflexus aurantiacus.* Journal of bacteriology, 2004. **186**(11): p. 3408-3414.
70. Youn, H.-D., et al., *A novel nickel-containing superoxide dismutase from Streptomyces spp.* Biochemical Journal, 1996. **318**(3): p. 889-896.
71. Youn, H.-D., et al., *Unique Isozymes of Superoxide Dismutase inStreptomyces griseus.* Archives of biochemistry and biophysics, 1996. **334**(2): p. 341-348.
72. Palenik, B., et al., *The genome of a motile marine Synechococcus.* Nature, 2003. **424**(6952): p. 1037-1042.
73. Schmidt, A., et al., *In silico analysis of nickel containing superoxide dismutase evolution and regulation.* Journal of basic microbiology, 2009. **49**(1): p. 109-118.
74. Chang, L., et al., *Molecular Immunochrochemistry of the Cu/Zn superoxide dismutase in rat hepatocytes.* J. Cell. Biol., 1988. **107**: p. 2169-2179.

75. Banci, L., et al., *Atomic-resolution monitoring of protein maturation in live human cells by NMR.* Nat Chem Biol, 2013. **9**(5): p. 297-9.
76. Bartnikas, T.B. and J.D. Gitlin, *Mechanisms of biosynthesis of mammalian copper/zinc superoxide dismutase.* J. Biol. Chem., 2003. **278**: p. 33602-33608.
77. M. Fetherolf, M., et al., *Oxygen-dependent activation of Cu,Zn-superoxide dismutase-1.* Metallomics, 2017.
78. Woodruff, R.C., J.P. Phillips, and A.J. Hilliker, *Increased spontaneous DNA damage in Cu/Zn superoxide dismutase (SOD1) deficient Drosophila.* Genome, 2004. **47**(6): p. 1029-1035.
79. Reaume, A.G., et al., *Motor neurons in Cu/Zn superoxide dismutase-deficient mice develop normally but exhibit enhanced cell death after axonal injury.* Nature Genetics, 1996. **13**(1): p. 43-47.
80. Elchuri, S., et al., *CuZnSOD deficiency leads to persistent and widespread oxidative damage and hepatocarcinogenesis later in life.* Oncogene, 2005. **24**(3): p. 367-80.
81. Montllor-Albalate, C., et al., *Extra-mitochondrial Cu/Zn superoxide dismutase (Sod1) is dispensable for protection against oxidative stress but mediates peroxide signaling in Saccharomyces cerevisiae.* Redox Biol, 2019. **21**: p. 101064.
82. Sturtz, L.A. and V.C. Culotta, *Superoxide dismutase null mutants of baker's yeast, Saccharomyces cerevisiae.* Methods Enzymol., 2002. **349**(Copyright (C) 2013 American Chemical Society (ACS). All Rights Reserved.): p. 167-172.
83. Strain, J., et al., *Suppressors of superoxide dismutase (SOD1) deficiency in Saccharomyces cerevisiae: identification of proteins predicted to mediate iron-sulfur cluster assembly.* J. Biol. Chem., 1998. **273**: p. 31138-31144.
84. Tainer, J.A., et al., *Determination and analysis of the 2 A-structure of copper, zinc superoxide dismutase.* J. Mol. Biol., 1982. **160**: p. 181-217.
85. Hart, P.J., et al., *A structure-based mechanism for copper− zinc superoxide dismutase.* Biochemistry, 1999. **38**(7): p. 2167-2178.
86. Hough, M.A. and S.S. Hasnain, *Structure of fully reduced bovine copper zinc superoxide dismutase at 1.15 Å.* Structure, 2003. **11**(8): p. 937-946.
87. Forman, H.J. and I. Fridovich, *On the stability of bovine superoxide dismutase.* J. Biol. Chem., 1973. **248**: p. 2645-2649.
88. Tainer, J.A., et al., *Structure and mechanism of copper, zinc superoxide dismutase.* Nature, 1983. **306**(5940): p. 284-7.
89. Rae, T.D., et al., *Undetectable intracellular free copper: the requirement of a copper chaperone for superoxide dismutase.* Science, 1999. **284**(5415): p. 805-8.
90. Sea, K.W., et al., *Yeast copper–zinc superoxide dismutase can be activated in the absence of its copper chaperone.* JBIC Journal of Biological Inorganic Chemistry, 2013. **18**(8): p. 985-992.
91. Kirby, K., et al., *Instability of superoxide dismutase 1 of Drosophila in mutants deficient for its cognate copper chaperone.* J. Biol. Chem., 2008. **283**: p. 35393-401.
92. Carroll, M.C., et al., *Mechanisms for activating Cu- and Zn-containing superoxide dismutase in the absence of the CCS Cu chaperone.* Proc Natl Acad Sci U S A, 2004. **101**(16): p. 5964-9.

93. Leitch, J.M., et al., *Activation of Cu,Zn-superoxide dismutase in the absence of oxygen and the copper chaperone CCS.* J. Biol. Chem., 2009. **284**(33): p. 21863-71.
94. Brown, N.M., et al., *Oxygen and the copper chaperone CCS regulate posttranslational activation of Cu,Zn superoxide dismutase.* Proc. Natl. Acad. Sci. U. S. A., 2004. **101**: p. 5518-23.
95. Leitch, J.M., P.J. Yick, and V.C. Culotta, *The right to choose: multiple pathways for activating copper,zinc superoxide dismutase.* J Biol Chem, 2009. **284**(37): p. 24679-83.
96. Lamb, A.L., et al., *Heterodimer formation between superoxide dismutase and its copper chaperone.* Biochemistry, 2000. **39**(48): p. 14720-7.
97. Lamb, A.L., et al., *Crystal structure of the copper chaperone for superoxide dismutase.* Nat Struct Biol, 1999. **6**(8): p. 724-9.
98. Schmidt, P., et al., *Multiple protein domains contribute to the action of the copper chaperone for superoxide dismutase.* J. Biol. Chem., 1999. **274**: p. 23719-23725.
99. Fetherolf, M.M., et al., *Copper-zinc superoxide dismutase is activated through a sulfenic acid intermediate at a copper ion entry site.* Journal of Biological Chemistry, 2017. **292**(29): p. 12025-12040.
100. Okado-Matsumoto, A. and I. Fridovich, *Subcellular distribution of superoxide dismutase (SOD) in rat liver. Cu/Zn SOD in mitochondria.* J. Biol. Chem., 2001. **276**: p. 38388-38393.
101. Keller, G.A., et al., *Cu,Zn superoxide dismutase is a peroxisomal enzyme in human fibroblasts and hepatoma cells.* Proc. Natl. Acad. Sci. U.S.A., 1991. **88**: p. 7381-7385.
102. Geller, B.L. and D.R. Winge, *Rat Liver Cu,Zn-superoxide dismutase.* J. Biol. Chem., 1982. **257**: p. 8945-8952.
103. Urushitani, M., et al., *Chromogranin-mediated secretion of mutant superoxide dismutase proteins linked to amyotrophic lateral sclerosis.* Nature neuroscience, 2006. **9**(1): p. 108-118.
104. Kikuchi, H., et al., *Spinal cord endoplasmic reticulum stress associated with a microsomal accumulation of mutant superoxide dismutase-1 in an ALS model.* Proceedings of the National Academy of Sciences, 2006. **103**(15): p. 6025-6030.
105. Tsang, C.K.w., et al., *Superoxide dismutase 1 acts as a nuclear transcription factor to regulate oxidative stress resistance.* Nature communications, 2014. **5**: p. 3446-3446.
106. Kawamata, H. and G. Manfredi, *Different regulation of wild-type and mutant Cu,Zn superoxide dismutase localization in mammalian mitochondria.* Hum Mol Genet, 2008. **17**(21): p. 3303-17.
107. Reddehase, S., et al., *The disulfide relay system of mitochondria is required for the biogenesis of mitochondrial Ccs1 and Sod1.* J Mol Biol, 2009. **385**(2): p. 331-8.
108. Mesecke, N., et al., *A disulfide relay system in the intermembrane space of mitochondria that mediates protein import.* Cell, 2005. **121**(7): p. 1059-69.
109. Han, D., E. WILLIAMS, and E. CADENAS, *Mitochondrial respiratory chain-dependent generation of superoxide anion and its release into the intermembrane space.* Biochemical Journal, 2001. **353**(2): p. 411-416.

110. Longo, V.D. and E.B. Gralla, *Superoxide Dismutase Activity Is Essential for Stationary Phase Survival in Saccharomyces cerevisiae.* JOURNAL OF BIOLOGICAL CHEMISTRY, 1996.
111. Goldsteins, G., et al., *Deleterious role of superoxide dismutase in the mitochondrial intermembrane space.* J Biol Chem, 2008.
112. Montllor-Albalate, C., et al., *Extra-mitochondrial Cu/Zn superoxide dismutase (Sod1) is dispensable for protection against oxidative stress but mediates peroxide signaling in Saccharomyces cerevisiae.* Redox biology, 2019. **21**: p. 101064.
113. Tsang, C.K., et al., *SOD1 Phosphorylation by mTORC1 Couples Nutrient Sensing and Redox Regulation.* Mol Cell, 2018. **70**(3): p. 502-515 e8.
114. Banks, C. and J. Andersen, *Mechanisms of SOD1 regulation by post-translational modifications.* Redox biology, 2019. **26**: p. 101270.
115. Banks, C.J., et al., *Acylation of Superoxide Dismutase 1 (SOD1) at K122 Governs SOD1-Mediated Inhibition of Mitochondrial Respiration.* Mol Cell Biol, 2017. **37**(20).
116. Sakanyan, V., et al., *Activation of EGFR by small compounds through coupling the generation of hydrogen peroxide to stable dimerization of Cu/Zn SOD1.* Sci Rep, 2016. **6**: p. 21088.
117. Juarez, J.C., et al., *Copper binding by tetrathiomolybdate attenuates angiogenesis and tumor cell proliferation through the inhibition of superoxide dismutase 1.* Clinical cancer research : an official journal of the American Association for Cancer Research, 2006. **12**(16): p. 4974-82.
118. Papa, L., et al., *SOD2 to SOD1 switch in breast cancer.* J Biol Chem, 2014. **289**(9): p. 5412-6.
119. Papa, L., G. Manfredi, and D. Germain, *SOD1, an unexpected novel target for cancer therapy.* Genes Cancer, 2014. **5**(1-2): p. 15-21.
120. Huang, P., et al., *Superoxide dismutase as a target for the selective killing of cancer cells.* Nature, 2000. **407**(6802): p. 390-5.
121. Somwar, R., et al., *Superoxide dismutase 1 (SOD1) is a target for a small molecule identified in a screen for inhibitors of the growth of lung adenocarcinoma cell lines.* Proc Natl Acad Sci U S A, 2011. **108**(39): p. 16375-80.
122. Flint, D.H., j.F. Tuminello, and M.H. Emptage, *The inactivation of Fe-S cluster containing hydro-lyases by superoxide.* J. Biol. Chem., 1993. **268**: p. 22369-22376.
123. Liochev, S.I. and I. Fridovich, *Superoxide and iron: partners in crime.* IUBMB Life, 1999. **48**(2): p. 157-61.
124. Bilinski, T., et al., *Is hydroxyl radical generated by the fenton reaction in vivo?* Biochem. Biophys. Res. Comm., 1985. **130**: p. 533-539.
125. Forman, H.J., M. Maiorino, and F. Ursini, *Signaling Functions of Reactive Oxygen Species.* Biochemistry, 2010. **49**(5): p. 835-842.
126. Veal, E.A., A.M. Day, and B.A. Morgan, *Hydrogen peroxide sensing and signaling.* Mol Cell, 2007. **26**(1): p. 1-14.
127. Veal, E. and A. Day, *Hydrogen peroxide as a signaling molecule.* Antioxid Redox Signal, 2011. **15**(1): p. 147-51.

128. Meng, T.C., T. Fukada, and N.K. Tonks, *Reversible oxidation and inactivation of protein tyrosine phosphatases in vivo.* Mol Cell, 2002. **9**(2): p. 387-99.
129. Denu, J.M. and K.G. Tanner, *Specific and reversible inactivation of protein tyrosine phosphatases by hydrogen peroxide: evidence for a sulfenic acid intermediate and implications for redox regulation.* Biochemistry, 1998. **37**(16): p. 5633-42.
130. Keyes, J.D., et al., *Endogenous, regulatory cysteine sulfenylation of ERK kinases in response to proliferative signals.* Free Radic Biol Med, 2017. **112**: p. 534-543.
131. Peralta, D., et al., *A proton relay enhances H2O2 sensitivity of GAPDH to facilitate metabolic adaptation.* Nat Chem Biol, 2015. **11**(2): p. 156-63.
132. Dinkova-Kostova, A.T., et al., *Direct evidence that sulfhydryl groups of Keap1 are the sensors regulating induction of phase 2 enzymes that protect against carcinogens and oxidants.* Proc. Natl. Acad. Sci. U. S. A., 2002. **99**(18): p. 11908-13.
133. Zhang, D.D., et al., *Keap1 is a redox-regulated substrate adaptor protein for a Cul3-dependent ubiquitin ligase complex.* Mol. Cell. Biol., 2004. **24**(24): p. 10941-53.
134. Shanmugasundaram, K., et al., *NOX4 functions as a mitochondrial energetic sensor coupling cancer metabolic reprogramming to drug resistance.* Nat Commun, 2017. **8**(1): p. 997.
135. Muller, F.L., Y. Liu, and H. Van Remmen, *Complex III releases superoxide to both sides of the inner mitochondrial membrane.* J Biol Chem, 2004. **279**(47): p. 49064-73.
136. Muller, F.L., et al., *High rates of superoxide production in skeletal-muscle mitochondria respiring on both complex I- and complex II-linked substrates.* Biochem J, 2008. **409**(2): p. 491-9.
137. Lustgarten, M.S., et al., *Complex I generated, mitochondrial matrix-directed superoxide is released from the mitochondria through voltage dependent anion channels.* Biochem Biophys Res Commun, 2012. **422**(3): p. 515-21.
138. Ichikawa, M., et al., *Subcellular localization of xanthine oxidase in rat hepatocytes: high-resolution immunoelectron microscopic study combined with biochemical analysis.* J Histochem Cytochem, 1992. **40**(8): p. 1097-103.
139. Jarasch, E.D., et al., *Localization of xanthine oxidase in mammary-gland epithelium and capillary endothelium.* Cell, 1981. **25**(1): p. 67-82.
140. Pizzinat, N., et al., *Reactive oxygen species production by monoamine oxidases in intact cells.* Naunyn Schmiedebergs Arch Pharmacol, 1999. **359**(5): p. 428-31.
141. Hrycay, E.G. and S.M. Bandiera, *Involvement of Cytochrome P450 in Reactive Oxygen Species Formation and Cancer.* Adv Pharmacol, 2015. **74**: p. 35-84.
142. Wallace, W.J., et al., *Mechanism of autooxidation for hemoglobins and myoglobins. Promotion of superoxide production by protons and anions.* J Biol Chem, 1982. **257**(9): p. 4966-77.
143. De Henau, S., et al., *A redox signalling globin is essential for reproduction in Caenorhabditis elegans.* Nat Commun, 2015. **6**: p. 8782.
144. Lei, X.G., et al., *Paradoxical Roles of Antioxidant Enzymes: Basic Mechanisms and Health Implications.* Physiol Rev, 2016. **96**(1): p. 307-64.
145. Weisiger, R.A. and I. Fridovich, *Mitochondrial superoxide dismutase.* J. Biol. Chem., 1973. **248**: p. 4793-4796.

146. Sturtz, L.A., et al., *A Fraction of Yeast Cu,Zn-Superoxide Dismutase and Its Metallochaperone, CCS, Localize to the Intermembrane Space of Mitochondria.* J. Biol. Chem., 2001. **276**: p. 38084-38089.
147. Tsang C. K., L., Y., Thomas, J., Zhang. Y., Zheng X. F., *Superoxide dismutase 1 acts as a nuclear transcription factor to regulate oxidative stress resistance.* Nat Commun, 2014. **5**: p. 3446.
148. Takeuchi, H., et al., *Mitochondrial localization of mutant superoxide dismutase 1 triggers caspase-dependent cell death in a cellular model of familial amyotrophic lateral sclerosis.* J Biol Chem, 2002. **277**(52): p. 50966-72.
149. Islinger, M., et al., *Hitchhiking of Cu/Zn superoxide dismutase to peroxisomes--evidence for a natural piggyback import mechanism in mammals.* Traffic, 2009. **10**(11): p. 1711-21.
150. Jackson, M.J., *Lack of CuZnSOD activity: a pointer to the mechanisms underlying age-related loss of muscle function, a commentary on "absence of CuZn superoxide dismutase leads to elevated oxidative stress and acceleration of age-dependent skeletal muscle atrophy".* Free. Radic. Biol. Med., 2006. **40**(11): p. 1900-2.
151. Muller, F.L., et al., *Absence of CuZn superoxide dismutase leads to elevated oxidative stress and acceleration of age-dependent skeletal muscle atrophy.* Free Radic. Biol. Med., 2006. **40**(11): p. 1993-2004.
152. Jang, Y.C., et al., *Increased superoxide in vivo accelerates age-associated muscle atrophy through mitochondrial dysfunction and neuromuscular junction degeneration.* FASEB J, 2010. **24**(5): p. 1376-90.
153. Sentman, M.L., et al., *Phenotypes of mice lacking extracellular superoxide dismutase and copper- and zinc-containing superoxide dismutase.* J Biol Chem, 2006. **281**(11): p. 6904-9.
154. Reaume, A.G., et al., *Motor neurons in Cu/Zn-SOD superoxide dismutase-deficient mice develop normally but exhibit enhanced cell death after axonal injury.* Nat. Genet., 1996. **13**: p. 43-47.
155. Phillips, J., et al., *Null mutations of copper/zinc superoxide in Drosophila confer hypersensitivity to paraquat and reduced longevity.* Proc. Natl. Acad. Sci. U.S.A., 1989. **83**: p. 3820-3824.
156. Chang, E. and D. Kosman, *O_2-dependent methionine auxotrophy in Cu,Zn Superoxide dismutase deficient mutants of Saccharomyces cerevisiae.* J. Bacteriol., 1990. **172**: p. 1840-1845.
157. Slekar, K.H., D. Kosman, and V.C. Culotta, *The yeast copper/zinc superoxide dismutase and the pentose phosphate pathway play overlapping roles in oxidative stress protection.* J. Biol. Chem., 1996. **271**: p. 28831-28836.
158. Sanchez, R.J., et al., *Exogenous manganous ion at millimolar levels rescues all known dioxygen-sensitive phenotypes of yeast lacking CuZnSOD.* J Biol Inorg Chem, 2005. **10**(8): p. 913-23.
159. Corson, L.B., et al., *Oxidative stress and iron are implicated in fragmenting vacuoles of Saccharomyces cerevisiae lacking Cu,Zn Superoxide dismtuase.* J. Biol. Chem., 1999. **274**: p. 27590-27596.

160. Freitas, J.M.D., et al., *Yeast Lacking Cu-Zn Superoxide Dismutase Show Altered Iron Homeostasis. Role of oxidative stress in iron metabolism.* J. Biol. Chem., 2000. **275**: p. 11645-11649.
161. Srinivasan, S.C., et al., *Yeast Lacking Superoxide Dismutase(s) Show Elevated Levels of "Free Iron" as Measured by Whole Cell Electron Paramagnetic Resonance.* J. Biol. Chem., 2000. **275**: p. 29187-29192.
162. Pardo, C.A., et al., *Superoxide dismutase is an abundant component in cell bodies, dendrites, and axons of motor neurons and in a subset of other neurons.* Proc. Natl. Acad. Sci. USA, 1995. **92**: p. 954-958.
163. Ghaemmaghami, S., et al., *Global analysis of protein expression in yeast.* Nature, 2003. **425**(6959): p. 737-41.
164. Kulak, N.A., et al., *Minimal, encapsulated proteomic-sample processing applied to copy-number estimation in eukaryotic cells.* Nat Methods, 2014. **11**(3): p. 319-24.
165. Reddi, A.R. and V.C. Culotta, *Regulation of Manganese Antioxidants by Nutrient Sensing Pathways in Saccharomyces cerevisiae.* Genetics, 2011. **189**: p. 1261-70.
166. Klug, D., J. Rabani, and I. Fridovich, *A direct demonstration of the catalytic action of superoxide dismutase through the use of pulse radiolysis.* J Biol Chem, 1972. **247**(15): p. 4839-42.
167. Neklesa, T.K. and R.W. Davis, *Superoxide anions regulate TORC1 and its ability to bind Fpr1:rapamycin complex.* Proc. Natl. Acad. Sci. U. S. A., 2008. **105**(39): p. 15166-71.
168. Wallace, M.A., et al., *Superoxide inhibits 4Fe-4S cluster enzymes involved in amino acid biosynthesis. Cross-compartment protection by CuZn-superoxide dismutase.* J. Biol. Chem., 2004. **279**(31): p. 32055-62.
169. Longo, V.D., E.B. Gralla, and J.S. Valentine, *Superoxide dismutase activity is essential for stationary phase survival in Saccharomyces cerevisiae: Mitochondrial production of toxic oxygen species in vivo.* J. Biol. Chem., 1996. **271**: p. 12275-12280.
170. Sehati, S., et al., *Metabolic alterations in yeast lacking copper-zinc superoxide dismutase.* Free Radic. Biol. Med., 2011. **50**(11): p. 1591-8.
171. Zielonka, J., J. Vasquez-Vivar, and B. Kalyanaraman, *Detection of 2-hydroxyethidium in cellular systems: a unique marker product of superoxide and hydroethidine.* Nat Protoc, 2008. **3**(1): p. 8-21.
172. Wood, L.K. and D.J. Thiele, *Transcriptional activation in yeast in response to copper deficiency involves copper-zinc superoxide dismutase.* J. Biol. Chem., 2009. **284**(1): p. 404-13.
173. Rinnerthaler, M., et al., *Yno1p/Aim14p, a NADPH-oxidase ortholog, controls extramitochondrial reactive oxygen species generation, apoptosis, and actin cable formation in yeast.* Proc. Natl. Acad. Sci. U. S. A., 2012. **109**(22): p. 8658-63.
174. Sawyer, D.T. and J.S. Valentine, *How super is superoxide?* Acc Chem Res, 1981. **14**: p. 393-400.
175. Fee, J.A., *Is superoxide important in oxygen poisoning?* Trends Biochem. Sci., 1982. **3**: p. 84-86.

176. Corson, L.B., et al., *Chaperone-facilitated copper binding is a property common to several classes of familial amyotrophic lateral sclerosis-linked superoxide dismutase mutants.* Proc. Natl. Acad. Sci. USA, 1998. **95**: p. 6361-6366.
177. Culotta, V.C., et al., *A physiological role for Saccharomyces cerevisiae copper/zinc superoxide dismutase in copper buffering.* J. Biol. Chem., 1995. **270**: p. 29991-29997.
178. Petrovic, N., A. Comi, and M.J. Ettinger, *Copper incorporation into superoxide dismutase in Menkes lymphoblasts.* J. Biol. Chem., 1996. **271**: p. 28335-28340.
179. Wang, P., et al., *Overexpression of human copper, zinc-superoxide dismutase (SOD1) prevents postischemic injury.* Proc Natl Acad Sci U S A, 1998. **95**(8): p. 4556-60.
180. Han, D., et al., *Voltage-dependent anion channels control the release of the superoxide anion from mitochondria to cytosol.* J Biol Chem, 2003. **278**(8): p. 5557-63.
181. Tormos, K.V., et al., *Mitochondrial complex III ROS regulate adipocyte differentiation.* Cell Metab, 2011. **14**(4): p. 537-44.
182. Hamanaka, R.B. and N.S. Chandel, *Mitochondrial reactive oxygen species regulate cellular signaling and dictate biological outcomes.* Trends Biochem Sci, 2010. **35**(9): p. 505-13.
183. Glasauer, A., et al., *Targeting SOD1 reduces experimental non-small-cell lung cancer.* J Clin Invest, 2014. **124**(1): p. 117-28.
184. Rowan, A., *SOD1 targeting in ALS.* Nature Reviews Neuroscience, 2004. **5**: p. 676.
185. Tokuda, E. and Y. Furukawa, *Copper Homeostasis as a Therapeutic Target in Amyotrophic Lateral Sclerosis with SOD1 Mutations.* Int J Mol Sci, 2016. **17**(5).
186. Zhang, Y., et al., *A new role for oxidative stress in aging: The accelerated aging phenotype in Sod1(-/)(-) mice is correlated to increased cellular senescence.* Redox Biol, 2017. **11**: p. 30-37.
187. Blander, G., et al., *Superoxide dismutase 1 knock-down induces senescence in human fibroblasts.* J Biol Chem, 2003. **278**(40): p. 38966-9.
188. Leitch, J.M., et al., *Post-translational modification of Cu/Zn superoxide dismutase under anaerobic conditions.* Biochemistry, 2012. **51**(2): p. 677-85.
189. Chernoff, Y.O., et al., *Evidence for a protein mutator in yeast: role of the Hsp70-related chaperone ssb in formation, stability, and toxicity of the [PSI] prion.* Mol Cell Biol, 1999. **19**(12): p. 8103-12.
190. Gietz, R.D. and R.H. Schiestl, *Applications of high efficiency lithium acetate trasformation of intact yeast cells using single-stranded nucleic acids as carrier.* Yeast, 1991. **7**: p. 253-263.
191. Ness, F., et al., *Sterol uptake in Saccharomyces cerevisiae heme auxotrophic mutants is affected by ergosterol and oleate but not by palmitoleate or by sterol esterification.* J Bacteriol, 1998. **180**(7): p. 1913-9.
192. Hanna, D.A., et al., *Heme dynamics and trafficking factors revealed by genetically encoded fluorescent heme sensors.* Proc Natl Acad Sci U S A, 2016. **113**(27): p. 7539-44.

193. Flohe, L. and F. Otting, *Superoxide dismutase assays*, in *Methods in enzymology: oxygen radicals in biological systems*, L. Packer, Editor. 1984, Academic press: New York. p. 93-104.
194. Luk, E., et al., *Manganese activation of superoxide dismutase 2 in the mitochondria of Saccharomyces cerevisiae.* J. Biol. Chem., 2005. **280**(24): p. 22715-20.
195. Srinivasan, C. and E.B. Gralla, *Measurement of "free" or electron paramagnetic resonance-detectable iron in whole yeast cells as indicator of superoxide stress.* Methods Enzymol, 2002. **349**: p. 173-80.
196. Petrat, F., U. Rauen, and H. de Groot, *Determination of the chelatable iron pool of isolated rat hepatocytes by digital fluorescence microscopy using the fluorescent probe, phen green SK.* Hepatology, 1999. **29**(4): p. 1171-9.
197. Irazusta, V., et al., *Major targets of iron-induced protein oxidative damage in frataxin-deficient yeasts are magnesium-binding proteins.* Free Radic Biol Med, 2008. **44**(9): p. 1712-23.
198. Fernandez-Castane, A., et al., *Flow cytometry as a rapid analytical tool to determine physiological responses to changing O2 and iron concentration by Magnetospirillum gryphiswaldense strain MSR-1.* Sci Rep, 2017. **7**(1): p. 13118.
199. Turrens, J.F., *Mitochondrial formation of reactive oxygen species.* J Physiol, 2003. **552**(Pt 2): p. 335-44.
200. Imlay, J.A., *Where in the world do bacteria experience oxidative stress?* Environ Microbiol, 2019. **21**(2): p. 521-530.
201. Sobotta, M.C., et al., *Peroxiredoxin-2 and STAT3 form a redox relay for H2O2 signaling.* Nat Chem Biol, 2015. **11**(1): p. 64-70.
202. Finkel, T., *Signal transduction by reactive oxygen species.* J Cell Biol, 2011. **194**(1): p. 7-15.
203. Moriya, H. and M. Johnston, *Glucose sensing and signaling in Saccharomyces cerevisiae through the Rgt2 glucose sensor and casein kinase I.* Proc. Natl. Acad. Sci. U. S. A., 2004. **101**(6): p. 1572-7.
204. Davidson, G., et al., *Casein kinase 1 gamma couples Wnt receptor activation to cytoplasmic signal transduction.* Nature, 2005. **438**(7069): p. 867-72.
205. Del Valle-Perez, B., et al., *Coordinated action of CK1 isoforms in canonical Wnt signaling.* Mol. Cell. Biol., 2011. **31**(14): p. 2877-88.
206. Lee, S.Y., et al., *Casein kinase-1gamma1 and 3 stimulate tumor necrosis factor-induced necroptosis through RIPK3.* Cell Death Dis, 2019. **10**(12): p. 923.
207. Luk, E., et al., *Manganese activation of superoxide dismutase 2 in Saccharomyces cerevisiae requires MTM1, a member of the mitochondrial carrier family.* Proc. Natl. Acad. Sci. USA, 2003. **100**: p. 10353-10357.
208. Geiger, T., et al., *Comparative proteomic analysis of eleven common cell lines reveals ubiquitous but varying expression of most proteins.* Mol Cell Proteomics, 2012. **11**(3): p. M111 014050.
209. Chen, Y., et al., *Activation of the Wnt/beta-catenin signaling pathway is associated with glial proliferation in the adult spinal cord of ALS transgenic mice.* Biochem Biophys Res Commun, 2012. **420**(2): p. 397-403.

210. Caliceti, C., et al., *ROS, Notch, and Wnt signaling pathways: crosstalk between three major regulators of cardiovascular biology.* Biomed Res Int, 2014. **2014**: p. 318714.
211. Korswagen, H.C., *Regulation of the Wnt/beta-catenin pathway by redox signaling.* Dev Cell, 2006. **10**(6): p. 687-8.
212. Shin, S.Y., et al., *Hydrogen peroxide negatively modulates Wnt signaling through downregulation of beta-catenin.* Cancer Lett, 2004. **212**(2): p. 225-31.
213. Funato, Y., et al., *The thioredoxin-related redox-regulating protein nucleoredoxin inhibits Wnt-beta-catenin signalling through dishevelled.* Nat Cell Biol, 2006. **8**(5): p. 501-8.
214. Li, L., et al., *Axin and Frat1 interact with dvl and GSK, bridging Dvl to GSK in Wnt-mediated regulation of LEF-1.* EMBO J, 1999. **18**(15): p. 4233-40.
215. Kajla, S., et al., *A crucial role for Nox 1 in redox-dependent regulation of Wnt-beta-catenin signaling.* FASEB J, 2012. **26**(5): p. 2049-59.
216. Guo, X., et al., *Ligand-dependent ubiquitination of Smad3 is regulated by casein kinase 1 gamma 2, an inhibitor of TGF-beta signaling.* Oncogene, 2008. **27**(58): p. 7235-47.
217. Gomez, M.L., et al., *SOD1 is essential for oncogene-driven mammary tumor formation but dispensable for normal development and proliferation.* Oncogene, 2019. **38**(29): p. 5751-5765.
218. Hua, Z., et al., *2-Phenylamino-6-cyano-1H-benzimidazole-based isoform selective casein kinase 1 gamma (CK1gamma) inhibitors.* Bioorg Med Chem Lett, 2012. **22**(17): p. 5392-5.
219. Tulalamba, W. and T. Janvilisri, *Nasopharyngeal carcinoma signaling pathway: an update on molecular biomarkers.* Int J Cell Biol, 2012. **2012**: p. 594681.
220. Li, S., et al., *Disrupting SOD1 activity inhibits cell growth and enhances lipid accumulation in nasopharyngeal carcinoma.* Cell Commun Signal, 2018. **16**(1): p. 28.
221. Stewart, D.J., et al., *Wnt signaling pathway pharmacogenetics in non-small cell lung cancer.* Pharmacogenomics J, 2014. **14**(6): p. 509-22.
222. Stewart, D.J., *Wnt signaling pathway in non-small cell lung cancer.* J Natl Cancer Inst, 2014. **106**(1): p. djt356.
223. Bansal, N., et al., *Broad phenotypic changes associated with gain of radiation resistance in head and neck squamous cell cancer.* Antioxid Redox Signal, 2014. **21**(2): p. 221-36.
224. Reddi, A.R. and V.C. Culotta, *Regulation of manganese antioxidants by nutrient sensing pathways in Saccharomyces cerevisiae.* Genetics, 2011. **189**(4): p. 1261-70.
225. Teixeira, H.D., R.I. Schumacher, and R. Meneghini, *Lower intracellular hydrogen peroxide levels in cells overexpressing CuZn-superoxide dismutase.* Proceedings of the National Academy of Sciences, 1998. **95**(14): p. 7872-7875.
226. Imlay, J.A., *Pathways of oxidative damage.* Annual Reviews in Microbiology, 2003. **57**(1): p. 395-418.

227. Gralla, E. and J.S. Valentine, *Null mutants of Saccharomyces cerevisiae Cu,Zn superoxide dismutase: characterization and spontaneous mutation rates.* J. Bacteriol., 1991. **173**: p. 5918-5920.
228. Liochev, S.I., *Commentary: The Role of Iron-Sulfur Clusters in In Vivo Hydroxyl Radical Production.* Free radical research, 1996. **25**(5): p. 369-384.
229. Liochev, S.I. and I. Fridovich, *The role of O2.− in the production of HO.: in vitro and in vivo.* Free Radical Biology and Medicine, 1994. **16**(1): p. 29-33.
230. Kirkman, H.N., S. Galiano, and G. Gaetani, *The function of catalase-bound NADPH.* Journal of Biological Chemistry, 1987. **262**(2): p. 660-666.
231. Jeon, S.-M., *Regulation and function of AMPK in physiology and diseases.* Experimental & molecular medicine, 2016. **48**(7): p. e245-e245.
232. Peralta, D., et al., *A proton relay enhances H2O2sensitivity of GAPDH to facilitate metabolic adaptation.* Nature Chemical Biology, 2015. **11**(2): p. 156-163.
233. van der Reest, J., et al., *Proteome-wide analysis of cysteine oxidation reveals metabolic sensitivity to redox stress.* Nature communications, 2018. **9**(1): p. 1-16.
234. Anastasiou, D., et al., *Inhibition of pyruvate kinase M2 by reactive oxygen species contributes to cellular antioxidant responses.* Science, 2011. **334**(6060): p. 1278-83.
235. Mitchell, A.R., et al., *Redox regulation of pyruvate kinase M2 by cysteine oxidation and S-nitrosation.* Biochemical Journal, 2018. **475**(20): p. 3275-3291.
236. Kunjithapatham, R. and S. Ganapathy-Kanniappan, *GAPDH with NAD+-binding site mutation competitively inhibits the wild-type and affects glucose metabolism in cancer.* Biochimica et Biophysica Acta (BBA)-General Subjects, 2018. **1862**(12): p. 2555-2563.
237. Diderich, J.A., et al., *Physiological properties of Saccharomyces cerevisiae from which hexokinase II has been deleted.* Appl. Environ. Microbiol., 2001. **67**(4): p. 1587-1593.
238. Bockus, L.B., et al., *Cardiac insulin signaling regulates glycolysis through phosphofructokinase 2 content and activity.* Journal of the American Heart Association, 2017. **6**(12): p. e007159.
239. Krüger, A., et al., *The Pentose Phosphate Pathway Is a Metabolic Redox Sensor and Regulates Transcription During the Antioxidant Response.* Antioxidants & Redox Signaling, 2011. **15**(2): p. 311-324.
240. Ralser, M., et al., *Dynamic rerouting of the carbohydrate flux is key to counteracting oxidative stress.* Journal of biology, 2007. **6**(4): p. 10.
241. Ralser, M., et al., *Metabolic reconfiguration precedes transcriptional regulation in the antioxidant response*. 2009. p. 604-605.
242. Kuehne, A., et al., *Acute activation of oxidative pentose phosphate pathway as first-line response to oxidative stress in human skin cells.* Molecular cell, 2015. **59**(3): p. 359-371.
243. Mullarky, E. and L.C. Cantley, *Diverting glycolysis to combat oxidative stress*, in *Innovative medicine*. 2015, Springer, Tokyo. p. 3-23.

244. Christodoulou, D., et al., *Reserve flux capacity in the pentose phosphate pathway enables Escherichia coli's rapid response to oxidative stress.* Cell systems, 2018. **6**(5): p. 569-578. e7.
245. Shestov, A.A., et al., *Quantitative determinants of aerobic glycolysis identify flux through the enzyme GAPDH as a limiting step.* elife, 2014. **3**: p. e03342.
246. Liberti, M.V., et al., *A predictive model for selective targeting of the Warburg effect through GAPDH inhibition with a natural product.* Cell metabolism, 2017. **26**(4): p. 648-659. e8.
247. Winterbourn, C.C. and M.B. Hampton, *Thiol chemistry and specificity in redox signaling*. 2008.
248. Jouhten, P., et al., *Oxygen dependence of metabolic fluxes and energy generation of Saccharomyces cerevisiae CEN. PK113-1A.* BMC systems biology, 2008. **2**(1): p. 60.
249. Viator, R.J., et al., *Hypoxia-induced increases in glucose uptake do not cause oxidative injury or advanced glycation end-product (AGE) formation in vascular endothelial cells.* Physiological reports, 2015. **3**(7): p. e12460.
250. Ouiddir, A., et al., *Hypoxia upregulates activity and expression of the glucose transporter GLUT1 in alveolar epithelial cells.* American journal of respiratory cell and molecular biology, 1999. **21**(6): p. 710-718.
251. Bruckner, B.A., et al., *Regulation of brain glucose transporters by glucose and oxygen deprivation.* Metabolism, 1999. **48**(4): p. 422-431.
252. Tarsio, M., et al., *Consequences of loss of Vph1 protein-containing vacuolar ATPases (V-ATPases) for overall cellular pH homeostasis.* Journal of Biological Chemistry, 2011. **286**(32): p. 28089-28096.
253. Baron, J.A., J.S. Chen, and V.C. Culotta, *Cu/Zn superoxide dismutase and the proton ATPase Pma1p of Saccharomyces cerevisiae.* Biochemical and biophysical research communications, 2015. **462**(3): p. 251-256.
254. van Leeuwen, L.A., et al., *Click-PEGylation–a mobility shift approach to assess the redox state of cysteines in candidate proteins.* Free Radical Biology and Medicine, 2017. **108**: p. 374-382.
255. Wood, L.K. and D.J. Thiele, *Transcriptional activation in yeast in response to copper deficiency involves copper-zinc superoxide dismutase.* Journal of Biological Chemistry, 2009. **284**(1): p. 404-413.
256. Rinnerthaler, M., et al., *Yno1p/Aim14p, a NADPH-oxidase ortholog, controls extramitochondrial reactive oxygen species generation, apoptosis, and actin cable formation in yeast.* Proceedings of the National Academy of Sciences, 2012. **109**(22): p. 8658-8663.
257. Papa, L., et al., *SOD2 to SOD1 switch in breast cancer.* Journal of biological chemistry, 2014. **289**(9): p. 5412-5416.
258. Araki, K., et al., *Redox sensitivities of global cellular cysteine residues under reductive and oxidative stress.* Journal of proteome research, 2016. **15**(8): p. 2548-2559.

259. Topf, U., et al., *Quantitative proteomics identifies redox switches for global translation modulation by mitochondrially produced reactive oxygen species.* Nature Communications, 2018.
260. Leichert, L.I., et al., *Quantifying changes in the thiol redox proteome upon oxidative stress in vivo.* Proceedings of the National Academy of Sciences, 2008. **105**(24): p. 8197-8202.
261. Fu, L., et al., *Systematic and quantitative assessment of hydrogen peroxide reactivity with cysteines across human proteomes.* Molecular & Cellular Proteomics, 2017. **16**(10): p. 1815-1828.
262. Xiao, H., et al., *A Quantitative Tissue-Specific Landscape of Protein Redox Regulation during Aging.* Cell, 2020. **180**(5): p. 968-983. e24.
263. Chouchani, E.T., et al., *Mitochondrial ROS regulate thermogenic energy expenditure and sulfenylation of UCP1.* Nature, 2016.
264. Garcia-Santamarina, S., et al., *Monitoring in vivo reversible cysteine oxidation in proteins using ICAT and mass spectrometry.* Nat Protoc, 2014. **9**(5): p. 1131-45.
265. Dick, T.P. and M. Ralser, *Metabolic remodeling in times of stress: who shoots faster than his shadow?* Molecular cell, 2015. **59**(4): p. 519-521.
266. Liu, C.-L., et al., *Targeting the pentose phosphate pathway increases reactive oxygen species and induces apoptosis in thyroid cancer cells.* Molecular and Cellular Endocrinology, 2020. **499**: p. 110595.
267. Chandel, N., et al., *Mitochondrial reactive oxygen species trigger hypoxia-induced transcription.* Proceedings of the National Academy of Sciences, 1998. **95**(20): p. 11715-11720.
268. Leichert, L.I., et al., *Quantifying changes in the thiol redox proteome upon oxidative stress in vivo.* Proc Natl Acad Sci U S A, 2008. **105**(24): p. 8197-202.
269. Xiao, H., et al., *A Quantitative Tissue-Specific Landscape of Protein Redox Regulation during Aging.* Cell, 2020. **180**(5): p. 968-983.e24.
270. Tonks, N.K., *Protein tyrosine phosphatases: from genes, to function, to disease.* Nature reviews Molecular cell biology, 2006. **7**(11): p. 833-846.
271. Lee, S.-R., et al., *Reversible inactivation of protein-tyrosine phosphatase 1B in A431 cells stimulated with epidermal growth factor.* Journal of Biological Chemistry, 1998. **273**(25): p. 15366-15372.
272. Leonard, S.E., K.G. Reddie, and K.S. Carroll, *Mining the thiol proteome for sulfenic acid modifications reveals new targets for oxidation in cells.* ACS Chem Biol, 2009. **4**(9): p. 783-99.
273. Gietz, R.D. and R.H. Schiestl, *Applications of high efficiency lithium acetate transformation of intact yeast cells using single-stranded nucleic acids as carrier.* Yeast, 1991. **7**(3): p. 253-263.
274. Ness, F., et al., *Sterol uptake in Saccharomyces cerevisiae heme auxotrophic mutants is affected by ergosterol and oleate but not by palmitoleate or by sterol esterification.* Journal of bacteriology, 1998. **180**(7): p. 1913-1919.
275. Perlin, D.S., et al., *Defective H(+)-ATPase of hygromycin B-resistant pma1 mutants fromSaccharomyces cerevisiae.* J. Biol. Chem., 1989. **264**(36): p. 21857-64.

276. Wessel, D.m. and U. Flügge, *A method for the quantitative recovery of protein in dilute solution in the presence of detergents and lipids.* Analytical biochemistry, 1984. **138**(1): p. 141-143.
277. Vander Heiden, M.G., L.C. Cantley, and C.B. Thompson, *Understanding the Warburg effect: the metabolic requirements of cell proliferation.* Science, 2009. **324**(5930): p. 1029-33.
278. Li, S., et al., *Disrupting SOD1 activity inhibits cell growth and enhances lipid accumulation in nasopharyngeal carcinoma.* Cell Communication and Signaling, 2018. **16**(1): p. 1-13.